

Development of an LCOE Optimization Tool used for the Siting and Planning of Hybrid Floating Wind and Wave Farms



Department of Wind Energy Master Report

Jorge Izquierdo Pérez

DTU Wind Energy-M-0323

August 2019

DTU Wind Energy
Department of Wind Energy



Author: Jorge Izquierdo Pérez

Title: Development of an LCOE Optimization Tool used for the Siting and Planning of Hybrid Floating Wind and Wave Farms

DTU Wind Energy-M-03233

August 2019

Project period:

February 2019 – August 2019

ECTS: 35

Education: Master of Science

Supervisor:

Niels-Erik Clausen

Antonio Manuel Pegalajar Jurado

DTU Wind Energy

Remarks:

This report is submitted as partial fulfillment of the requirements for graduation in the above education at the Technical University of Denmark.

DTU Wind Energy is a department of the Technical University of Denmark with a unique integration of research, education, innovation and public/private sector consulting in the field of wind energy. Our activities develop new opportunities and technology for the global and Danish exploitation of wind energy. Research focuses on key technical-scientific fields, which are central for the development, innovation and use of wind energy and provides the basis for advanced education at the education.

We have more than 240 staff members of which approximately 60 are PhD students. Research is conducted within nine research programmes organized into three main topics: Wind energy systems, Wind turbine technology and Basics for wind energy.

Technical University of Denmark

Department of Wind Energy
Frederiksborgvej 399
4000 Roskilde
Denmark

www.vindenergi.dtu.dk

Abstract

Offshore floating hybrid wind and wave energy is a young technology that still needs to be scaled up. To ensure its competitiveness in the sustainable energy market, the total costs of the energy production must be reduced by either improving the technology or maximizing the farm's efficiency. The key indicator to be minimized is the Levelized Cost of Energy, subject of optimization in the model developed in this work.

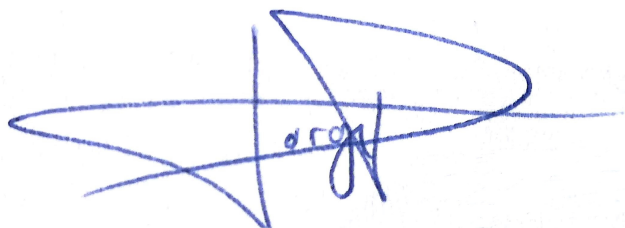
A full energy production and costs model has been built for the hybrid P80 concept designed by the company Floating Power Plant A/S. The technical aspects involved in the model include the wakes and waves shadow, the power output conversion values of both wind and waves generators, as well as all the expenditures and economical factors involved in the project: CAPEX, OPEX, and discount rate. The site-dependent parameters considered are: the wind and wave resources, the bathymetry, and the distances to shore, to the harbors and to the grid. A Particle Swarm Optimization algorithm consummates the tool, taking as decision variables the layout, the offshore substation position, and the export cable choice. It was found that more sophisticated algorithms are needed to find consistent results in this kind of optimization process.

The model has been applied off the west coast of Ireland in a site of interest for the company. With a layout of 25 platforms in 5 rows, the LCOE was minimized to a value of 116.56 €/MWh when using the considered base parameters. The main vessel routes, the area's grid strength, and the visual impact of the farm were also studied. It was then found that lower costs of about 85 €/MWh can be reached in the short-term, and the room for improvement in the structure's design and materials was highlighted, with an LCOE reduction potential of up to a 32%. It is also proved that a model of this kind serves usefully as a preliminary analysis, but the uncertainty estimate of an 11% indicates that site-specific studies and measurements are essential.

Preface

This MSc thesis was prepared at the department of Wind Energy at the Technical University of Denmark in Risø, in collaboration with the company Floating Power Plant A/S, in fulfillment of the requirements for acquiring a Master of Science degree in Sustainable Energy with a specialization in Wind Energy.

Copenhagen, August 1, 2019

A handwritten signature in blue ink, appearing to be 'Jorge Izquierdo Pérez', written over a faint grid background.

Jorge Izquierdo Pérez (s172587)

Acknowledgements

I would like to express my gratitude to my supervisors Niels-Erik Clausen and Antonio Manuel Pegalajar Jurado for giving me freedom and autonomy throughout the whole Master Thesis, not only always supporting me but also giving me new insights and offering constructive solutions to any challenge encountered. They opened the door to their department, helped me with my organization and always directed me in the right direction and towards the right people.

I am also very grateful with the help provided by FPP, specially from Nis Ebsem, my supervisor in the company, who was always quick and generous at answering questions and providing useful information and documentation, not to forget about Sarah, Pilar and Anders, that let me in the company with their arms open and offered their help and advice. Also, thanks to Morten and Chris for efficiently providing information when I asked for it.

I would also like to thank Niels, Daniel, Andreas and Nikolay, that received me, in some cases more than once, and offered their knowledge and support. A special thanks to Alfredo, that granted me access to his work and let me use it in my tool, and Neil, who provided crucial data for the model. Also thanks to Hugo and Gyde, for allowing me to have a basis from where to build my work and take inspiration, specially in the unclear and abstract beginning.

Particularly, I want to express my special gratitude to Joaquín and Bruno for offering their priceless help from a very different environment in a completely altruistic effort. And finally thank you very much to my loving family, friends, and the fellowship of the Ring for their everyday support.

Contents

Abstract	i
Preface	iii
Acknowledgements	v
Contents	vii
List of Abbreviations	ix
1 Introduction	1
1.1 Motivation	3
1.2 Content	4
2 The Technology	5
2.1 Floating Power Plant A/S	5
2.2 P80: the concept used in the model	8
3 The Model	15
3.1 Wave energy model	17
3.2 Wind energy model	24
3.3 Costs model	29
3.4 Optimization algorithm	43
4 Case Study: Siting in the Republic of Ireland	51
4.1 General description	52
4.2 Implementation of the model	57
5 Results and Discussion	69
5.1 Sensitivity analysis	75
5.2 Uncertainty analysis	80
6 Conclusion	83
6.1 Future work	85

Bibliography	87
A Costs Figures: Sources and Assumptions	93
A.1 Design and project management	93
A.2 Wind turbines	94
A.3 Electrical infrastructure	95
A.4 Decommissioning	97
A.5 Discount rate	98
A.6 Vessel speeds	99
B Confidential data from Floating Power Plant A/S	101

List of Abbreviations

AEP	Annual Energy Production
ASO	Agent Swarm Optimization
CAPEX	Capital Expenditures
DHI	Danish Hydraulics Institute
EI	Electrical Infrastructure
FPP	Floating Power Plant A/S
GWA	Global Wind Atlas
H_s	Wave's significant height
HV	High Voltage
LCOE	Levelized Cost of Energy
L_w	Waves wavelength
MV	Medium Voltage
NEWA	New European Wind Atlas
OPEX	Operational Expenditures
O&G	Oil & Gas
O&M	Operation & Maintenance
PSO	Particle Swarm Optimization
PTO	Power Take-Off unit
T_e	Wave's energy period
T_z	Wave's zero-crossing period
WEC	Wave Energy Converter
w.s.	Wind speed
WTG	Wind Turbine Generator
θ_{wa}	Waves direction
θ_{wi}	Wind direction

CHAPTER 1

Introduction

One of the main issues that determine the future of planet Earth, the environment, and human civilization since the industrial revolution is climate change. Global warming as a consequence of greenhouse gases in the atmosphere is a reality, and there is a consensus among more than 97% of the scientific community on the fact that human emissions are the main reason of this phenomenon [1].

As a consequence, since the late 1990s, several arguably soft agreements and efforts such as the Kyoto protocol in 1997, the pact at the COP 21 summit in 2015 or the 2020 targets proposed by the European Commission, have been launched at the international level. These actions are becoming urgent as latest findings and studies already predict inevitable catastrophic consequences from climate change [2].

Among other targets, middle term national green new deals point at a transition to a full sustainable energy generation system, as one of the main sources of these greenhouse gas emissions is, in fact, electricity generation, which represents around 25% of the total emissions, according to the Intergovernmental Panel on Climate Change (IPCC) [3], as shown in Fig. 1.1:

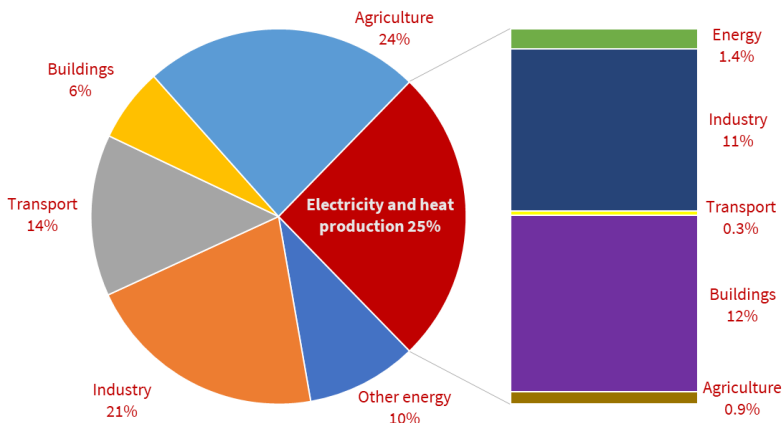


Figure 1.1: Total anthropogenic greenhouse gas emissions (GtCO₂eq/yr) by economic sector in 2010 (based on [3]).

Together with other technologies such as solar photovoltaic (PV), wind energy plays a crucial role in this transition, in part thanks to the irruption of offshore wind farms, that are contributing to propel the wind energy potential worldwide. In fact, the installed wind capacity around the globe has been increased from 432 GW in 2015 to 597 GW by the end of 2018, currently supplying a 14% of Europe's and 6% of the world's total electricity demand [4–6], of which 23 GW corresponds to offshore farms worldwide [7], with growth expectations of other 8 GW by 2023 [8].

The newly exploitable offshore resource presents significant advantages with respect to that available onshore as it is both more constant and powerful, two very valuable characteristics for the energy market. These features combined with the lower spatial restraints in the sea have allowed the manufacturers to develop bigger and taller turbines that can be placed further from each other and which already reach capacities of up to 8, 10 or even 12 MW in the case of General Electric's Haliade-X, which can provide energy to 16,000 European households, according to GE [9].

State of the art technologies keep allowing access to more convenient and previously unexploitable wind resources; while mass installation of offshore bottom-fixed wind turbines is already a reality, it is now pilot farms and projects with floating platforms such as Hywind Scotland, IDEOL's Floatgen, Fukushima FORWARD and the upcoming PLOCAN Canary Islands wind hub which are exploring and expanding this market.

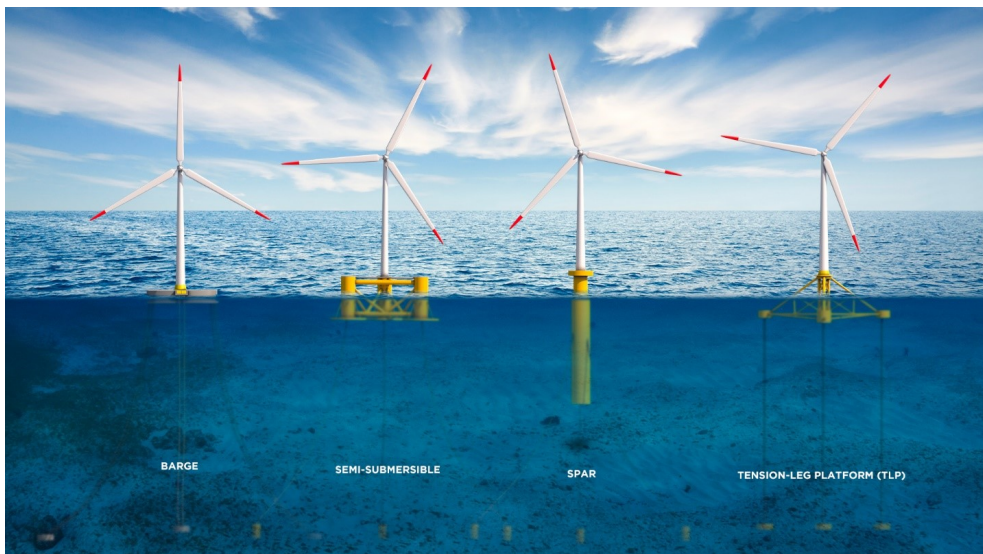


Figure 1.2: Main concepts of floating wind turbines [10].

The floating concepts, showed in Fig.1.2, present new attractive advantages: they can be installed in sites where the seabed is too deep for the feasible installation of bottom-fixed foundations. This way, the turbines can be placed further offshore, where the wind resource is often of even better quality; and also off the shore of regions with steep seabeds like Europe's West coast in the Atlantic Ocean, the Mediterranean Sea or California's coast. In contrast, the main downside of floating technology is the need of big amounts of material (generally steel) that can enclose enough air to ensure the whole structure's buoyancy, thus increasing its cost significantly. Concepts like Stiesdal's TetraSpar, about to be tested in Norway, aim to find a solution to this issue, in this case by reusing old decommissioned turbine towers as floaters [11].

A new twist in the latest offshore floating technologies are the hybrid concepts that combine different sources of energy, thus allowing the efficient use of resources for more than a single process: these are the so-called synergies. One of the most developed concepts is the hybrid wind and wave technology, which combines Wind Turbine Generators (WTG) and Wave Energy Converters (WEC). This combination of technologies leads to the following synergies: the possibility of finding a common regulatory framework for both energy generation methods with regards to the licensing and planning of space and infrastructure; the increase of spatial efficiency of the energy yield; the improvement of the output power, which is smoother and more reliable; and the opening of the Operation and Maintenance (O&M) window of both devices thanks to the WEC's waves shadow effect, thus reducing the costs [12, 13].

This leads to the device object of this study: the P80, a semi-submersible hybrid wind and wave energy production concept designed by Floating Power Plant A/S (FPP) in Denmark, further analyzed in Section 2.2.

1.1 Motivation

As it is usual in every state-of-the-art technology, the new hybrid concepts currently struggle to be cost-competitive in the energy market and to prove themselves feasible so that they can be object of a power generation project. Their competitiveness may be achieved in different ways: by improving the technology design itself, reducing the amount of material needed (as mentioned above), or maximizing the usage efficiency of the existing designs.

The latter is the target of the present study, in which a P80 farm layout optimization model has been developed in MATLAB in order to minimize the total energy generation costs of a project taking into account all the expenses involved, as well as the technical characteristics of the energy generators, the conditions of the geographic site of interest, the available wind and wave resources, and the interaction between the different generators (wind wakes and waves shadows). The optimization is carried out by means of a Particle Swarm Optimization (PSO) algorithm, as this or

another type of metaheuristic evolutionary algorithm is needed due to the non-linear characteristics of a problem of this nature.

The indicator subject to be minimized in the model is the Levelized Cost of Energy (LCOE) since, as it is fully explained in Section 3.3.1, it represents the average generation cost of a unit of energy along the lifetime of a project, thus being a powerful indicator that allows investors to compare the variation of costs with time, among different arrangements and technologies.

1.2 Content

The following sections of the report provide a logical and structured explanation of the model developed with its further application and discussion: In **Chapter 2**, the state of the art P80 concept engineered by FPP is presented. Following the technology analysis, in **Chapter 3** all the details regarding the model's construction are explained: its main parts, the logic behind it, the equations used, the assumptions made and its consequent limitations. Next, in **Chapter 4**, after a qualitative study, the numerical model is applied in a geographical area of relevance for FPP located off the west coast of the Republic of Ireland: different sites within the area are considered and an ideal final site and layout are chosen after a description of the optimization process that was followed. Finally, a discussion about the results, together with sensitivity and uncertainty analyses, and a study of the technology's projection in the future are made in **Chapter 5**; and **Chapter 6** serves as a summary of the work carried out, where the conclusions extracted are presented to culminate the report. Additionally, the appendices contain all the figures and sources of the costs and technical parameters used in the model: Appendix A shows the data obtained from the literature research regarding the design and project management, wind turbines, electrical infrastructure and decommissioning related costs, as well as the discount rate value and the vessel speeds used. Finally, the sensitive data from FPP is specified in a confidential appendix.

CHAPTER 2

The Technology

As it has been anticipated, the hybrid wind and wave concept that has been used in the model is Floating Power Plant's P80. Therefore, all its technical and economical characteristics are implemented as inputs in the model: these are the WTG power curve, the WEC power output matrix, and all the costs figures related to the device. These now rather straightforward input parameters are the output magnitudes of a complex technology that is analyzed in the chapter after a brief introduction to the company.

2.1 Floating Power Plant A/S

FPP is a rather recent international engineering company based in Denmark, the United Kingdom and Norway. It emerged in the late 90s from the conception of a new wave energy generation system, being the company finally established in 2004. Since then, the first offshore-proven combined floating wind and wave device to have delivered power to the grid has been engineered, upscaled, and is now being commercialized. The company's progression is shown in Fig. 2.1.

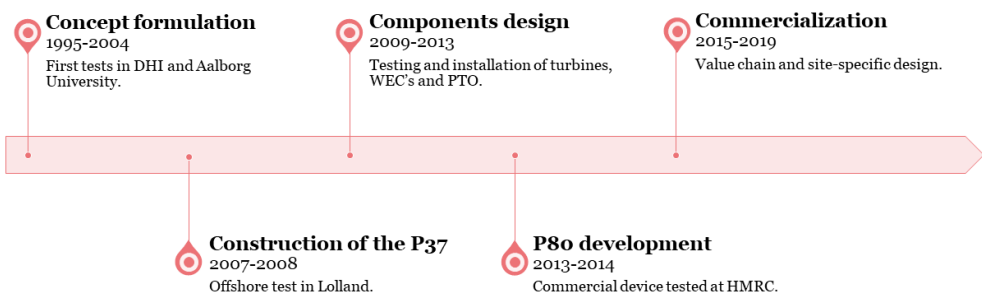


Figure 2.1: FPP's history timeline (diagram based on [14]).

Given its European origins, FPP's most immediate objectives are several particular areas off the shore of European countries. However, the company's target by

2050 is to exploit 20 GW of the worldwide wind and waves resources available in the offshore areas depicted in Fig. 2.2, where the rather deeper seafloor, the good wind resource, and the strong waves are best suitable for their hybrid concept, in comparison to other existing bottom fixed and floating wind energy concepts.



Figure 2.2: FPP’s worldwide potential market [14].

Up to now, the company has developed two models of their hybrid product: the P37 and the P80 (shown in Fig. 2.3 and 2.4 respectively). The former, named after “Poseidon” and its 37 m length characteristic, was the first ever wind and wave concept to produce energy for the grid from an offshore environment. It was installed off the shore of Lolland, Denmark, as a demo device and it has been used for testing, improvement and implementation of its main components: the wave absorbers and the Power Take Off system (PTO). All of this with the goal of developing the P80 large-scale production model.

With regards to the P80 version, the product is in early stages of commercialization and the company currently aims at two possible markets for it: on the one hand, the goal in the long run is to use it in large-scale electricity generation farms (which is the application for which it is modeled in this study); and on the other, in the short term, the concept is meant to be used as the energy source for offshore oil extraction processes in the oil and gas (O&G) sector. This will play a non-negligible role in the decarbonization of fuel extraction processes, and it will serve for further testing, quality proving and market demonstration of the technology.

Currently, FPP is involved in several potential projects (the most advanced ones in

the United Kingdom), and latest news are the signature of a Memorandum of Understanding with the Oceanic Platform of the Canary Islands (PLOCAN) for a potential deployment of FPP's technology in the testing facilities in the Spanish archipelago; also, together with Aalborg's University, FPP has been conceded grants from the Danish EUDP program for developing and testing advanced control strategies for the waves PTO system, and for further developing FPPs technology towards the O&G market.



Figure 2.3: P37 concept installed in Lolland, Denmark [14].

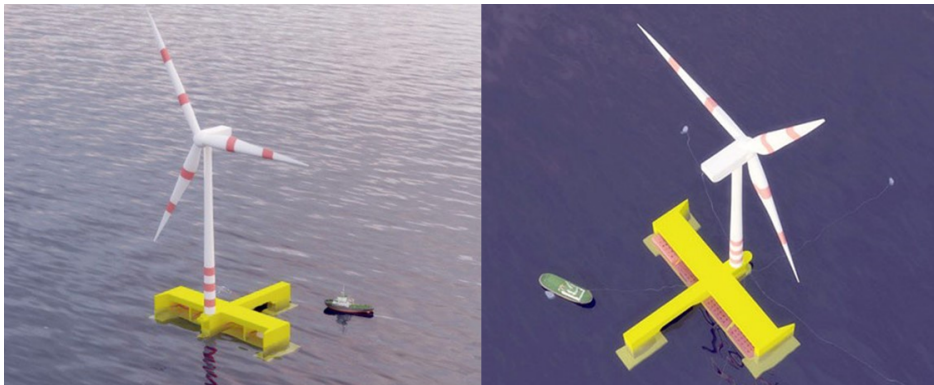


Figure 2.4: Virtual model of the commercial P80 concept [14].

2.2 P80: the concept used in the model

Among the several existent types of combined offshore energy generation systems, the P80 is a hybrid multipurpose floating platform that is capable of extracting energy simultaneously from the waves (not to be confounded with tidal energy) with its WEC system, and from the wind, as an offshore wind turbine is also installed on the structure. The platform is 80 meters wide, the beam along that dimension hosts four wave absorbers, depicted in red in the figures, two at each side of the central axis beam, which is 90 m long and where the WTG, the turret (connecting point of the mooring and electrical output systems) and the third leg of the platform are placed. In terms of height, depending on its site specific characteristics, the wind turbine hub can currently be in the order of 100-150 meters tall.

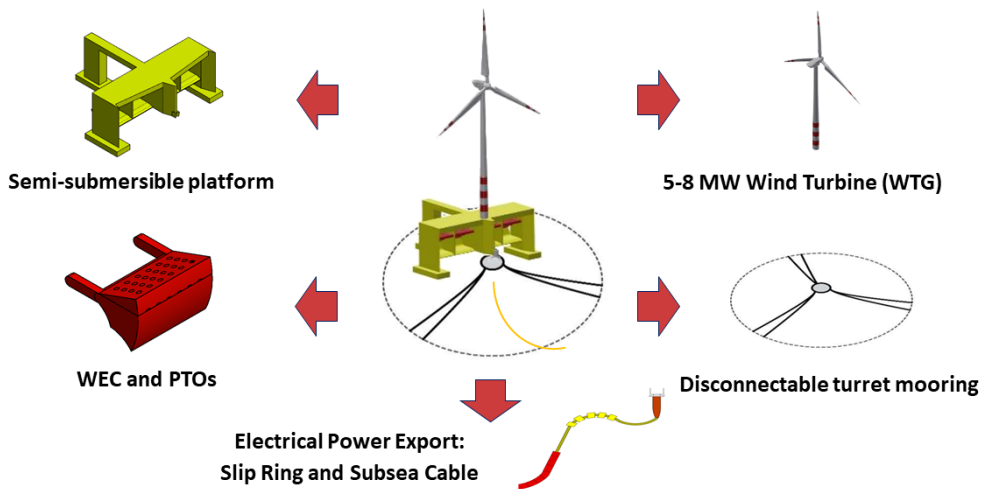


Figure 2.5: Components of the P80 (figure obtained from FPP).

2.2.1 Semi-sub platform

The platform is a semi-submersible (see Fig.1.2) floating structure made of steel that has the functions of hosting all the components of the P80, ensuring the proper buoyancy of the structure, controlling the draft by means of hollow chambers that can be filled or emptied of water with the installed water pumps, and, together with the WECs, passively vaning (rotating) the whole structure around the turret mooring point, so it faces the main waves direction thanks to the interaction of the waves with its geometry.

The passive vanning is an important and cumbersome behavior as it will limit the amount of energy that can be extracted from the waves (thus implying a vanning efficiency), and it will be affected by the direction of not only the different types of waves (wind and swell waves) but also the direction of the tides.

2.2.2 Wave Energy Converter (WEC)

The WEC is a state of the art commercial design, developed in FPP. As it has been mentioned, there are four WECs installed in the front side of the P80, each of which has a capacity of 500-800 kW, a total of 2-3.2 MW per platform. The exact power magnitude will depend on its ultimate site-specific design, according to the size of the waves. The main components of the WEC, showed in Fig. 2.6, are presented below.

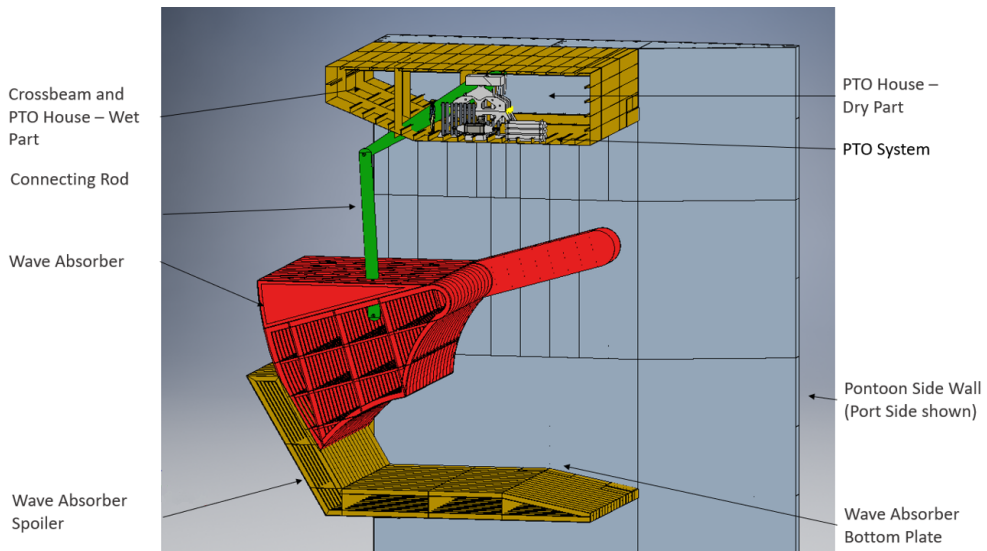


Figure 2.6: Wave Energy Converter (WEC) components (figure obtained from FPP).

A 18.5 m wide front pivot **Wave Absorber** with one degree of freedom that rotates within its hosting chamber converts the wave energy into pitch kinetic energy with an efficiency of 60-70% and transmits the waves mechanical energy through a connecting rod to the PTO.

The **Power Take-Off (PTO)** system is a complex hydro-electronic device that, by means of automatic control, actively changes its damping characteristics so as to

absorb as much energy as possible from the waves. It has two main functions: converting the energy carried by the absorber into electricity (reaching PTO efficiencies of 55-70%), and smoothing out the electricity output.

Naturally, the produced electricity depends on the instantaneous characteristics of the waves, which (as it is further explained in the following sections) are characterized by their significant height (H_s) and energy period (T_e), consequently originating an electrical output power matrix that is a function of these two parameters. The maximum power produced is limited, so when the waves are bigger than the size that the system is designed for, the PTO automatically locks the wave absorbers to maintain their integrity.

2.2.3 Wind Turbine Generator (WTG)

The WTG is placed just in front of the intersection of the platform's two main beams as showed in Fig. 2.7, the supported capacity being 5-8 MW, which represents the biggest share of electricity production of the P80. Due to the motion of the WECs, the system has four extra degrees of freedom on top of the six d.o.f. involved in a standard floating wind turbine, so the WTG controller needs to be optimized for the complex motion pattern that this entails.

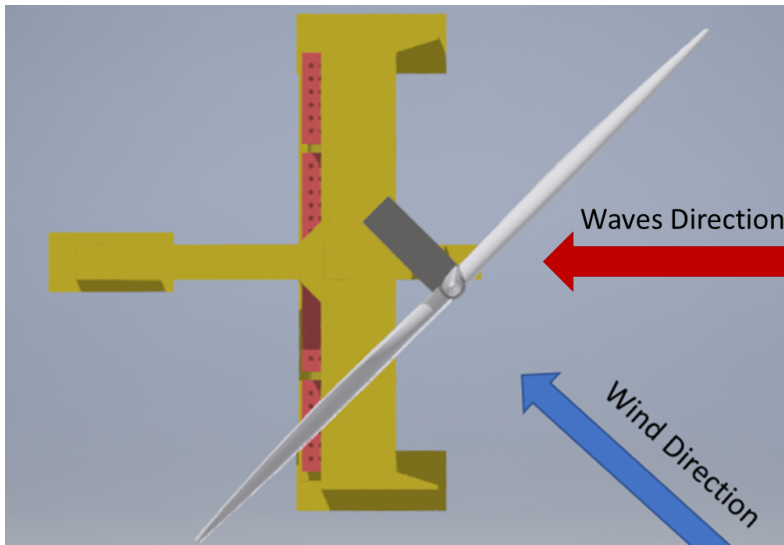


Figure 2.7: Position of the WTG on the P80 (figure obtained from FPP).

As every wind turbine nowadays, the P80s WTG hub yaws (rotates around its

vertical axis) actively to face the wind direction, and therefore its orientation is independent from that of the platform. The WTG is also placed very close to the turret mooring point, so the forces and moments affecting it have the least possible influence on the passive vaning of the platform.

2.2.4 Turret Mooring and Power Export System

The turret is the point around which the platform has the freedom to rotate and where the mooring lines and the electrical output power system are connected to the platform. The turret has the fundamental characteristic of being detachable, so both the mooring system and the electrical infrastructure can be installed before towing the actual platform to the site. A buoy keeps the connectable end of the mooring lines floating at a certain depth under water for their later connection.

FPP works with different configurations of mooring lines, but the one that is currently most defined and developed is the redundant system, which consists of three double-lines separated by 120° and is designed to work from 40 to 200 m of depth. Figure 2.8 shows the disposition and elements of the mooring lines.

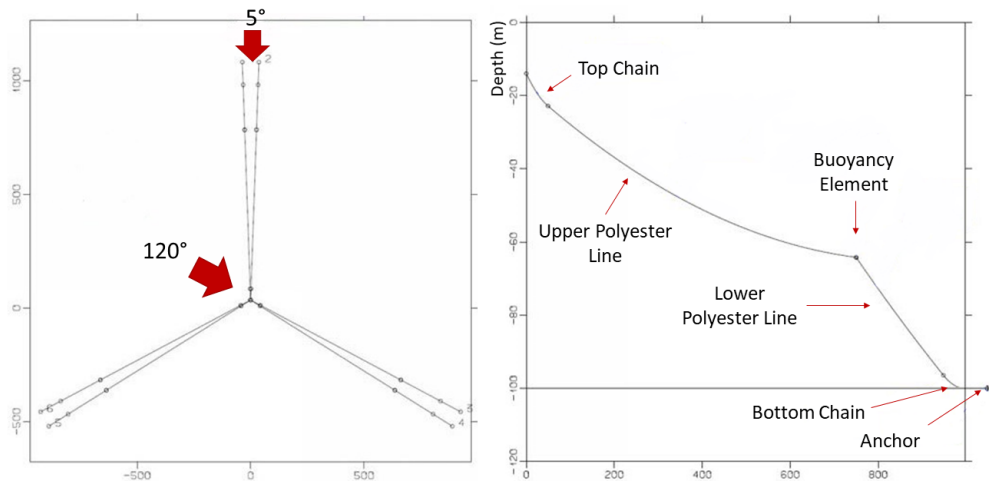


Figure 2.8: Mooring lines disposition and components (figure obtained from FPP).

As for the electrical system, the electricity is exported through a 33 kV, 50-70 mm^2 flexible stainless steel armored copper cable. In order to allow the platform to rotate independently from the export cable, a slip ring connects it with the turret. The cable is stress-terminated and fitted with some buoyancy modules as shown in Fig. 2.9. The dynamic cable thus floats underwater in a similar way as it occurs with

the mooring lines, and it is further equipped with protections along the area where it makes contact with the seafloor.

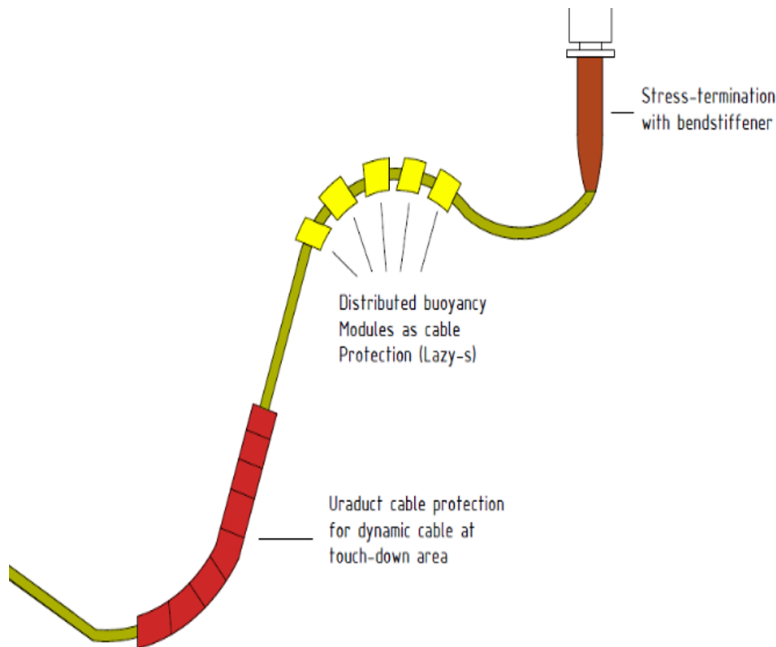


Figure 2.9: Dynamic power cable (figure obtained from FPP).

As a wrap up on the P80, all the above presented devices and technology make up a device that, as most floating concepts, has its main disadvantage in the excessive amount of steel needed for its structure, but which presents several characteristics that make it interesting in an engineering and economical way:

- The provided energy output is smoother and more predictable than that of only-wind concepts, thus reducing the system balancing costs and improving the power generation reliability. This is caused by the following facts: the wave energy output is generally flatter; also, as very often wind and waves are not correlated, the energy produced from both sources balance quite well the peaks and valleys of each other; on top of this, sea states can be predicted accurately with two to three days in advance, whereas accurate wind forecasts are available just a few hours ahead [15, 16].

- A direct effect of taking energy from the waves is the flattening of the water surface behind the platform, i.e. the significant reduction of the waves height behind the absorbers, which increases considerably the amount of hours when the sea state is suitable for O&M, something specially sensitive in the winter season. This reduces

the platforms downtime and thus increases the Annual Energy Production (AEP).

- The third advantage is the fact that the platform can be built onshore, in the harbor (which is how it has been modeled) and it can be towed to the site afterwards, so expensive installation vessels with cranes are not needed in the process. The same happens when the O&M process requires to tow the platform back to the harbor. In fact, the feature of being able to regulate the platform's height from a draft of 8 meters to 24 meters is specially useful for this application.

CHAPTER 3

The Model

The model developed in the present study is untangled in this chapter. In general terms, it consists in a lifetime costs calculation of an offshore hybrid farm project composed of P80 platforms, in relation to the many inputs and variables involved in the project, all of which are explained in the following sections. The type of farm that can be calculated by the model has the following structure: the P80s are connected to an offshore floating electrical substation through inter-array cables; from the offshore substation, an export cable transmits the electricity produced in the farm to an inland electrical substation which is connected to the grid; furthermore, a harbor is used to carry out certain necessary operations in the farm along the project that will also influence the costs.

The model is composed of four main modules: the wind and waves power generation models, the costs calculation model, and in a different plane, the optimization algorithm. With the intention of providing a big picture of the model so the reader can understand its general logic, a diagram of its components is shown in Figure 3.1.

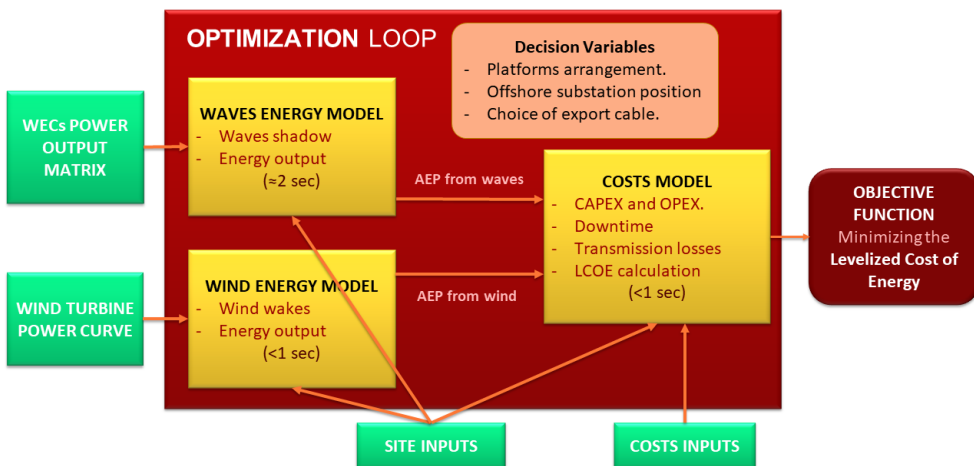


Figure 3.1: General diagram of the model.

The **waves** and **wind** power production models aim at simulating the physical and technical phenomena that result in a certain Annual Energy Production (AEP). This energy output depends, on the one hand, on the quality of the wind and waves climate, which determines the energy that could be potentially extracted from nature, and on the other, on the characteristics of the devices that convert the available energy into electricity: the WTG and WEC respectively.

In contrast, the **costs** model is a series of economical calculations that uses these AEP results as inputs to find the costs of the project in relation to the energy production by means of the LCOE indicator. Additionally, the energy losses due to downtime periods and transmission of electricity are calculated in the costs model.

A **Particle Swarm Optimization (PSO)** algorithm has been set up to obtain the minimum LCOE in any site with its specific inputs. It does so by modifying some decision variables like the platforms layout. The algorithm foundations and its implementation process are explained in the last section of this chapter.

The model was built under three main principles: first of all, minimizing as much as possible the many uncertainties involved in this complex calculation, naturally still assuming some limitations; secondly, reducing its running time, specially for the sake of the optimization process; and in the third place, developing it in a user friendly way, so the tool results useful for the company.

The model code was developed in MATLAB. However, in order to achieve the two latter goals presented above, all the inputs to the model were introduced in the form of Excel spreadsheets, instead of directly through the code. This way, specific values that may be reconsidered or subject to change in time, can be easily modified. In order to avoid the increase of computational time that this may cause, the inputs' loading is done outside of the optimization loop, as it is shown in Fig. 3.1, only keeping the strictly necessary calculations in it.

3.1 Wave energy model

The first module to be described is the waves model, where the AEP obtained from the waves (AEP_{waves}) is calculated. This model is based on a prior model developed in 2014 between DTU and FPP by Hugo de Sevin [17]. Some modifications were done to adapt it, improve significantly its computation speed (from about 30 to 2 seconds), and to match newer physical considerations and findings made in FPP since then. A diagram with the flows of information of the waves model is shown in Fig. 3.2.

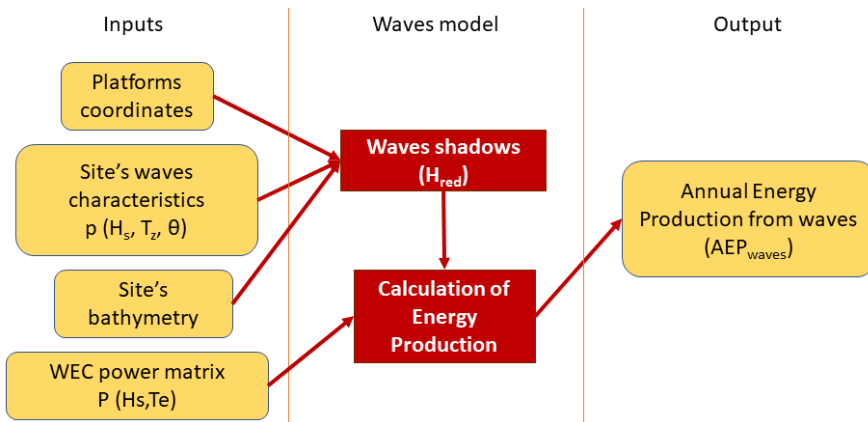


Figure 3.2: Waves model diagram.

3.1.1 Inputs: loading and processing

As it is shown in Fig. 3.2, the inputs to the model are the platforms' coordinates (which depend entirely on either the user or the optimization tool, as it is the main decision variable), the bathymetry and waves characteristics of the site, and the WEC power output matrix (obtained in FPP), that provides the electrical power output as a function of the waves characteristics, taking into account the technology and efficiencies involved in the waves absorber and PTO.

The most straightforward site-dependent input is the **bathymetry**. It is directly introduced in the model through a spreadsheet that contains information of the seafloor depth at every coordinate point in a grid. This data can be obtained from the Digital Terrain Model of the online portal of the European Marine Observation and Data Network (EMODnet) [18], that provides the seafloor depth from survey data-sets, composite DTMs, and Satellite Derive Bathymetry (SDB) data products.

With regards to the **waves climate**, the parameters that best describe its energy content are the significant height (H_s), which represents the average height of the

third highest waves, and the energy period (T_e), a non-direct parameter that describes the period of the waves [19]. The third characteristic that has much influence in the potential waves energy exploitation is their direction (θ_{wa}), as it will influence the power output of the WECs depending on their relative position due to the shadow effect, further explained in this section.

Given the high economic cost of obtaining time series with this information, the interest of the company from the beginning was to develop the tool using probabilistic scattered tables instead: three matrices that indicate the probability of occurrence of three parameters, two by two, i.e.: $p(H_s, T_z)$, $p(H_s, \theta_{wa})$, and $p(T_z, \theta_{wa})$, being T_z the zero-crossing period of the wave:

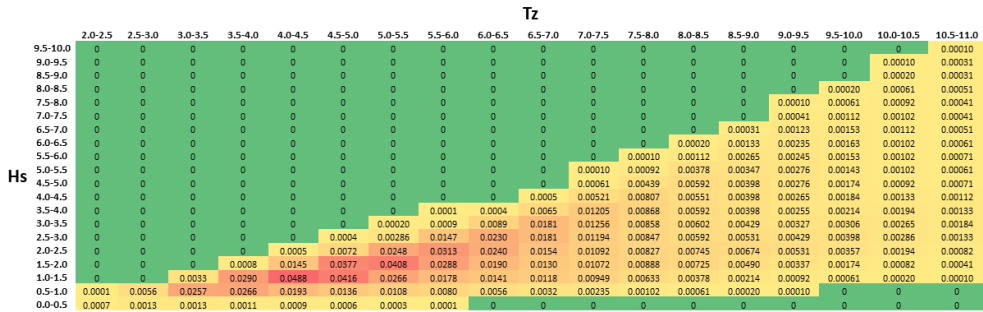


Figure 3.3: Example of a scattered matrix $p(H_s, T_z)$.

In the model, it has been considered that the waves characteristics are, in general, decoupled to each other and also to the wind speed. Even though some studies indicate their dependence in some areas (e.g.: the joint distribution in the Northern North Sea [20]), in bigger and more open oceans this may not be the case.

These input matrices can be obtained by FPP in the portal of the Danish Hydraulic Institute (DHI A/S) [21] for any site, at a cost zero for the company. As it is recurrently evinced further in the text, this transformed data implies a loss of information and therefore a slight increase in the uncertainty of the results. Indeed, the most immediate issue that rises is the fact that the values of $p(H_s, T_e, \theta_{wa})$ are unknown. None of the three probabilistic matrices provide the whole picture.

For this reason, in an early stage of the study, the scattered matrices were combined to obtain the probability of occurrence of the three parameters in the form of a 3-D matrix calculated as follows:

$$p(H_s, T_e, \theta_{wa}) = \frac{p(H_s, T_e) \cdot p(H_s, \theta_{wa}) \cdot p(T_e, \theta_{wa})}{\sum p(H_s, T_e) \cdot p(H_s, \theta_{wa}) \cdot p(T_e, \theta_{wa})} \quad (3.1)$$

Being $\sum p(H_s, T_e, \theta_{wa}) = 1$. If the 3-D matrix is subsequently multiplied by the number of hours in a year, the amount of hours of occurrence of each type of wave is obtained, and thus the AEP_{waves} can be calculated as it is explained further in this section. The method described in Eqn. (3.1) was checked and compared with a time series set of data of a specific site owned by FPP, obtaining more than fairly accurate AEP_{waves} results with an error that remained below 5%.

As the reader may have noticed, previously it has been stated that the energy content of a wave is best described with the energy period (T_e), and the scattered matrices provide the information for the zero-crossing period (T_z) instead. In fact, in the WECs power matrix, the power output is expressed as a function of the former: $P(H_s, T_e)$ in MWh.

The two periods are closely linked, but their relation depends on the type of sea or ocean: the peak enhancement factor (γ) of the site's wave spectrum defines it and it is used in the model to convert T_z into T_e by means of the following empirical equation developed by FPP, which was included in the model:

$$T_e = T_z \cdot (0.0017 \cdot \gamma^2 - 0.0246 \cdot \gamma + 1.2093) \quad (3.2)$$

The value of γ depends on the level of development of the sea climate. If the exact figure in the site is unknown, lower values may be used for more open and fully developed seas such as the Atlantic Ocean (e.g.: $\gamma = 1.5$) where waves are mainly generated by local winds, and higher ones for fetch-limited wind seas where waves are not fully developed (e.g.: $\gamma = 3.3$), as observed in the Joint North Sea Wave Observation Project (JONSWAP) for the North Sea [22].

One last parameter is needed as an input to the waves shadow model: the wavelength (L_w), which depends on T_z and the depth (introduced in this model as the site's average depth). On the one hand, the wave's angular frequency (ω) is expressed as:

$$\omega = \frac{2 \cdot \pi}{T_z} \quad (3.3)$$

On the other, the following dispersion equation is defined [19]:

$$\omega^2 = g \cdot k(\omega) \cdot \tanh k(\omega) \cdot d \quad (3.4)$$

Being g the gravity, and d the depth. A third equation allows then an iterative process to obtain L_w [17]:

$$L_w = \frac{-2 \cdot \pi}{k} \quad (3.5)$$

This iteration process, implemented in the original model by de Sevin, has been optimized and extracted from the optimization loop, being this one of the places

where the computational speed was improved.

3.1.2 Waves shadow calculation

The wave shadow effect is defined as the reduction of the waves' mean height (not so of their wavelength) in the wake of a WEC as a consequence of the energy extraction from the waves [13], similarly to what happens with the wind speed at the wake of a WTG. This reduction of the waves' height and thus of their energy content is negative in terms of further energy exploitation, and therefore it needs to be taken into account when deciding the position of the WECs. The function to calculate this effect is the main contribution of the original model developed by de Sevin, even though a few changes have also been made.

The inputs to the function have been introduced previously: the platforms positions (x and y coordinates) and the discrete values of L_w and θ_{wa} . As an output, a **wave height reduction factor** H_{red} (with values between 0 and 1) is obtained at the position of each WEC, for each wavelength and direction of the waves.

The model is based on the measurements obtained in a test made in Cork, Ireland, in 2015 [23]. A down-scaled version of the WEC was submitted to waves with different wavelengths and heights, and the height reduction was measured in the positions shown in Fig. 3.4:

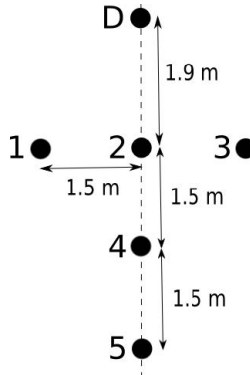


Figure 3.4: Diagram of the test carried out in Cork, Ireland [17].

In de Sevin's model, this height reduction, then converted into the H_{red} fractional factor, is linearly upscaled, extrapolated and fitted in the two dimensions: along the direction of the waves (x), and in the perpendicular direction (y); finding finally the following expression:

$$H_{red}(L, x, y) = 1 + f(L, x) \cdot e^{-\frac{y^2}{D(L)}} \quad (3.6)$$

where:

$$f(L, x) = 1 + \frac{1}{A(L) \cdot x + B(L)} \quad (3.7)$$

The original model was slightly corrected as it was found that a mistake had been made when introducing one of the test's distances. Also, the curve fitting function used was modified in order to increase the computing speed of the calculation.

As a general remark, further concept specific, non-linear hydro-dynamic models should be subject of development in the future, as the upscaling of the measurements means an assumption that may result inaccurate. On the other hand, general models can not be applied in this case, as the behavior of the waves depends directly on the geometry of the specific type of WEC.

3.1.3 Calculation of the AEP from the waves (AEP_{waves})

Once the H_{red} has been obtained for each wavelength, direction and platform position, the significant heights (H_s) from the wave scatter will now be platform dependent, i.e.: the wave resource in each P80 will be different. Therefore, for each platform i , the new H_s is calculated as follows:

$$H_{s,i}(H_s, T_e, \theta_{wa}) = H_{s,waves} \cdot H_{red,i}(T_e, \theta_{wa}) \quad (3.8)$$

Being $H_{s,waves}$, the significant height values of the wave scatter data. It should not be forgotten that T_e and L_{wa} are directly related. Each value of T_e corresponds to a value of L_{wa} , and therefore, even though H_{red} depends on L_{wa} , it can also be expressed as a function of T_e as it is done in Eqn. (3.8).

As the yearly number of hours of occurrence of the three characteristics for each P80 is known, now the wave resource is fully characterized in all the platforms, and thus the energy output in a year (AEP_{waves} , in MWh) can be obtained just by multiplying these time values by the power output corresponding to each H_s and T_e (this information is, of course, stored in the WEC's power output matrix). The described calculation has the following shape:

$$AEP_{waves,gross} = \sum_{i=1}^{n_{plat}} \sum_{H_s} \sum_{T_e} \sum_{\theta_{wa}} t(H_{s,i}, T_{e,i}) \cdot P(H_s, T_e) \quad (3.9)$$

As additional information, this way of calculating the waves energy output has been implemented in this work. In the original model, the efficiency of the WEC depended on the WEC-to-waves size rate, a consideration that was regarded as doubtful

later on in the company. The power output matrix was eventually developed experimentally and therefore it could be integrated in the model in this project, both providing more reliable results and allowing a faster computation.

3.1.3.1 Vanning losses

The energy production obtained in the previous question is not quite the output value of the waves model, as there is one last efficiency that needs to be considered. Two types of waves are generally found in a typical waves climate: the wind and swell waves. The **wind sea** is defined as those waves which are generated by the wind in the area where they are observed or measured, whereas the **swell climate** is the result of the propagation of these waves away from the initial area, the latter being the prominent carrier of energy in the ocean [24].

The two types of waves coexist simultaneously together with the sea tide, and their directions are, in general, different, very much depending on the site where they are observed. Bringing the discussion to the P80, the passive vanning behavior of the platform will align it with an intermediate direction, depending on the amount of energy carried by each one of the two types of waves, as well as that of the tide. In terms of energy output, this phenomenon is translated into a reduction of the exploitable energy of the waves. Figure 3.5 shows the directional efficiency of the WEC when it is not aligned with the incoming waves.

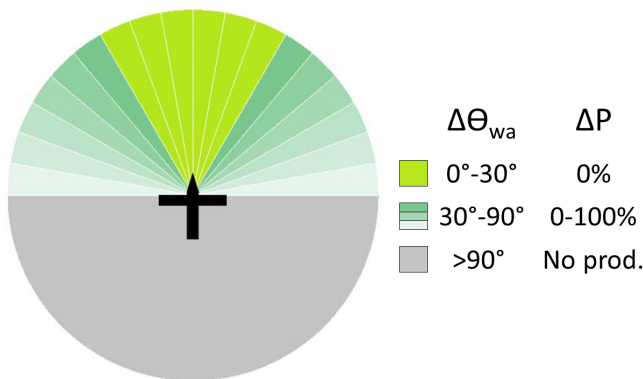


Figure 3.5: Efficiency as a function of vanning misalignment (figure obtained from FPP).

As the waves input data is not detailed enough (it only contains mean probabilistic values), the exact energy output loss cannot be calculated in the model and an assumption needs to be made based on other previously analyzed full sets of data. After consulting with the company, it was concluded that the vanning efficiency generally lays in the range of 85-95%, an energy loss not negligible. In order to remain

in the safe side, a value of an 85% of efficiency was adopted in the model.

The vanning efficiency (eff_{van}) is applied on the gross annual energy production from waves calculated above, obtaining the final AEP_{waves} , the output of the waves model:

$$AEP_{waves} = AEP_{waves, gross} \cdot eff_{van}(\%) \quad (3.10)$$

3.2 Wind energy model

Concurrently with the waves model, the Annual Energy Production from the wind (AEP_{wind}) is calculated in the second part of the model. Its proper calculation is specially relevant since, as it has been mentioned in Section 2.2.3, the energy from the wind represents the biggest share of the electricity generated in the P80. The computing time of the model is kept under 1 second, something very convenient for the optimization loop.

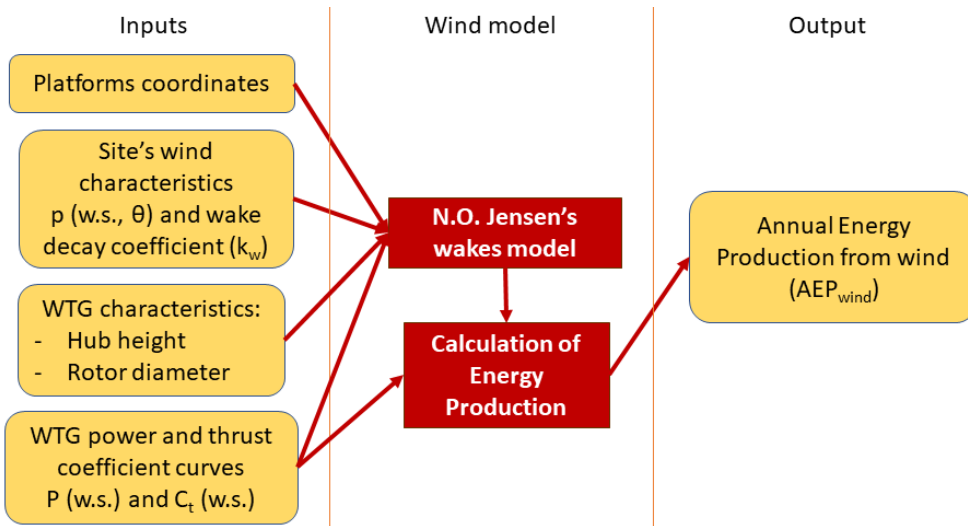


Figure 3.6: Wind model diagram.

3.2.1 Data inputs

As it is depicted in Fig. 3.6, the inputs to the model are the WTG's coordinates (platform's coordinates), the site's characteristics (in this case, only the wind resource is relevant), and the WTG specifications, which include the power curve, thrust coefficient curve, hub height and rotor diameter.

The **power** ($P(w.s.)$) and **thrust coefficient** ($C_T(w.s.)$) **curves** provide information about the power produced and the thrust forces experimented by a WTG as a function of the wind speed (w.s.), the latter being due to the pressure difference between the front and the back of the rotor. As an example, Fig. 3.7 shows these two curves for a simulated 8 MW WTG being developed currently in the company [25].

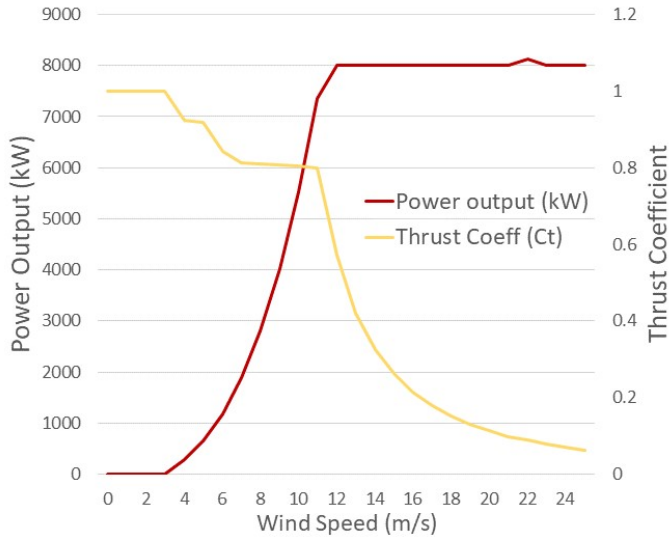


Figure 3.7: Power and thrust coefficient curves of the WTG being modeled between FPP and DTU (graph based on [25]).

The 8 MW maximum values of the power curve determines the capacity of the WTG. Also, cut-in and cut-out wind speeds of 4 and 25 m/s can be observed: these magnitudes represent respectively the minimum profitable w.s. and the maximum working w.s. in which the safety is secured.

		Wind direction (°)															
		0	10	20	30	40	50	60	70	80	90	100	110	120	130	140	150
Wind speed (m/s)	0	0	0	0	0	0	0	0	0	0	0	0	0	0	0	0	0
	1	0.000645	0.000645	0.000649	0.000649	0.000649	0.000646	0.000646	0.000646	0.000652	0.000652	0.000652	0.000673	0.000673	0.000556	0.000556	0.000556
	2	0.001151	0.001151	0.001103	0.001103	0.001103	0.001103	0.001103	0.001103	0.001103	0.001103	0.001103	0.001167	0.001167	0.001167	0.001144	0.001144
	3	0.001544	0.001544	0.001423	0.001423	0.001423	0.001423	0.001423	0.001423	0.001423	0.001423	0.001423	0.001423	0.001423	0.001423	0.001423	0.001423
	4	0.001817	0.001817	0.001612	0.001612	0.001612	0.001612	0.001612	0.001612	0.001612	0.001612	0.001612	0.001612	0.001612	0.001612	0.001612	0.001612
	5	0.001969	0.001969	0.001679	0.001679	0.001679	0.001679	0.001679	0.001679	0.001679	0.001679	0.001679	0.001679	0.001679	0.001679	0.001679	0.001679
	6	0.002008	0.002008	0.001644	0.001644	0.001644	0.001644	0.001644	0.001644	0.001644	0.001644	0.001644	0.001644	0.001644	0.001644	0.001644	0.001644
	7	0.00195	0.00195	0.00153	0.00153	0.00153	0.00153	0.00153	0.00153	0.00153	0.00153	0.00153	0.00153	0.00153	0.00153	0.00153	0.00153
	8	0.001816	0.001816	0.001362	0.001362	0.001362	0.001362	0.001362	0.001362	0.001362	0.001362	0.001362	0.001362	0.001362	0.001362	0.001362	0.001362
	9	0.001631	0.001631	0.001167	0.001167	0.001167	0.001167	0.001167	0.001167	0.001167	0.001167	0.001167	0.001167	0.001167	0.001167	0.001167	0.001167
	10	0.001415	0.001415	0.000964	0.000964	0.000964	0.000964	0.000964	0.000964	0.000964	0.000964	0.000964	0.000964	0.000964	0.000964	0.000964	0.000964
	11	0.001191	0.001191	0.00077	0.00077	0.00077	0.00077	0.00077	0.00077	0.00077	0.00077	0.00077	0.00077	0.00077	0.00077	0.00077	0.00077
	12	0.000973	0.000973	0.000596	0.000596	0.000596	0.000596	0.000596	0.000596	0.000596	0.000596	0.000596	0.000596	0.000596	0.000596	0.000596	0.000596
	13	0.000772	0.000772	0.000448	0.000448	0.000448	0.000448	0.000448	0.000448	0.000448	0.000448	0.000448	0.000448	0.000448	0.000448	0.000448	0.000448
	14	0.000597	0.000597	0.000327	0.000327	0.000327	0.000327	0.000327	0.000327	0.000327	0.000327	0.000327	0.000327	0.000327	0.000327	0.000327	0.000327
	15	0.000449	0.000449	0.000232	0.000232	0.000232	0.000232	0.000232	0.000232	0.000232	0.000232	0.000232	0.000232	0.000232	0.000232	0.000232	0.000232
	16	0.00033	0.00033	0.00016	0.00016	0.00016	0.00016	0.00016	0.00016	0.00016	0.00016	0.00016	0.00016	0.00016	0.00016	0.00016	0.00016
	17	0.000236	0.000236	0.000108	0.000108	0.000108	0.000108	0.000108	0.000108	0.000108	0.000108	0.000108	0.000108	0.000108	0.000108	0.000108	0.000108
	18	0.000165	0.000165	7.06E-05	7.06E-05	7.06E-05	7.06E-05	4.41E-05	4.41E-05	4.41E-05	4.41E-05	6.92E-05	6.92E-05	6.92E-05	0.000187	0.000187	0.000187
	19	0.000113	0.000113	4.51E-05	4.51E-05	4.51E-05	4.51E-05	2.8E-05	2.8E-05	2.8E-05	2.8E-05	2.8E-05	4.59E-05	4.59E-05	4.59E-05	0.000131	0.000131
	20	7.51E-05	7.51E-05	2.81E-05	2.81E-05	2.81E-05	1.74E-05	1.74E-05	1.74E-05	1.74E-05	2.99E-05	2.99E-05	2.99E-05	9.02E-05	9.02E-05	9.02E-05	0.000226

Figure 3.8: Extract of a probabilistic wind resource matrix with wind speeds from 0 to 20 m/s and wind directions from 0 to 150°.

Regarding the **wind resource**, similarly to the waves scattered matrices, the input to the model consists of a matrix that provides the probability of occurrence of every wind speed and direction $p(w.s., \theta_{wi})$ at a certain height, the only two parameters needed to obtain the energy content of the wind in the model. An example of such matrix is shown in Fig. 3.8. This information is usually not found in this shape, but rather in regional Generalized Wind Climates (GWC) or time series. In Section 4.2.2 it is explained in detail how the wind resource was obtained and processed for its use in the case study.

An assumption is being made with regards to the wind resource. As the P80 concept is generally meant to be used at seabeds deeper than those suitable for bottom-fixed concepts, it is assumed that the location of any site in the model is far offshore enough for the wind climate to be considered identical at every point in the site. After consulting with experts in Risø it was found that, as a rule of thumb, this assumption can be made from distances to shore 100 times the height of the WTG, i.e.: 10 km for a hub height of 100 m.

Therefore, just a single matrix of information is needed for the whole farm site, assuming all the probabilistic values of wind speeds and directions identical for every position. This means an important advantage, since otherwise, as it is generally done in onshore and near-shore wind farms, the regional GWC would need to be transformed into a localized wind climate at each point, being influenced by the different land elevations, obstacles, roughness lengths and atmospheric conditions [26]. This would either complicate the coding significantly and increase the running time or it would make necessary the use of external tools.

3.2.2 Wind wakes calculation

In comparison to the wave energy sector, both the research and the industry scenes of the wind energy field are much more developed, and therefore there are more calculation tools available in the market. Focusing on the calculation of the Annual Energy Production of wind farms, WAsP [27] (developed and supported in DTU) is the reference software nowadays. In an early stage of the project, the possibility of linking WAsP to the model was considered in order to carry out the wind related calculations. However, this was soon discarded given the different coding language embedded in the software, and the incompatibility of this option with running fast enough optimization loops.

Alternately, it was possible to get access and make use of two MATLAB codes: the code developed by de Sevin [17] together with his waves model, and a function developed by A. Peña in the Wind Energy department of DTU in Risø, Denmark [28]. In a similar way as the waves shadow function does, these codes calculate the wind speed reduction behind a WTG due to its wake. They are both based on the so-called

PARK calculation developed by N.O. Jensen, which uses momentum deficit theory to predict the flow field, assuming a linear expansion of the wake behind the rotor [29].

De Sevin's and Peña's models were compared with the results obtained after carrying out identical calculations in WASP, which also makes use of the same theory. Considering these results as a reference, different arrangements with different numbers of platforms, positions and wind resources were tried, obtaining significantly smaller errors in the wake losses calculation (and therefore in the AEP_{wind} calculation) in Peña's model. Given the results shown in Table 3.1, Model 2 (Peña's) was considered as a reliable model that could be used with guarantees in the study.

	Net AEP wind		Wake Losses	
	Model 1	Model 2	Model 1	Model 2
Case 1	1.53%	0.75%	17.56%	8.17%
Case 2	0.14%	0.16%	3.33%	5.33%
Case 3	1.59%	0.86%	18.95%	9.47%
Case 4	1.23%	0.70%	15.58%	8.44%
Case 5	0.33%	0.08%	5.35%	0.15%
Maximum	1.59%	0.86%	18.95%	9.47%
Minimum	0.14%	0.08%	3.33%	0.15%
Average	0.67%	0.35%	9.84%	3.49%

Table 3.1: Error of wakes models with respect to calculation in WASP in five different scenarios (Model 1: de Sevin's; Model 2: Peña's).

As it has already been advanced, the wake losses are translated into a reduced speed (V) at a distance (X) behind the WTG, which depends on the free stream speed (U), the WTG's diameter (D), the thrust coefficient (C_T), and the wake decay coefficient (k). The reduced wind speed is then calculated as follows [29]:

$$V = U \cdot \left[1 - \left(1 - \sqrt{1 - C_T} \right) \left(\frac{D}{D + 2 \cdot k \cdot X} \right)^2 \right] \quad (3.11)$$

A scheme with all the variables is shown in Fig. 3.9. The only non-straightforward parameter involved in the calculation is the wake decay coefficient (k), which determines both the downstream reduction and also the wake's opening angle. In principle, this value is determined by semi-empirical means with the following expression [29]:

$$k = \frac{A}{\ln(h/z_0)} \quad (3.12)$$

Where $A \approx 0.5$ is a constant, h is the hub height and z_0 is the roughness length, which, in the offshore cases, would be very close to zero. However, according to the

literature, the wake decay coefficient can be simply approximated to a general value of $k = 0.05$ in offshore wind farms [28], and so it was done in the model.

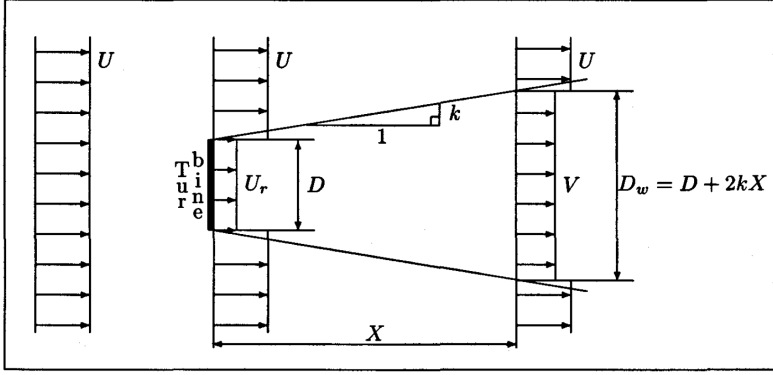


Figure 3.9: Wind speed in the wake of a WTG and parameters involved [29].

A couple of general remarks about the wakes model shall be made: some modifications were done so the particular energy output from each WTG can now also be found, information that can be useful so as to find the efficiencies of the different WTGs, or even to eventually particularize electrical transmission losses at each platform's export cable; most importantly, it was found that in order to get results with enough accuracy, the probabilistic input matrix should provide directional information at least every 10° . Otherwise, directional empty areas may result in hidden WTGs for the model, meaning wake losses calculation errors.

3.2.3 Calculation of the AEP from the wind (AEP_{wind})

Once the reduced wind speed $w.s.red$ has been obtained at every WTG for every $w.s.$ and θ_{wi} according to the relative positions of all the platforms, the energy output (AEP_{wind}) is calculated by multiplying these wind speeds with the WTG's power curve, the probability matrix and the number of hours in a year:

$$AEP_{wind} = \sum_{i=1}^{n_{plat}} \sum_{w.s.} \sum_{\theta_{wi}} w.s.red, i \cdot P(w.s.) \cdot t(w.s., \theta_{wi}) \quad (3.13)$$

In this case, no other efficiencies are involved in the wind energy output alone. However, as it is explained in the next section, further energy losses due to downtime periods and electrical transmission are applied to the final merged energy output which, at this point, after the wakes and shadow effect ($AEP_{gross} = AEP_{after\ wakes}$), is simply calculated as follows:

$$AEP_{gross} = AEP_{after\ wakes} = AEP_{wind} + AEP_{waves} \quad (3.14)$$

3.3 Costs model

The costs model is the last module inside the tool's optimization loop and, as its name indicates, all the costs involved in the farm project (from before the start until the end of its lifetime) are calculated by it: the ones due to the capital expenses (CAPEX), those derived from the operational expenditures (OPEX) and the costs associated to the inevitable energy losses due to the generators' downtime periods and transmission of the electricity. The costs model also continues the energy flow: the gross power generation has been calculated in the wind and wave models alongside with their respective wakes and shadow losses, and now these energy inputs see individual yearly decrements due to the mentioned downtime and transmission losses as illustrated in Fig. 3.10.

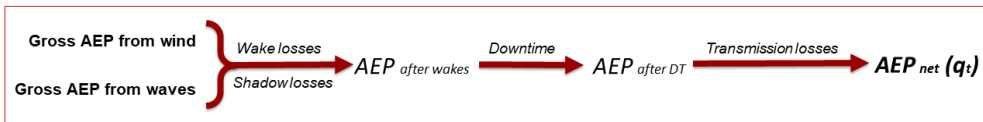


Figure 3.10: Energy flow along the model.

The inputs to the costs model are, on the one hand, the gross AEP from wind and waves after the wakes and shadow losses (constant along the years at this point); and on the other, the values relative to the site characterization (its bathymetry and coordinates, and the inland substation, harbor and shore positions), and more than 140 costs related figures, many of which have been obtained directly from FPP and compared with existent models from external literature (the values used in the model are depicted in Appendix A). The output is no other than the Levelized Cost of Energy (LCOE), arguably the most useful indicator for seeking financing, as it represents the average lifetime cost in the lifetime of a project, and it is ideal to compare the costs of different technologies [30, 31].

3.3.1 LCOE

The *LCOE*, expressed in €/MWh, indicates the average cost of the energy produced along the lifetime of a project, and therefore, the minimum average price at which the energy should be sold in order for the project to be profitable [32]. Unlike other more simple indicators, the *LCOE* takes into account the time value of money, as it weights the annual expenses TC_t in each year t by means of a discount rate r , which is determined by the investors according to the inflation and the estimated risk of the project. The *LCOE* is calculated in the model as follows:

$$LCOE = \frac{\sum_{t=0}^{LT} \frac{TC_t}{(1+r)^t}}{\sum_{i=0}^{LT} \frac{q_t}{(1+r)^t}} \quad (3.15)$$

Where q_t represents the yearly energy production in period t , and LT the lifetime of the project. As a clarification, the discount rate is a purely economic factor and the apparent discounting of the energy production in Eqn. (3.15) is just a result of algebraic rearrangement.

Even though some sources include further costs, neither taxes nor any other socio-economic factors have been considered in this study for being often subjective or highly dependent on the country or area. Therefore, it was concluded that including these terms would only increase the uncertainty of the results. The calculation methodology of the costs (sorted into CAPEX and OPEX) and energy transformations are exposed below.

3.3.2 CAPEX

The capital expenditures of a project involve all the investment, administrative, acquisition and installation costs that make the project possible, before and along the project's lifetime. With regards to this model, almost all the costs are considered to be executed in the year immediately before the start of the project (i.e.: year 0). The exception is the so-called decommissioning cost, executed in the last year of the project, and which is often regarded as an independent expenditure (DECEX). However, as its influence in the final LCOE value is very small (specially after discounting it), this expenditure has been calculated as a part of the CAPEX in this study.

The CAPEX categories considered in the model are the following: design and project management expenses (C_{PM}), wind turbine costs (C_{WTG}), P80 costs (C_{P80}), mooring costs (C_{Moor}), costs associated to the electrical infrastructure (C_{EI}), installation costs (C_{Inst}) and decommissioning costs (C_{Decom}); all of them expressed in €. The installation costs associated to each one of these categories are calculated separately. The simple CAPEX calculation is shown below, i being the year of the expenditure:

$$CAPEX_i = C_{PM,i} + C_{WTG,i} + C_{P80,i} + C_{Moor,i} + C_{EI,i} + C_{Inst,i} + C_{Decom,i} \quad (3.16)$$

Below, the calculation of the different introduced costs categories is explained.

3.3.2.1 Design and project management

This expenditure includes all the administrative, design, engineering and project management related costs and also all the expenses originated from the site specific analyses and studies that are needed before the start of the project: these analyses have to

do with resource data acquisition, the environment, the parts involved/ affected by the project and so on [33, 34]. The design and project management costs are applied in year zero and they are divided into **concession** ($C_{concession}$) and **design** (C_{design}) costs:

$$C_{PM} = C_{concession} + C_{design} \quad (3.17)$$

where:

$C_{concession}$ [€] : costs relative to the Environmental Impact Assessment (EIA), site analyses (bathymetry measurements, meteorological mast, wind monitoring), surveys, site-specific design engineering, administrative fees, grid analyses and consent application.

C_{design} [€] : FPP's total margin.

The two new categories are calculated in the model as follows:

$$C_{concession} = C_{con.,cap} \cdot Cap_{Tot} \quad (3.18)$$

$$C_{design} = Margin \cdot (C_{P80} + C_{transp} + C_{ass}) \quad (3.19)$$

with:

$C_{con.,cap}$ [€/MW] : estimation of concession costs per capacity unit.

Cap_{Tot} [MW] : total capacity of the farm.

$Margin$ [%] : FPP's margin as a percentage of investment costs.

C_{P80} [€] : acquisition cost of the P80.

C_{transp} [€] : cost of components' transportation to assembly site.

C_{ass} [€] : P80 assembly costs.

3.3.2.2 Wind turbines

The acquisition cost of the wind turbines (C_{WTG} , in €) is one of the most relevant expenditures in the lifetime of the project. Naturally, this is a pure investment cost and it is therefore applied in year 0. In the present study, as in most works of the kind, it is calculated as a linear function of the wind turbine capacity. Since it is linear, for the whole farm, the cost is found by multiplying the total capacity of the WTGs of the farm (Cap_{wind} , in MW) by a considered cost per capacity ($C_{WTcap.}$, in €/MW):

$$C_{WTG} = C_{WTcap.} \cdot Cap_{WT} \quad (3.20)$$

As a reminder, the figure of the cost per capacity used in the model and the logic behind it can be found in Appendix A.2.

3.3.2.3 P80

The acquisition costs involved in the P80 platform and WEC (C_{P80} , in €) are numerous and very diverse. However, they are modeled in a very simple way, and, as most of the CAPEX, they are also applied in year 0 of the project. The costs figures are obtained from FPP:

$$C_{P80} = C_{plat} \cdot n_{plat} + C_{site} \quad (3.21)$$

As it can be inferred from Eqn. (3.21), some of them are unit dependent (C_{plat} , in €/P80) and therefore, they are multiplied by the number of platforms (n_{plat}). These include the acquisition costs of the **platform** (hull fabrication, corrosion protection and marine systems outfitting), the **absorbers** (fabrication, hull bearing, locking and control systems), the **PTO** (hydraulic and control systems, connection rod and yoke), the **power system**, and some **data acquisition** related costs.

On the other hand, there are other costs that are considered constant, so they do not depend on the size of the farm (C_{site} , in €). These are the costs associated to condition monitoring and SCADA system.

3.3.2.4 Mooring system

The mooring costs (C_{Moor} , in €), also obtained from the company, are divided into the **anchor acquisition costs**, which include the six anchor kits needed in each P80 unit; and the **mooring line costs** that are considered to increase linearly with the depth. Again, this cost is applied in year 0:

$$C_{Moor} = \sum_{i=1}^{n_{plat}} C_{anch.} + C_{lines} \cdot \frac{l}{d} \cdot d_i \quad (3.22)$$

having:

- $C_{anch.}$ [€/P80] : fixed cost of a platform's mooring system (anchors, shackles, buoyancy elements, etc.).
- C_{lines} [€/m] : length dependent cost of the mooring lines (which includes both the chains and polyester lines costs, depicted in Fig. 2.8).
- l/d : linear rate of mooring lines length per seafloor depth.
- d_i [m] : depth under platform i .

In reality, attending to site dependent physical conditions (like natural frequencies originated from the wind and the waves, or the seabed characteristics), the length of the mooring line would not necessarily increase linearly with the depth. Instead, its buoyancy, horizontal length, and the length and size of its elements would be designed according to these site specific parameters. However, as this is clearly off the scope of the present study, and after consulting with experts in the company, a linear growth

has been assumed in this case, making use of an existent design of a 100 m depth as the base case.

3.3.2.5 Electrical infrastructure

The investment costs associated to the electrical infrastructure (EI) are an intricate aspect to model as, on the one hand, there is not much information available on the prices of certain key components, and on the other, depending on the country and even on the year of commissioning, the state may assume all the costs, part of them, or the developer might have to take charge of the whole investment.

For this reason and since it represents an expense of the project, independently of who takes responsibility for it, the costs associated to the electrical infrastructure (C_{EI} , in €), are included in the LCOE calculation, although it could be argued that the inland infrastructure costs (underground bedding or overhead lines) are not included. The reason is that they were considered way too uncertain and completely site dependent.

The expenses involved are the following: acquisition costs of **inter-array cables** (C_{MV}), offshore and onshore **export cable** (C_{HV}), **offshore substation** (C_{sub}), and **other costs** ($C_{el.other}$), which include those associated to devices like reactive power dynamic compensators, connector sets and so on [35, 36]. All of them are expressed in €.

$$C_{EI} = C_{MV} + C_{HV} + C_{sub} + C_{el.other} \quad (3.23)$$

Regarding the inter-array and export cables, both of their costs are modeled as a linear function of their length, having been the latter considered identical in its onshore and offshore stretch, so both distances are considered in the calculation. In the case of the inter-array cables, they are modeled as independent cables that connect each platform with the offshore substation, since this is the preferred disposition in the company at the moment given the quite dynamic characteristics of the concept.

$$C_{MV} = \sum_{i=1}^{n_{plat}} l_{MV,i} \cdot C_{dyn.cab.} \quad (3.24)$$

$$C_{HV} = C_{HV,length} \cdot (l_{HV,off} + l_{HV,on.}) \quad (3.25)$$

with:

- $l_{MV,i}$ [km] : length of the inter-array cable of each platform.
- $C_{dyn.cab.}$ [€/km] : acquisition cost per length of the inter-array MV dynamic cables (described in Section 2.2.4).
- $C_{HV,length}$ [€/km] : acquisition cost per length of the export HV cable.

$l_{HV,off}$ [km] : length of subsea HV export cable (distance from offshore substation to shore).

$l_{HB,on}$ [km] : length of inland HV export cable (distance from shore to onshore substation).

The offshore substation is one of the project's cost components that was found to be more difficult to obtain costs information for, not to talk about intending to find data for all the devices involved in it. After some research was made, it was decided to use the method proposed by Gonzalez-Rodriguez [33], as it uses costs data from several existent projects as a reference. Exceptionally, as in this case its acquisition expense includes the mooring costs, they are not taken into account in their pertinent section.

$$C_{sub.} = 539,000 \cdot Cap_{Tot}^{0.687} \quad (3.26)$$

Being Cap_{Tot} , in MW, the total capacity of the farm (including both the wind and waves capacity). Finally, a platform dependent value ($C_{el.other plat.}$, €/P80), obtained from FPP, was used to calculate the costs of the additional equipment introduced above:

$$C_{el.other} = C_{el.other plat.} \cdot n_{plat} \quad (3.27)$$

3.3.2.6 Installation costs

After the acquisition costs, depicted in the previous sections, the installation costs are calculated. They are those expenses associated to both the human workforce and the technology used in the transportation, assembly, connection and testing of all the infrastructure involved in the construction of the project before it has started. Any other operation on the infrastructure during the lifetime of the project is considered as part of the operational expenses (OPEX), presented later in this chapter.

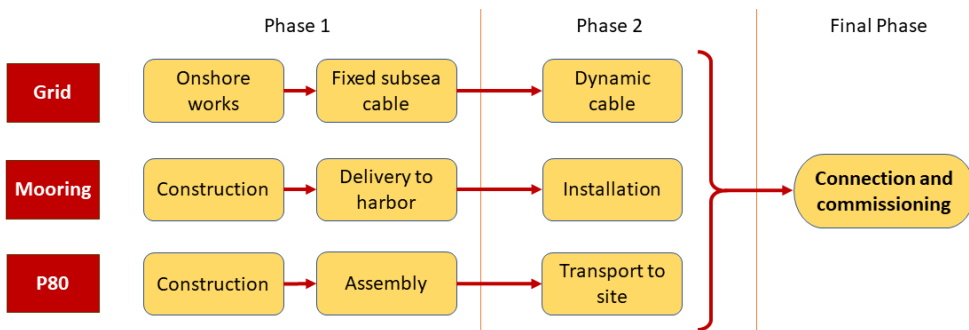


Figure 3.11: Flowchart of the installation process (based on information from FPP).

An approximate flowchart of the installation process considered most optimal in the company can be seen in Figure 3.11. The different processes depicted in the flowchart divide the expenses into: the **cost of transportation** of the components to the assembly site ($C_{transp.}$), **assembly costs** ($C_{ass.}$), **mooring installation costs** ($C_{inst. moor.}$), costs of **installation of the EI** ($C_{inst. elec.}$), costs of on-site **platforms installation** ($C_{inst. P80}$), and **commissioning or connection costs** ($C_{connec.}$).

$$C_{Inst.} = C_{transp.} + C_{ass.} + C_{inst. moor.} + C_{inst. elec.} + C_{inst. P80} + C_{connec.} \quad (3.28)$$

As it was advanced in Chapter 2, one of the advantages of the P80 is the possibility of assembling it in the harbor and afterwards towing the whole structure to the site, thus avoiding the costly offshore assembly process, but of course, still involving some assembly and component transportation related costs. The latter component is modeled as a percentage of the acquisition costs of the devices involved (WTG, P80, EI and mooring system), this being an estimation made by FPP:

$$C_{transp.} = 10\% \cdot (C_{WTG} + C_{P80} + C_{E.I.} + C_{Moor}) \quad (3.29)$$

As for the assembly costs, that of a single P80 ($C_{ass. P80}$, in €/platform) is defined by the company taking into account all the devices involved in the process, and the personnel and infrastructure needed for it:

$$C_{ass.} = C_{ass. P80} \cdot n_{plat} \quad (3.30)$$

Moving on to the installation processes that take place on-site, the mooring systems of all the platforms and the substation are installed before the rest of the infrastructure is transported to the site, and as it was also mentioned before, its attachable end is left floating underwater at a desired depth:

$$C_{inst. moor} = C_{inst. anch.} \cdot (n_{plat} + 1) \quad (3.31)$$

Being $C_{inst. anch.}$, in €/P80, the anchors installation cost per platform and substation. It is assumed that the mooring costs of the substation and the platforms are identical, which probably means overestimating the ones relative to the substation, remaining this way in the safe side, as the loads on the floating substation are quite smaller.

The installation of the EI ($C_{inst. elec}$, in €) is divided in four different processes: on the one hand, the offshore HV export cable ($C_{inst. HV}$), the MV inter-array cables ($C_{inst. MV}$) and the onshore export cables ($C_{inst. HV, on.}$) are installed in different operations, and on the other, the substation is considered to be installed as if it was just one more platform, just towing it from the harbor, and this is therefore modeled later on.

$$C_{inst. elec} = C_{inst. MV} + C_{inst. HV} + C_{inst. HV, on}. \quad (3.32)$$

Being the three components calculated as follows:

$$C_{inst. MV} = C_{inst. dy. cab.} \cdot n_{plat} \quad (3.33)$$

$$C_{inst. HV} = C_{inst. HV fix.} + C_{c.l. vessel} \cdot \left(\frac{l_{HV}}{s_{c.l.}} + \frac{d_{harb}}{s_{ret. c.l.}} \cdot 24^{-1} \right) \quad (3.34)$$

$$C_{inst. HV, on} = C_{HV on.} \cdot inst_{rate} \quad (3.35)$$

with:

- $C_{inst. dy. cab.}$ [€/P80] : inter array cables installation cost per platform (data from FPP).
- $C_{inst. HV fix.}$ [€] : cable laying vessel and team mobilization cost and other fixed costs.
- $C_{c.l. vessel}$ [€/day] : daily cost of cable laying vessel and team.
- l_{HV} [km] : HV subsea export cable length.
- $s_{c.l.}$ [km/h] : cable laying speed.
- $s_{ret. c.l.}$ [km/h] : cruise speed of cable laying vessel.
- $inst_{rate}$ [%] : estimated costs of installation of the onshore EI as a percentage of the acquisition costs (again, this figure is hard to model as there is very little information about this type of cost).

Finally, once the fixed part of the installation is prepared, the platforms and the substation are ready to be towed to the site and prepared to operate. Below, the calculation of the costs of both processes is shown:

$$C_{inst. P80} = (n_{plat} + 1) \cdot \left[C_{inst. P80 fix} + C_{tow vess.} \cdot \left(\frac{d_{harbor}}{s_{tow}} + \frac{d_{harb}}{s_{ret. t.v.}} \right) \cdot 24^{-1} \right] \quad (3.36)$$

$$C_{connec.} = C_{con. P80} \cdot n_{plat} \quad (3.37)$$

having:

- $C_{inst. P80 fix}$ [€/P80] : costs per P80 of towing team, vessel, equipment, etc.
- $C_{tow vess.}$ [€/day] : towing vessel cost per day.
- s_{tow} [km/h] : towing speed of P80 and offshore substation.
- $s_{ret. t.v.}$ [km/h] : return speed of towing vessel.
- $C_{con. P80}$ [€/P80] : testing and commissioning costs per P80 (from FPP).

3.3.2.7 Decommissioning

In the last place with regards to the CAPEX, the decommissioning costs are obtained. It is worth reminding once again that these costs are applied in the last year of the lifetime of the project, and therefore, due to the presence of the discount rate, their influence is quite low in the LCOE value.

Now all the devices and infrastructure installed in the project need to be removed. Therefore, the categories of decommissioning costs are the **EI** ($C_{d.grid}$), the **platforms** ($C_{d.P80}$), the **mooring system** ($C_{d.moor.}$) and the **paperwork** involved in the process ($C_{d.other}$). All of them, once again, expressed in €.

$$C_{Decom} = C_{d.grid} + C_{d.P80} + C_{d.moor.} + C_{d.other} \quad (3.38)$$

In the same way as it was done with the installation costs, the offshore substation towing process is calculated as if it was one more platform. Therefore, the EI decommissioning costs can be modeled by separating that due to the MV inter-array cables ($C_{d.grid MV}$) and the one associated to the removal of the HV export cable ($C_{d.grid HV}$):

$$C_{d.grid} = C_{d.grid MV} + C_{d.grid HV} \quad (3.39)$$

$$C_{d.grid MV} = C_{d.g.mob.} + C_{d.g.day} \cdot \left[\left(\frac{l_{MV}}{s_{cab.rem.}} + 2 \cdot \frac{d_{harb}}{s_{ret.}} \right) \cdot 24^{-1} \right] \quad (3.40)$$

$$C_{d.grid HV} = C_{d.g.mob.} + C_{d.g.day} \cdot \left[\left(\frac{l_{HB}}{s_{cab.rem.}} + \frac{d_{harb}}{s_{ret.}} \right) \cdot 24^{-1} \right] \quad (3.41)$$

being:

- $C_{d.g.mob.}$ [€] : mobilization costs of cable removal vessel and team.
- $C_{d.g.day}$ [€/day] : daily cost of cable removal vessel and team.
- l_{MV} [km] : total length of inter array cables.
- $s_{cab.rem.}$ [km/h] : cable removal speed of the vessel.
- d_{harb} [km] : distance from site to harbor.
- $s_{ret.}$ [km/h] : cruise speed of the cable removal vessel.
- l_{HV} [km] : length of subsea HV export cable.

It is assumed that the huge amounts of decommissioned steel and other materials from the platforms is collected by external companies for which these are valuable, and therefore, for the sake of this model, the direct decommissioning costs associated to the P80s and offshore substation ($C_{d.P80}$, in €) are just the expenditure of towing them back to harbor, which is calculated as follows:

$$C_{d.P80} = C_{d.P80\text{mob}} + (n_{\text{plat}} + 1) \cdot C_{d.P80\text{day}} \cdot \left[\left(\frac{d_{\text{harb}}}{s_{\text{tow.ret.}}} + \frac{d_{\text{harb}}}{s_{\text{tow}}} \right) \cdot 24^{-1} \right] \quad (3.42)$$

with:

$C_{d.P80\text{mob}}$ [€] : mobilization cost of towing vessel and operations team.

$C_{d.P80\text{day}}$ [€/day] : daily cost of towing vessel and team.

$s_{\text{tow.ret.}}$ [km/h] : cruise speed of towing vessel.

s_{tow} [km/h] : tug speed of towing vessel.

Similarly as in their installation process, the cost of decommissioning the mooring systems of both the platforms and offshore substation is calculated by means of a cost per platform ($C_{r.anch.}$, in €/P80) derived from removing the anchors and turret in each of them:

$$C_{d.moor.} = (n_{\text{plat}} + 1) \cdot C_{r.anch.} \quad (3.43)$$

The last expenditure with regards to the decommissioning process is that derived from surveys, reports and the bureaucracy that comes with it, being estimated by FPP a cost per platform ($C_{r.surv.}$ in €/P80):

$$C_{d.other} = n_{\text{plat}} \cdot C_{r.surv.} \quad (3.44)$$

3.3.3 OPEX

The Operational Expenditures (OPEX) include the costs associated to all types of maintenance and any other operation along the lifetime of a project (e.g.: inspections, checks, testing, cleaning, painting, replacement of components, etc.), being often divided into planned and unplanned or unscheduled O&M [37]. These maintenance operations have an associated energy generation downtime, as they often involve a failure or require shutting down the generators. The generation downtime is thus modeled together with the O&M costs as part of the OPEX.

As it has been done when modeling the CAPEX, and more relevantly in this case due to its distribution along the years, the annual costs associated to the OPEX are calculated individually every year, so they can be discounted in the LCOE calculation as explained above. Thus, in the broadest level, for each year i in the project's lifetime, the maintenance operations ($O\&M_i$, in €) and their associated downtime (DT_i , in hours) are calculated as follows:

$$O\&M_i = O\&M_{\text{planned},i} + O\&M_{\text{unplanned},i} \quad (3.45)$$

$$DT_i = DT_{\text{planned},i} + DT_{\text{unplanned},i} \quad (3.46)$$

Initially, it was considered to carry out an O&M strategy optimization, however the uncertainty associated to the components' failure rates, their dependence on the climate, and the lack of information regarding the interaction between the different devices involved in the technology, made the optimization attempt too unreliable. For this reason, estimations from FPP were regarded as the best option for the present study, even though these operational strategies have never actually been carried out before. The strategy is based on experience with similar structures in the offshore wind energy and O&G sectors, and it considers the materials and devices used in the concept and their behavior under typical offshore conditions.

Planned O&M and Downtime

Three types of planned operations are defined in FPP's maintenance strategy, each of which presents a specific estimated cost and downtime. They are the following:

- An **annual operation** that involves inspections of the platform's corrosion, the WTG and the WEC, as well as maintenance of the ballast, electrical and cooling systems.
- An **intermediate survey** every 3-4 years, which consists in a further analysis of some elements like the mooring lines and the EI.
- And a **major inspection** every 7 years that involves towing the platform to the harbor for an exhaustive onshore examination and the replacement of a number of internal components.

Currently, it is considered that the major operations could be potentially avoidable, as it is not clear whether the full process of towing the platforms to land will be strictly necessary or not. For this reason, its impact in the LCOE is analyzed in the sensitivity analysis further in the report (Section 5.1).

For each year i in the project's lifetime, the planned O&M and its associated downtime periods are expressed as follows:

$$O\&M_{planned,i} = C_{O\&M\ site} + n_{plat} \cdot C_{O\&M\ P80,i} \quad (3.47)$$

$$DT_{planned,i} = t_{O\&M,i} \quad (3.48)$$

being:

$C_{O\&M\ site}$ [€/year]	: the fixed yearly O&M cost: port charges, warehouse, fixed costs of vessels and personnel...
$C_{O\&M\ P80,i}$ [€/P80/year]	: the O&M cost per platform in year i , which may include costs of yearly, intermediate and/or major operations, depending on the year.
$t_{O\&M,i}$ [h/year]	: hours of downtime in year i , which may include those due to yearly, intermediate and/or major operations, depending on the year.

Unplanned O&M and Downtime

In the case of the operations due to unexpected or sudden breakdowns, the costs and their associated downtimes are implemented by sorting the failures into five different severity levels: **remote reset**, **minor fault/ inspection**, **medium fault** (module replacement), **large fault** (offshore repair), and **major fault** (harbor repair). Each one of these categories presents a certain occurrence probability that is translated in the model as a number of incidents per year.

The yearly unplanned O&M costs and downtime are thus implemented in the model as shown in Equations (3.49) and (3.50):

$$O\&M_{unplanned} = \sum_{i=1}^5 \left\{ n_{plat} \cdot f_{fail,i} \cdot \left[C_{fixed,i} + C_{h,i} \cdot \left(t_{rep,i} + \frac{d_{harb}}{s_{go,i}} + \frac{d_{harb}}{s_{ret.,i}} \right) \right] \right\} \quad (3.49)$$

$$DT_{unplanned} = \sum_{i=1}^5 \left[f_{fail,i} \cdot \left(t_{rep,i} + \frac{d_{harb}}{s_{go,i}} \right) \right] \quad (3.50)$$

with:

- $f_{fail,i}$: estimated number for failures per year for failure type i .
- $C_{fixed,i}$ [€/P80] : fixed repair cost per failure for failure type i (mobilization costs, etc.).
- $C_{h,i}$ [€/h/P80] : time dependent cost for failure type i (it includes personnel, vessel costs, etc.).
- $t_{rep,i}$ [h] : repair time for failure type i .
- d_{harb} [km] : average distance to harbor.
- $s_{go,i}$ [km/h] : going speed of the vessel used in failure type i .
- $s_{ret.,i}$ [km/h] : return speed of the vessel used in failure type i (it involves towing the platform in the case a major fault).

Two assumptions were made regarding the downtime: it is considered that the O&M affects the energy production of the whole P80, and not only the individual wind or waves energy production, as many operations may need a full shut down of the platform for control or safety related reasons, giving it, this way, a conservative approach; on top of this, the downtime is modeled as a number of hours that represents a fraction of an entire year, being this figure multiplied by the gross energy generation of the farm (after wakes and waves shadow losses) to obtain the total energy loss, instead of particularizing the energy output of each platform. The AEP after wake losses and downtime is then the following:

$$AEP_{after\ DT,i} = AEP_{gross} - \left(AEP_{gross} \cdot \frac{DT_i}{8760} \right) \quad (3.51)$$

where AEP_{gross} , in MWh, is the energy output in a year after deducting the wakes and waves shadow losses.

3.3.4 Transmission losses

The transmission losses are the last step before obtaining the net AEP of a farm, and therefore they are included in the costs submodel after discounting the O&M downtime from the gross AEP. In reality, they directly depend on many factors: power input of the transmission lines, temperature, material of the cables, grid frequency, insulation thickness, rated values and other characteristics that make its precise calculation very complex. For this reason, as a fair approximation that also allows quick computing, the following simplified loss model is used to calculate the transmission losses (P_{loss} , in MW) [38]:

$$P_{loss} = P_0 \cdot l + C_0 \cdot l^3 + P_k \cdot l \cdot \frac{S_{in}^2}{S_n^2} \quad (3.52)$$

being:

P_0, C_0 : no load parameters that depend on the cable's rated voltage.

P_k : load parameter that depends on the cable's rated voltage.

l [km] : cable's length.

S_{in} [VA] : cable's input apparent power.

S_n [VA] : cable's rated apparent power ($= \sqrt{3} \cdot V_r \cdot I_r$, for a triphase system).

As the input data of neither the wind nor the waves are time series but non-joint probabilistic data, the value of the simultaneous power output of both at all times is by all means unknown. On top of this, as the input apparent power in Eqn. (3.52) is squared, the simultaneous power outputs of both technologies cannot just be summed afterwards to obtain the total power losses. As a compromise solution, an assumption was made to estimate the power in the cables (S_{in}): as wind energy production predominates, the wind power output was up-scaled by the P80-to-wind capacity rate and it was considered as the total power output of the wind farm, as it is defined in Eqn. (3.56) and (3.57). Subsequently, the number of hours per year for each power output case (cables power input) is obtained from the wind scatter, so the yearly transmission losses ($T_{losses, i}$, in MWh) are implemented as follows:

$$T_{losses, i} = T_{l, MV, i} + T_{l, HV, i} \quad (3.53)$$

$$T_{l, MV, i} = \sum_{w.s.} \sum_{\theta_{wi.}} P_{loss, ins.}(S_{in MV}) \cdot t_{w.s., \theta_{wi.}} \quad (3.54)$$

$$T_{l, HV, i} = \sum_{w.s.} \sum_{\theta_{wi.}} P_{loss, ins.}(S_{in HV}) \cdot t_{w.s., \theta_{wi.}} \quad (3.55)$$

with:

$T_{l, MV, i}$ [MWh] : transmission losses in the inter array cables.

$T_{l, HV, i}$ [MWh] : transmission losses in the export cable.

$P_{loss, ins.}$ [MW] : power loss calculated as in Eqn. 3.52 (it is a function of the power input, and cable's characteristics).

$t_{w.s., \theta_{wi}}$ [h/year] : yearly hours of a wind speed and direction.
 $S_{in\ MV}$ [VA] : inter-array cables' input apparent power.
 $S_{in\ HV}$ [VA] : export cable's input apparent power.

Taking, as mentioned before, the input power of both the inter-array and export cables as the wind energy production (which of course depends on the wind speed) up-scaled to simulate the capacity of the platform:

$$S_{in\ MV} = S_{wind}(w.s.) \cdot \frac{Cap_{P80}}{Cap_{wind}} \quad (3.56)$$

$$S_{in\ HV} = \sum_{i=1}^{n_{plat}} S_{wind,i}(w.s.) \cdot \frac{Cap_{P80}}{Cap_{wind}} \quad (3.57)$$

being:

$S_{wind,i}$ [MW] : power output of turbine i at a certain wind speed and direction.
 Cap_{P80} [MW] : P80 capacity.
 Cap_{wind} [MW] : WTG capacity.

The presence of reactive power implicates various undesired effects in the electrical infrastructure: it increases the transmission losses of the cables and it also puts in risk the safety of the grid [35]. For these reasons, sets of power factor correction capacitors are often used to maintain the reactive power at low levels, and thus, the power factor ($\cos(\phi)$) values as close to 1 as possible. Normally, figures in the range of 0.85 to 0.95 are obtained [39, 40]. In order to remain in the safe side, a power factor of 0.85 has been used in the present study. This parameter has a direct effect on the transmission losses and on the maximum output capacity of a farm for a given export cable, as the apparent power in the cable depends on it ($S_{cable} = P_{gen.}/\cos(\phi)$).

After discounting the transmission losses, the net AEP for every year along the lifetime is obtained. As introduced previously, it is the energy that will actually be sold to the grid and it is therefore the value used in the LCOE calculation.

3.4 Optimization algorithm

Once the full LCOE calculation model is ready, it can be executed in two different ways: the user can define manually all the inputs (platforms coordinates, substation position, export cable to be used, harbor chosen for operations, inland substation chosen...) and run the model to find a solution; or certain variables can be left open to modification by an optimization algorithm so as to find a solution that minimizes the LCOE result, being this a single objective optimization problem.

Given the complexity of the model, it is impossible to carry out a classical analytical or gradient based optimization. This is due to the wide range of variables and the nature of many of the parameters involved: discrete scattered matrices that cannot be defined with a function, choices among different available options for a given parameter, spatial restraints and convexity (the problem presents several localized minimums) [41, 42].

For this reason, it is necessary to use other metaheuristic algorithms that are not based in the classic differential methods to solve the problems. These are the evolutive algorithms: calculation methods that take metaphorical inspiration on certain processes that occur in nature [43]. Most generally, they work by improving the obtained results in an iterative way, modifying the variables (called decision variables) each time according to each algorithm's working principle or logic.

Among the most extended evolutive methods, the Genetic Algorithm (GA) and the Particle Swarm Optimization (PSO) can be found. The former, extensively used in the wind energy field [41, 44, 45], emulates the principles of evolution theory by, for example, mixing solutions that give birth to new ones, or mutating offspring solutions to find other exotic ones. With regards to the PSO, it is based in bird flocking, fish schooling, and swarming theory, having also ties with the GA [46].

After consulting with experts in the optimization field, and taking into consideration the description of the problem, the first intention was to use a new type of algorithm that has not been used in the wind energy sector up to now (the algorithm comes from the water systems dimensioning sector). It is called Agent Swarm Optimization (ASO) and it integrates behaviors of the two described algorithms, among others, preventing it from terminating in localized minimums, increasing the computational speed, and allowing multi-objective optimizations [47, 48].

However, the implementation of this algorithm was finally not possible due to the lack of time to translate it into MATLAB and the unavailability of the developers. As also very often the good functioning of the algorithms depends mostly on the way it has been implemented rather than in the type of algorithm used, it was finally decided to use the PSO algorithm (*particleswarm* function in MATLAB).

3.4.1 Particle Swarm Optimization (PSO)

The PSO is primarily based on the movement of the different individuals (in this case known as particles, each of which, after all, represents a set of decision variables) with respect to the rest of the members (population) of the swarm [46]. The new variables tried in each iteration shift from the previous ones according to three different components, shown in Fig. 3.12:

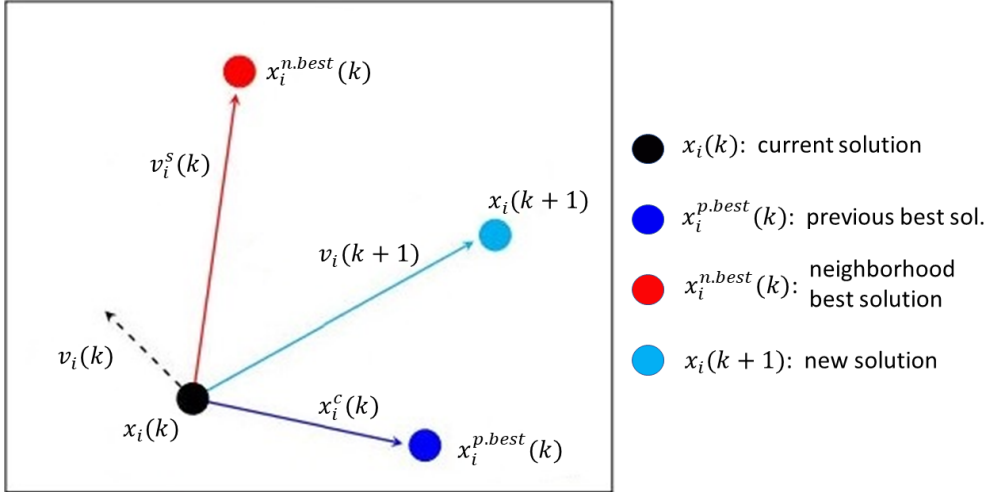


Figure 3.12: Illustration of PSO velocity and particle position [49].

After the modification of the algorithm in 1998 by Eiberhardt [50], the weight of each one of these components is determined by the following equation:

$$v_i(k+1) = \omega \cdot v_i(k) + c_1 \cdot r_1 \cdot (x_i^{p.best}(k) - x_i(k)) + c_2 \cdot r_2 \cdot (x_i^{n.best}(k) - x_i(k)) \quad (3.58)$$

being ω the inertia parameter, c_1 the cognitive/ own-best position/ self adjustment weight, and c_2 the neighborhood/social/group adjustment weight, the factors that influence the particle's motion.

3.4.2 Algorithm configuration

Four main parties are involved in the way the optimization process is built: the **objective function** (minimization of the LCOE), the **decision variables** (subject of change to improve the result), the decision variables' associated **restraints**, and the **penalizations** (worsening of the objective value due to the infringement of the restrictions).

3.4.2.1 Decision variables

Among the wide range of parameters that could be subject of change to minimize the LCOE, in the last version of the optimization algorithm eight parameters, divided in three groups, were chosen as decision variables:

First, the decision variables associated to the positions of the platforms: arguably, the most relevant decision variables of the model. With a set number of platforms in the farm, in an early stage the platforms were free to be located independently within the limited site's area. However, rather messy and unorganized arrangements were obtained, and this option was soon discarded due to negative visual impact and the operational difficulties that this may involve (e.g.: difficulty to define boat routes and safe access areas). Moreover, this arrangement method involved having 2 decision variables per platform (x and y coordinate for each one of them), which increased the computational time significantly.

In order to solve these issues, the platforms were finally forced to be arranged in rows and a total of five decision variables were found to be necessary to define completely the positions of all the platforms: these are the **number of rows** ($d.var_1$), the **separation between rows** ($d.var_2$), the **separation between platforms in each row** ($d.var_3$), the **row offset** ($d.var_4$), which is the relative positional shift along the rows' direction of consecutive rows, and the **angle of orientation of the rows** ($d.var_5$). These decision variables are shown in Fig. 3.13:

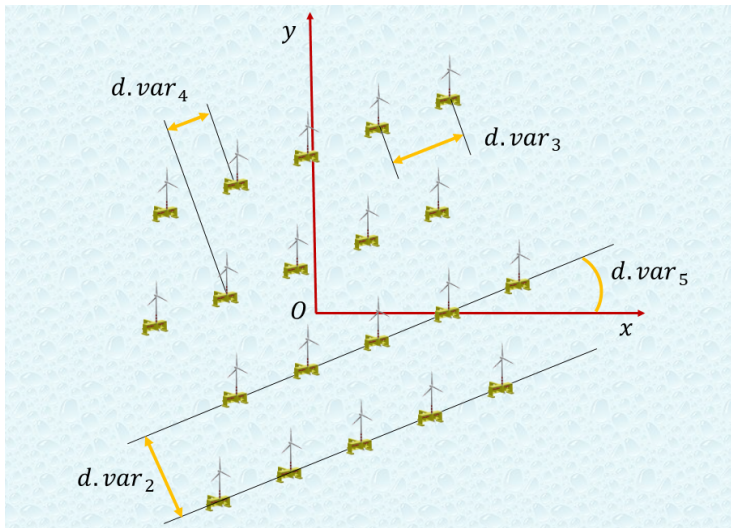


Figure 3.13: Decision variables associated to the platforms positions (being O the center of the site).

As it can be seen in the figure, the platforms are located around the site's center coordinates, so the rows are distributed equally to each side. Needless to say, these optimizer input parameters or decision variables were needed to be converted into the platforms coordinates inside the function: first, the number of platforms and rows is read, and therefore the rows are created with their specified spacing ($d.var_2$ and $d.var_3$); then the uneven extra platforms are successively added from the last row towards the first one; and finally, the orientation angle is applied by multiplying each platform's coordinates by a two-dimensional rotation matrix (R_θ) as follows:

$$\begin{bmatrix} x_{rot} \\ y_{rot} \end{bmatrix} = R_\theta \cdot \begin{bmatrix} x_{coord.} \\ y_{coord.} \end{bmatrix} \quad (3.59)$$

being: $R_\theta = \begin{bmatrix} \cos(\theta) & -\sin(\theta) \\ \sin(\theta) & \cos(\theta) \end{bmatrix}$ and $\theta = d.var_5$ the orientation angle.

The second group of decision variables ($d.var_6$ and $d.var_7$) are the **coordinates of the offshore substation**, specified as x and y distances with respect to the center of the site O . Finally, the last decision variable ($d.var_8$) is the **export cable choice** among the available ones (of course, this depends on the inputs, in the next section the considered export cables in the case study are specified); the chosen cable will therefore have its own specifications. As an extra remark, as the PSO does not allow to choose input decision variables as integers, $d.var_1$ and $d.var_8$ had to be rounded up or down inside the function to integer values. However, undesired behavior was observed due to the rounding of integer variables. In Section 4.2.5 it is explained what was done to deal with this issue.

A few other parameters that *a priori* seemed subject of also being optimized were eventually discarded as decision variables for various reasons. These parameters are the following:

- Harbor and inland substation choice among the available ones in the area: even though the LCOE output definitely depends on this decision, there are many external factors that condition it as this choice highly depends on the state legislation and planning; it also depends on particular characteristics of both the harbour and substation: their size, availability and so on. Therefore, it is very difficult to model these factors and it has been considered that it should be the user who makes this decision, after a site-specific study.

- The number of platforms: similarly, this factor depends mainly on the region and country where the farm would be installed. Factors like the strength of the grid or the need of power in the surrounding area will determine the total capacity of the farm, and thus it is something that must be chosen manually after studying these particularities. The procedure followed in the case study to determine this parameter is explained in Section 4.1.2.

- **WTG size:** it was one of the initial decision variables considered. However, as the P80 is currently designed to host a 8 MW WTG, it was finally decided to develop the model with it. Another type of WTG would imply different input costs, a different hub height and therefore different wind speed inputs, and probably also a different size of the platforms and WEC.

- **Lifetime:** this parameter depends entirely on the design of the structures involved in the project, not on the project planning itself. As the P80 design is given for granted in the model with its consequent costs and characteristics, it does not make sense to optimize the lifetime. In fact, the model would tend to increase the lifetime indefinitely, in order to share the investment costs with the maximum energy production possible, thus decreasing the LCOE. This is clearly unrealistic. It was also considered to model an aging rate, but this was regarded as being too uncertain due to the lack of information about a real behavior along time of the P80.

3.4.2.2 Restraints and penalizations

All the decision variables have restraints that are directly or indirectly associated to them as, on the one hand, they cannot adopt any size due to their nature, and on the other, third party variables which depend on the values of these decision variables may also have their own restraints. Below, the **restraints** involved in the model are listed:

- **Minimum separation between platforms:** they cannot be placed closer than a certain distance (because of wakes turbulence, mooring lines length, etc.). Again, the particular values decided in the case analysis are explained in Section 4.2.4.

- **Site delimitation:** the available space can not be infinite as the model is considering a single climate for the whole site. The site area is defined with a radius of 10 km around the center coordinates. These two first restraints affect directly the coordinates of the platforms, and indirectly the decision variables that determine their arrangement (*d.var₁* to *d.var₅*).

- **Depth range:** which is determined by the depth boundaries of the mooring system (from 40 to 200 m, as presented in Chapter 2).

- **Minimum separation between platforms and substation:** similarly to the first restraint.

- **Rated power of the export cable:** so the algorithm chooses an export cable that can bear the farm's maximum output power.

On top of these restraints, the eight decision variables specified have associated boundary parameters that define the maximum and minimum values they can adopt. Technically, this would not be necessary as long as the restraints specified above are

fulfilled. However, setting these values is convenient in order to minimize, once again, the computing time (e.g.: setting the orientation angle from -180° to $+180^\circ$), so that the optimizer does not try values out of this range.

As advanced above, these restraints have associated **penalizations** that prevent the algorithm from choosing a non-feasible result as an optimal solution. These penalizations are applied at the beginning of the LCOE function, before the waves energy calculation. If the value they adopt is greater than zero (a restraint has not been fulfilled), the LCOE output also adopts a certain value in an order of magnitude greater than that of a reasonable result. If so is the case, the rest of the function is not computed (this is done by means of a *return* command) so as to decrease the computing time. Furthermore, these penalizations have to be modeled in a way that the further away the variables are from fulfilling their restraints, the greater the penalizations become: thus the LCOE value obtained is a function of the degree of unfulfillment of the restraint. This way, the particles will evolve towards feasible solutions. Figure 3.14 shows this principle visually:

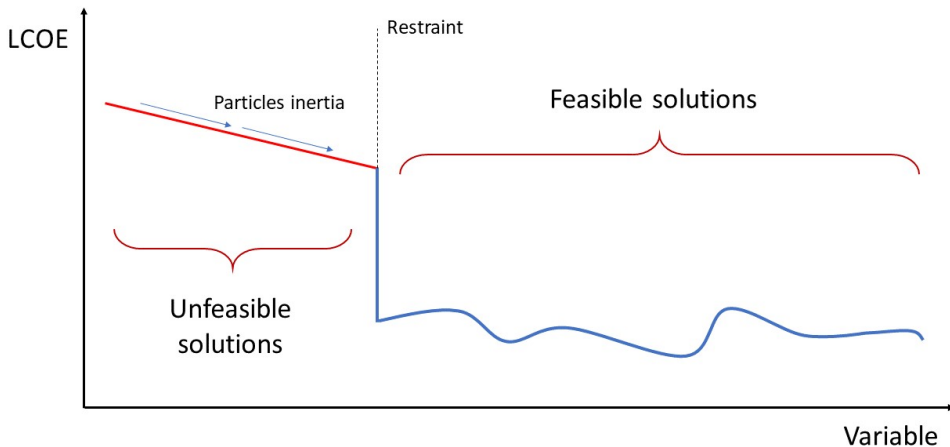


Figure 3.14: Working principle of the penalizations.

3.4.2.3 Performance improvement

Several parameters can be modified in order to optimize the performance of the algorithm. This performance is basically determined by two aspects: the computing speed of the algorithm (how long it takes to find an optimized minimum), and the ability to avoid the choice of local minimums as the final solution. It has been tried to deal with these issues as explained below:

Once the algorithm has found what looks like the surrounding area of a minimum, it often starts to modify the values of the particles (decision variables) in a very small scale, technically still improving the output result, but actually doing so very slowly and irrelevantly, as the tiny changes may improve the output value in very small values, which, apart from not really making a difference and preventing the algorithm from finishing the optimization quickly, the resolution of the results at that point is actually too precise if the uncertainties and error tolerance associated to the model are taken into consideration. In order to prevent this from happening several actions were tried:

First, all the decision variables (not only the integers) were rounded to a certain decimal base that was regarded as a reasonable resolution according to its nature. For example, the angles were rounded to integers, having a change resolution of 1° , or the separation between platforms were rounded to the nearest hundred meters. However, it was found that this solution resulted in a termination of the optimization too prematurely, as the algorithm would often see no change in the objective function when modifying the values of the inputs, sometimes preventing it from finding and jumping to a new better local minimum.

Secondly, the rounding was also applied to the LCOE output value, which was found to provide better results. This solution satisfactorily stops the algorithm from trying to find irrelevant better solutions for too long, however still with a risk of ending the optimization too soon in a non-global minimum. Something similar is achieved when modifying the option *TolFun* of the algorithm, which determines the tolerance in the change of the objective function for the algorithm to consider it as an improvement.

The third modification made was adjusting the values of the previously described inertia weight (*InertiaRange* option in MATLAB), which can also be dynamic (i.e.: it can change along the optimization loops), the self adjustment weight (*SelfAdjustmentWeight*) and the social adjustment weight (*SocialAdjustmentWeight*). Optimum values for them and for the amount of particles in each iteration (*SwarmSize*) were found in literature [51] given the number of input variables, although this also very much depends on the structure of the function being optimized. Three sets of optimum parameters are given:

Problem dimensions	Fitness evaluations	PSO Parameters			
		<i>SwarmSize</i>	ω	c_1	c_2
10	2,000	63	0.6571	1.6319	0.6239
		204	-0.2134	-0.3344	2.3259
	20,000	53	-0.3488	-0.2746	4.8976

Table 3.2: Optimum PSO parameters [51].

Being the problem dimensions of 10, the case found in literature closest to the 8 decision variables of this optimization case. After implanting these changes, it was observed an improvement in the results but an increase in the optimization time, as it is presented in Section 4.2.5.3.

The last modification made to improve the performance of the algorithm was running successive optimizations, defining each time the optimum result found in the previous optimization process as one of the initial particles/decision variables (*InitialSwarmMatrix*) of the next loop. A slight improvement in the final value was found as a result. However, it again exists the risk of limiting the search area of the algorithm to a local minimum.

CHAPTER 4

Case Study: Siting in the Republic of Ireland

In this chapter, an application case of the model is presented. Sligo bay, at the North-West of the Republic of Ireland, is the target area of this study. Given the significant wave power density in the Northern Atlantic Ocean (the waves climate is too powerful for current wind floating concepts), this site presents an appropriate climate for the P80 concept. The area's particularities in terms of power generation and costs calculation are analyzed, together with relevant factors such as the bathymetry, the electrical system and the activities taking place in the area.



Figure 4.1: Area of interest: Sligo Bay (figure obtained from Google Earth).

4.1 General description

The Republic of Ireland is one of the countries in Europe with the highest share of wind power production, currently entailing a 29% of the country's electricity demand. And this is only growing: 19 new wind farms were built in 2018, and latest news are the target of increasing the share of renewables from 30% to 70% by adding 12 GW of clean energy capacity by 2030, 3.5 GW of which are reserved for offshore capacity [52, 53].

One of the measures being launched to achieve this target is the new Renewable Electricity Support Scheme (RESS), after several years without support from the state since the Feed-in Tariff scheme closed in 2015 [54]. This new scheme consists in an auctions based system that will take into account not only the bid generation price but also aspects like the communities' ownership of the project, the demand-supply ratio of the area and the financial structure of the project. The auctions also include Floating Feed-in Premiums, a relevant aspect for a concept like the P80 [55].

Focusing on the wind energy field, most of the Irish wind farms are placed onshore, spread all around the country. At this point, only one offshore wind farm has been commissioned. Placed in the East coast, the Arklow Bank Wind Park consists of 7 WTGs that produce a total of 25 MW, very little capacity in comparison to the ambitious aspirations of the country.

4.1.1 The Irish energy system

A Single Electricity Market was established in 2007 enclosing both Northern Ireland's and the Republic of Ireland's Transmission System Operators (TSOs): these are the System Operator of Northern Ireland and EirGrid respectively. The grid is further interconnected with Scotland and Wales, and a future connection with mainland Europe is planned.

The most demanding area of the island in terms of power is the East coast, mainly due to Dublin and its metropolitan area, and also that of Belfast. For this reason, a big offshore project in the West coast as the one considered in this study may not seem the most suitable from the point of view of demand-supply ratio and grid strength at first sight. Nevertheless, the suitability of this type of project is guaranteed, given the state's ambitious plans of shifting to renewables (phasing out non-renewable capacity, which leaves space for generation), and the on-going North-West Project, which precisely has the goal of strengthening the grid in the area for future wind energy capacity by connecting the Srananagh and Clogher substations [56]. Figure 4.2 depicts a map of the grid system in the area of interest.

As it can be seen, most of the substations found in the area have a rated voltage of 110 kV, the smallest type of high voltage station among the existent ones in the all-

island grid system. However, a bigger 220 kV substation can be found in Srananagh, only 10 km away from Sligo, which is the largest town in the area with about 20,000 inhabitants.

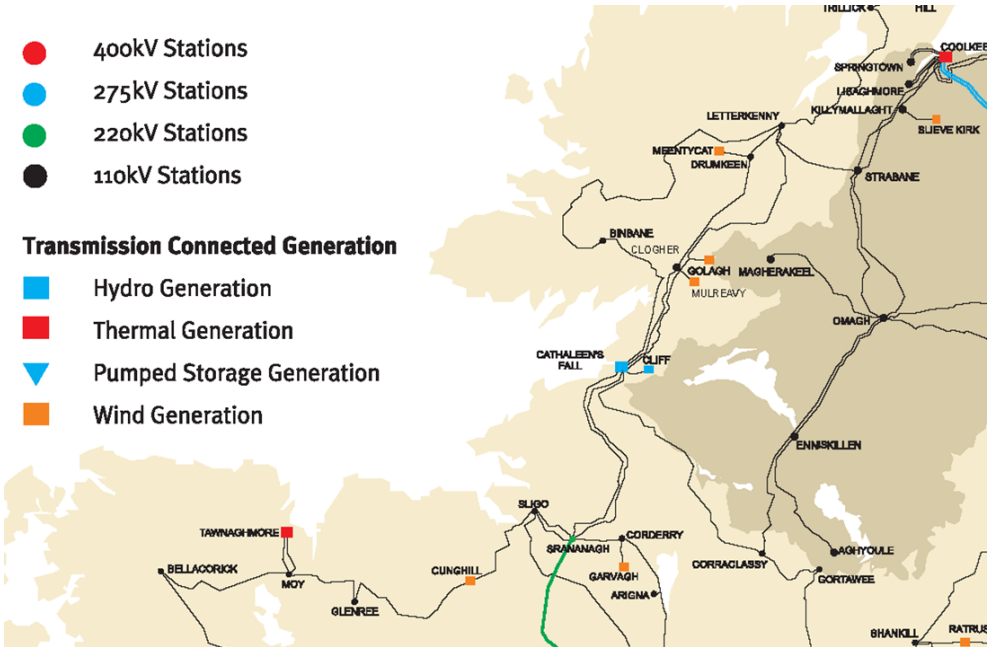


Figure 4.2: Transmission system map of the Sligo Bay area [56].

4.1.2 Grid strength and farm size

Given that the TSO specifies that large generation stations of more than 100 MW of capacity shall be connected to 220 kV, 270 kV or 400 kV stations [56], and since no other transformer of these characteristics can be found in the area, **Srananagh 220 kV substation** was chosen in an early stage as the inland grid substation to which connect the farm. As it can be seen in Fig. 4.2, a couple of wind farms are located close by, also a hydro power plant can be found further North, and the Thawnaghmore 153 MW thermal generation plant, which may be subject of decommissioning soon, is located to the West, not far from the chosen station.

The grid strength determines the reliability of the network, as a new generator may have a big impact on a weak grid, reaching the thermal limit of its cables, suffering voltage changes and emitting harmonic frequencies (flickering). The short-circuit impedance expressed in ohms ($Z_{k,\Omega}$) needs to be calculated in order to quantify

this grid strength. For the sake of this calculation, the general characteristics of Srananagh's transformer, necessary to obtain of the short-circuit impedance of the system, are shown below together with the calculation made:

Name	Rating (MVA)	HV/LV (kV)	Impedance (p.u. with 100 MVA base)	
T2101	250	220/110	R=0.001	X=0.064

Table 4.1: Srananagh's transformer characteristics [56].

$$Z_{base} = \frac{u_{base}^2 (kV)}{S_{base} (MVA)} = \frac{220^2}{250} = 484 \Omega \quad (4.1)$$

$$Z_{k,\Omega} = Z_{base} \cdot Z_{p.u.} = 484 \cdot \sqrt{0.001^2 + 0.064^2} = 30.98 \Omega \quad (4.2)$$

Moreover, the short circuit current of the transformer (I_k) is presented in Table 4.2, which shows the maximum and minimum values for Srananagh's station (those of 2016 and the predicted ones for 2019 and 2022):

		Year		
		2016	2019	2022
Summer	Max	3.89	3.98	4
	Min	3.72	3.83	3.84
Winter	Max	4.99	5.33	6.71
	Min	4.75	5.07	6.26

Table 4.2: Srananagh transformer short circuit currents (I_k) in kA [56].

Taking into account the minimum value (when the grid is the weakest), and considering that the farm would not be commissioned before 2022, the short circuit power of the station can then be calculated as follows:

$$S_k = 3 \cdot |Z_{k,\Omega}| \cdot I_k^2 = 3 \cdot |30.98| \cdot 3.84^2 = 1370.45 \text{ MVA} \quad (4.3)$$

Finally, the grid strength is best represented by the short circuit ratio (rate between the wind farm's capacity and the short circuit power) which should be kept below a controlled value. This value, unknown in this case, depends on the country and substation. In general, according to [36], the short circuit ratio should lay within the following boundaries:

$$2\% \leq \frac{Cap_{Tot}}{S_k} \leq 20\% \quad (4.4)$$

Therefore, in this case, for a short-circuit ratio of 20%, the maximum wind farm capacity would be that of $Cap_{Tot} = 274 \text{ MVA}$. Taking into account the previously explained grid-strengthening project and the phasing-out of non renewable generation plants, it was considered a farm size of **25 platforms, i.e.: 250 MW** (even though, according to the figures, this capacity would be very tight if the grid is not modified at all, specially taking into account the influence of the reactive power).

4.1.3 Analysis of the area of interest

Sixteen possible sites spread throughout the bay have been analyzed for the sake of this study. These sites were chosen according to the wind and waves resources' discrete resolution (being placed 25-30 km apart from each other), covering as much as possible the entire area of the bay.

The studied location is an open ocean bay with the fishing practice as its main activity, being most of the bustle due to boats coming in and out from the **port of Sligo**, which was the harbor chosen for all the operations involved in the project given its greater dimensions in comparison to the only other harbor in the area: Killybegs Harbour. The vessel activity density of the area (obtained from Marine Traffic), as well as the location of the considered sites and that of the harbors, are shown in Fig. 4.3.

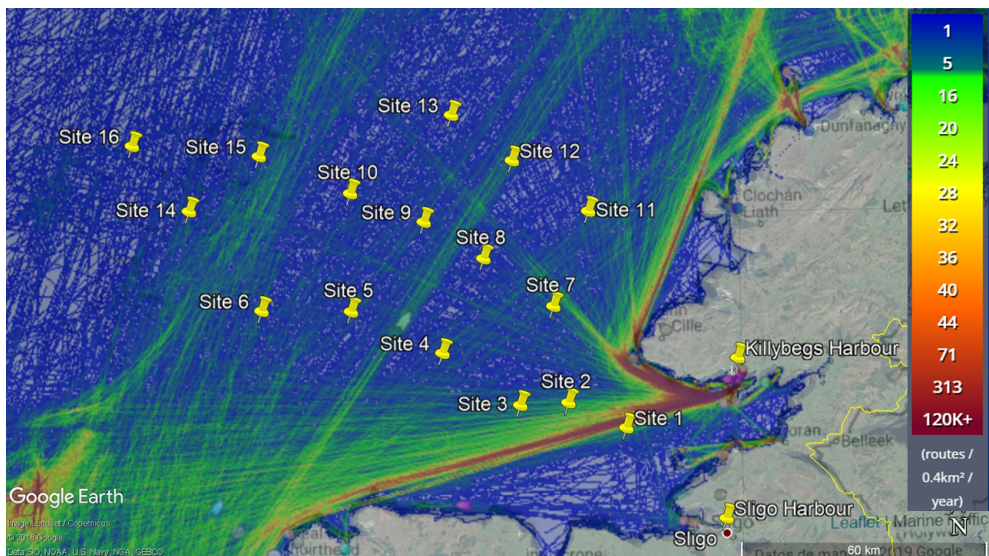


Figure 4.3: Position of the possible sites and boat routes [57].

As it can be deduced from the figure, the area is not very concurred. However, the sites 1, 2, and 3, placed at the South part of the bay, have to be discarded since they lay in the main shipping route of the bay. On top of this, Site 1 was considered to be placed too close to shore, where both its visual impact and the shallow seafloor make it an unsuitable site.

Regarding possible environmental issues that may condition the siting, the only protected areas that can be found are the estuaries of the three rivers that flow into the bay: the Drumcliff, Garavogue and Bonet rivers. These estuaries are protected by the European Union and they have been defined as Natural Heritage areas. However, these areas are placed very close to shore, thus not meaning an issue for a far-shore farm of this kind.

The third main factor that may involve a direct elimination of further sites is the seafloor depth (as a reminder, the mooring system of the P80 can be installed in depths from 40 to 200 m). The depth of the seafloor throughout the bay is depicted in Fig. 4.4:

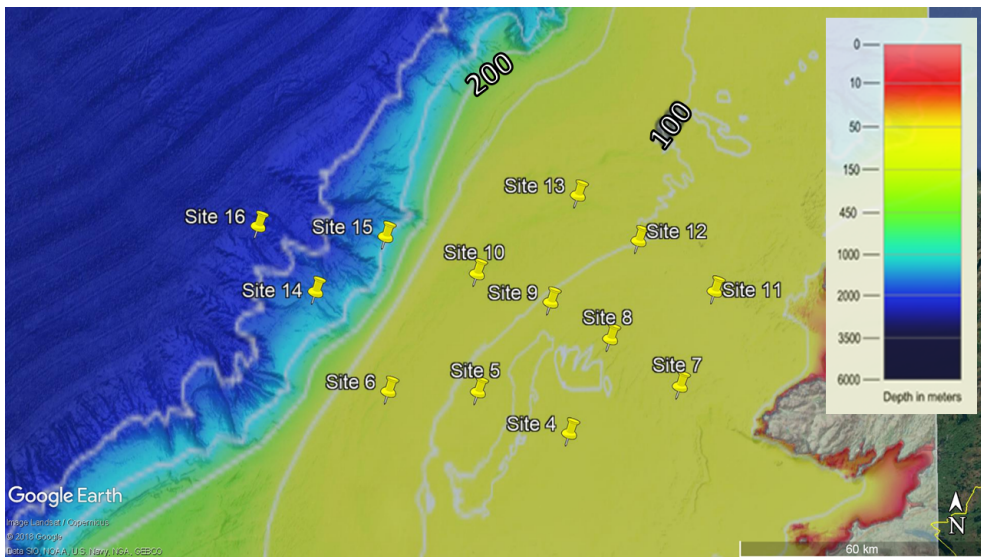


Figure 4.4: Seafloor depth of the bay [18].

As it can be observed, most of the sites present a suitable seafloor depth, which is out of the range of bottom-fixed concepts and which lays in the P80 range. However, a very steep depth increase up to thousands of meters is observed just before the three sites placed further offshore (Sites 14, 15 and 16), making impossible the installation of

the platforms. Finally, after this primary analysis, the suitable locations are reduced to Sites 4 to 13.

4.2 Implementation of the model

Up to this point, the choice of harbor and inland station (and therefore their coordinates) has been established. Furthermore, several sites were discarded due to a prior analysis, and the number of platforms in the farm has been determined given the grid characteristics. Before the model can be run, now all the site-specific inputs and parameters need to be determined and loaded in the model.

4.2.1 WTG used in the model

Several 8 MW WTGs were considered for the study, one of them being the WTG developed in DTU and used in Section 3.2.1 as an example. However, given the availability of its data and its level of development and detail, it was finally decided to use **LEANWIND's reference 8 MW wind turbine** [58], which is based in both the 5 MW turbine designed in the National Renewable Energy Laboratory (NREL), and DTU's 10 MW reference wind turbine. Its power and thrust coefficient curves are the following:

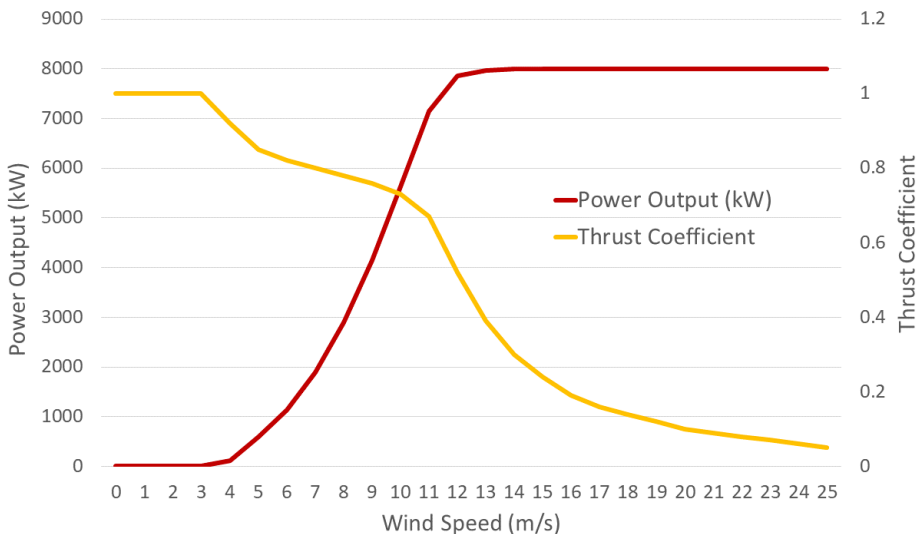


Figure 4.5: Power and Thrust Coefficient curve of the LEANWIND 8 MW WTG.

Furthermore, the chosen WTG has the following relevant specifications that are used in the model:

- Rated Power: 8 MW
- Hub height: 110 m
- Rotor diameter: 164 m
- Cut-in wind speed: 4 m/s
- Cut-out wind speed: 25 m/s

4.2.2 Wind resource

The most up-to-date wind data has been used in the case analysis after an investigation of the different sources available. The data used, in the form of a Generalized Wind Climate, was obtained from the New European Wind Atlas (NEWA) developing team.

The NEWA [59] is soon going to be launched, becoming the newest and most advanced source of wind climate data available. Following the work done in the Global Wind Atlas (GWA), the NEWA will provide the results obtained by the Weather Research and Forecasting (WRF) model [60], which consists of new down-scaling methodologies that have been implemented using new long-term data sets. Unlike the GWA, the NEWA data also includes information of distances up to 100 or even 200 km offshore.

For this study case, it was possible to contact the developers, who provided the data of the locations specified. This was very valuable due to the lack of information about the sites placed furthest offshore in the currently available GWA, and also due to the significant differences between both sets of data. Figure 4.6 shows these differences in the wind profiles, which give an idea of the importance of having a good and trustworthy data source.

As mentioned, in this case the wind data was obtained in the form of Generalized Wind Climate (GWC) files, which contain information about the different wind speeds' frequency of occurrence in the form of the parameters of a Weibull distribution (extensively used to describe wind speed variations) for twelve directions (every 30°), several heights (50, 75, 100, 150 and 200 m) and terrain roughness lengths (using, in this case, a roughness length of 0 m, as the wind farm is placed offshore). However, once the GWC is obtained, this information needs to be processed and transformed in every site to make it suitable and readable by the model.

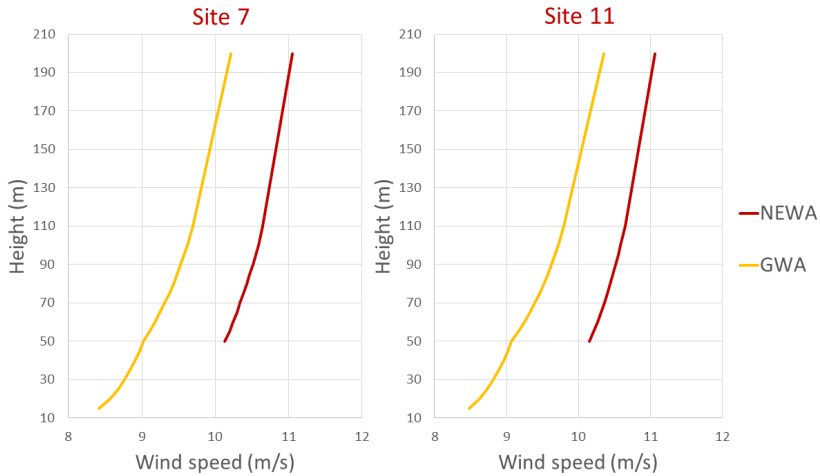


Figure 4.6: Wind profiles of Sites 7 and 11.

Given the characteristics of the model and the WTG used, the wind data in the form of $p(w.s., \theta_{wi.})$ is needed for a hub height of 110 m. Since there is no specific information about this particular height in the GWC, the first step is to load the file in WAsP, where the Weibull distributions at all heights are interpolated taking into account the atmospheric conditions of the site's geographical area. Then, a *reference site* with the desired height is placed so the Weibull parameters at 110 m can be read and extracted from WAsP. These parameters have the following structure:

Sector	Wind direction	Weibull A [m/s]	Weibull k	Mean w.s. [m/s]
1	0	9.4	2.44	8.29
2	30	9.5	2.2	8.42
3	60	8.5	2.42	7.55
4	90	8.1	2.62	7.24
5	120	9.9	2.17	8.78
6	150	12.3	2.35	10.92
7	180	12.5	2.51	11.08
8	210	13.1	2.38	11.57
9	240	12.3	2.47	10.89
10	270	10.6	2.05	9.43
11	300	10	2.26	8.85
12	330	9.1	1.94	8.05

Table 4.3: Example of Weibull parameters at 110 m obtained from WAsP.

This information now needs to be transformed into the probabilistic values for each wind speed and direction $p(w.s., \theta_{wi.})$, since it is the way the model can read it as explained in Section 3.2.1. Since the Weibull parameters for the twelve directions are known, the probabilities are calculated using the Weibull distribution, shown below:

$$p(w.s.) = \frac{k}{A} \cdot \left(\frac{w.s.}{A}\right)^{k-1} \cdot \exp\left(-\left(\frac{w.s.}{A}\right)^k\right) \quad (4.5)$$

being A the Weibull scale parameter in m/s and k the Weibull form parameter.

Finally, as it explained in Section 3.2.2, the wind speed probabilities that, at this point, are defined every 30° , need to be converted to a resolution of every 10° so the wakes can read them properly. In the absence of a better method (the result can only be as accurate as the data is), this was done by dividing each one of these probabilities' values in three sectors (e.g.: the probabilities obtained for 90° were divided by three and distributed equally for 80° , 90° and 100°). In fact, the matrix depicted in Fig. 3.8, used as an example of a wind speed scattered matrix, has this shape.

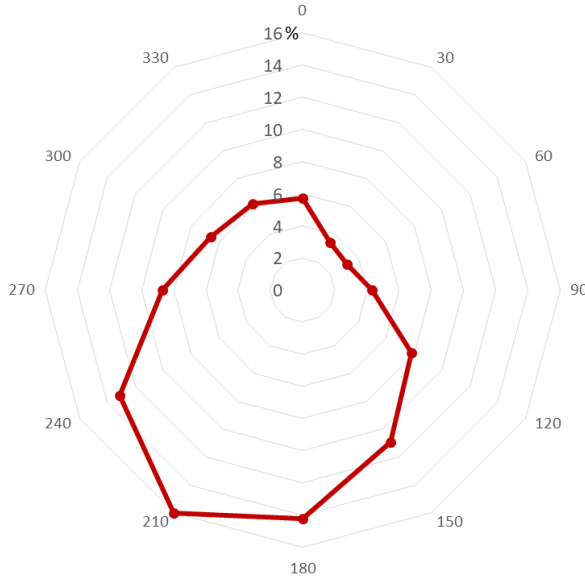


Figure 4.7: Example of wind rose (Site 11).

Focusing back on the analyzed area, as it can be seen in Fig. 4.7, the wind was found to come predominantly from the South-West in every site, which is not surprising given that the land is placed at the East side of the bay. On the other

hand, the obtained average wind speeds at 110 m go from 10.65 m/s in Site 11 to 10.85 m/s in Site 6. As a preliminary observation before the calculations are run, it is worth mentioning that the increase of the wind speed when going further offshore is not as steep as it could seem, probably meaning that the sites placed far offshore may not be feasible when taking into consideration the costs involved in this increment of distance to shore.

4.2.3 Waves resource

In the case of the waves climate, as advanced in Section 3.1.1, the data is obtained from the DHI in the form of three scattered matrices. The generation method of this data is the MIKE 21 Spectral Wave numerical model [61] developed in the DHI. As it can be seen in Fig. 4.8, the prevailing and almost exclusive waves direction in the area is from West to East: coming from ocean to land.

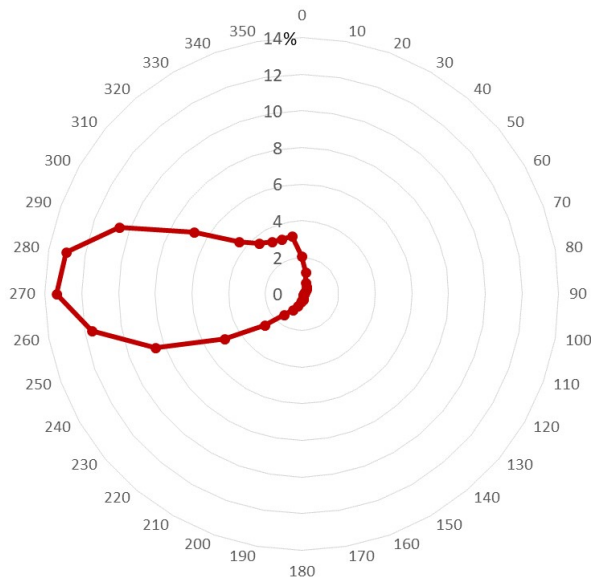


Figure 4.8: Example of waves rose (Site 11).

At this point, it is worth mentioning that, in principle, the wind wakes are much more determinant for the positioning of the platforms than the waves shadows. This is due to two main facts: as it has already been discussed in the report, the highest share of energy is produced by the wind so a decrease in the wind energy production reduces more significantly the value of the LCOE; and, on the other hand, the WTGs wakes have a longer spatial range than that of the waves shadows, meaning that the

proportional loss of energy at longer distances is higher in the case of the WTGs. The results from the lay-out optimization process should be clarifying in this regard.

4.2.4 Definition of the rest of the parameters

Once all the site dependent inputs have been determined, only the parameters that influence the decision variables (restraints) and the discount rate are left to be established.

Regarding the minimum separation between the platforms, two main factors influence this value: on the one hand, unlike the waves shadows, which only have an effect on wave height reduction (thus creating a more still water surface), one of the main issues involved in the wind wakes of a WTG is the appearance of turbulence, which causes undesired and uneven loads (wind shear) in the WTGs placed close by. For this reason, as a rule of thumb, a minimum separation between WTGs of five to seven times the diameter of the WTG is often used as the minimum separation.

On the other hand, the mooring systems also needs to be taken into account, specially given the dynamic nature of the platform in this concept. As shown in Fig. 2.8, the P80 mooring system is designed to be quite spread in the horizontal direction in comparison to the depth. In the example shown in the picture, this horizontal distance is in the range of a thousand meters, or even more if the last laying chain stretch is considered. However, this rather long distance is, in general, oversized, and it is believed in FPP that there is still room to optimize the depth-width rate of the mooring system.

Given the exposed reasons above, the minimum separation between platforms (sep_{plat}) was modeled as follows:

$$sep_{plat} = max \left\{ 5 \cdot diam_{WTG}, 2 \cdot 80\% \cdot \frac{1000}{100} \cdot depth \right\} \quad (4.6)$$

having considered as 80% the reduction in horizontal distance after optimizing the mooring system.

The second restraint to be established was the minimum separation between the platforms and the offshore substation. It was decided to use a value of 1000 m. Given that the mooring system of the substation is considered to be much more simple and static than that of the P80s, this separation is more than enough, even in the cases where the depth may be greater than 100 m. Furthermore, it is assumed that no further interaction between substation and generators exists in terms of wind blocking and waves shadow.

The 16 types of HV export cables considered in this case analysis, and their nominal current (I_r), section (Sec), nominal voltage (V_r) and rated power (S_r) where chosen among the most typical ones found in the literature and data sheets. Their characteristics are presented below:

S_r (MW)	Sec (mm ²)				
	500	630	800	1000	
	I_r (A)				
	655	715	775	825	
U_r (kV)	110	124.8	136.2	147.7	157.2
	132	149.8	163.5	177.2	188.6
	220	249.6	272.5	295.3	314.4
	275	312	340.6	369.1	393

Table 4.4: Available cables and their section area, and rated voltage, current and apparent power.

All these cables are subject to be chosen by the optimizer, which will intend to find a balance between their cost and transmission losses. Further characteristics like the loss coefficients and prices of the different types of cables are presented in Appendix A.3.

Furthermore, it is worth reminding that the site delimitation was set to a circular area with a radius of 10 km around the site's center coordinates, due to the fact that the wind and waves resources cannot be considered constant at higher distances and, as it is proven in the following sections, having the security that the optimum coordinates perfectly fit within this delimited area, this not being a constraining factor.

Finally, as it is explained more in depth in Appendix A.5, after consulting several sources, the discount rate value that has been considered for this type of technology and that has been used throughout the optimization process in this case analysis is that of 9%, although this is one of the parameters with the highest level of uncertainty. In fact, the value considered in the company is generally a 7%. The influence of the variation of this parameter is analyzed in Section 5.1.

4.2.5 Optimization Methodology

In this section, it is explained how the optimization was carried out after narrowing down all the determinant factors that influence the calculation: the successive steps taken in the optimization process and the results obtained in each one of them.

4.2.5.1 Step 1: finding the best sites

The first part of the process had the goal of discarding the least feasible sites considered up to this point. The model was run for every site with the same identical decision variables and layout (shown in Fig. 4.9), composed of 25 platforms. This way, the long optimization process could be avoided in many of these sites. In the layout figure and in all the figures of the kind from now on, the small blue and red circles represent the positions of the P80s and that of the offshore substation respectively, and the big red circle depicts the site's delimited area.

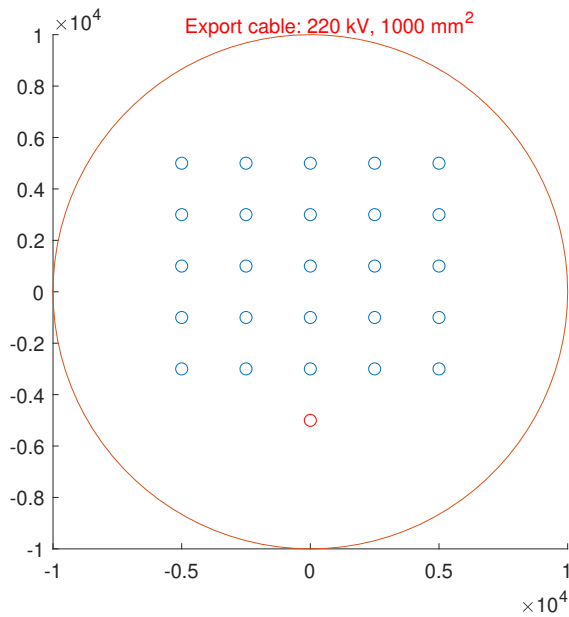


Figure 4.9: Base layout in Step 1 (in blue, the positions of the platforms; and in red, that of the offshore substation).

Furthermore, the site's mean depth, and the AEP_{wind} , AEP_{wave} , and $LCOE$ values obtained in the different sites are shown in Table 4.5. As it can be deduced from the results, Sites 4, 7, 8, and 11 (in green) were found to provide the best figures due to a better balance between the energy production and the costs associated to the distance from shore. It is easy to realize that these four sites are the ones placed closer to shore and also those ones where the seafloor is more shallow (although this second factor does not have such a big impact in the $LCOE$).

On the other hand, even though both the wind and waves energy production

in the rest of the sites is generally higher (with the exception of Site 4), this fact is not enough to balance their longer distance to shore, which increases their costs significantly. This is specially observed in the sites marked in red (Site 6, 10, and 13), the ones placed the furthest from shore. Given the significant difference in the *LCOE* value, only the green sites were chosen for the second step of the process.

	<i>LCOE</i> (€/MWh)	Mean Depth (m)	<i>AEP_{wi}</i> (GWh)	<i>AEP_{wa}</i> (GWh)
Site 4	121.2	97	1045.65	156.06
Site 5	127.3	97	1042.64	171.79
Site 6	133.1	120	1046.66	179.13
Site 7	119.1	83	1034.70	146.79
Site 8	123.3	95	1036.96	163.40
Site 9	127.5	98	1038.64	171.13
Site 10	132.5	119	1044.93	177.91
Site 11	123.1	76	1032.88	152.41
Site 12	127.9	98	1036.38	165.73
Site 13	132.6	109	1038.71	174.05

Table 4.5: Results of Step 1.

As it is discussed more in depth further in the report, a conclusion that may be extracted from these preliminary results is that in this area the climate's power growth with distance is not steep enough. It is also worth remarking the big difference obtained between the wind and waves energy generation, as advanced in the previous chapters. In every site, the latter only represents 10-15% of that of the wind in all the sites.

4.2.5.2 Step 2: optimization and choice of the best site

The second step of the process consisted in finally carrying out the optimization in the selected best sites. From the results obtained in the previous step, it seems like Site 7 is the clear favorite as its *LCOE* value is around 2 €/MWh lower than that of the second best site. However, given that the energy production of this second one is higher (better wind resource), the optimization of the layout could have a more relevant effect in the minimization of its *LCOE*.

A last minute dismissal was made. Given the nature of the model, which takes into account the linear distances (between site, harbor, onshore substation and shore connection point), a modification should be made in Site 11. Since it is located behind a cape, the length of the export cable and the distances of the O&M and installation operations are actually higher than the ones considered in the first approach as their path should go around the prominent land. These factors, together with the fact that

its *LCOE* is one of the highest in the selected group (and it cannot be minimized too much since the site's wind and waves power is not very high), were considered enough to also discard Site 11 for this step.

As it has been advanced in Section 3.4.2.1, after a few prior optimization attempts, it was noticed that the integer decision variables of the optimization problem presented some issues, as the algorithm would get trapped in a localized minimum. Two integer decision variables are part of the optimization: the number of rows and the choice of the HV export cable.

Regarding the latter, after running the model several times, it was observed straightforwardly that given the orders of magnitude of the distances to shore and the power generation, one of the cables was providing the best results in every case: the 220kV, 800mm² and 775A cable. Therefore, this decision variable was eliminated and this specific cable was set as a fixed parameter in every case.

As for the number of rows, the solution was not so simple. Five different optimizations for each number of rows were carried out in one of the three sites: Site 4. This way, similarly as it was done when discarding sites in Step 1, the best numbers of rows were found and the optimization process with other less optimal numbers of rows in the rest of the sites was avoided. An example of these types of successive optimizations can be seen in Fig. 4.10, where the graph at the left depicts the improvement in the *LCOE* in each optimization process until it stabilizes, and the graph at the right shows the layout that provides the newest value of LCOE.

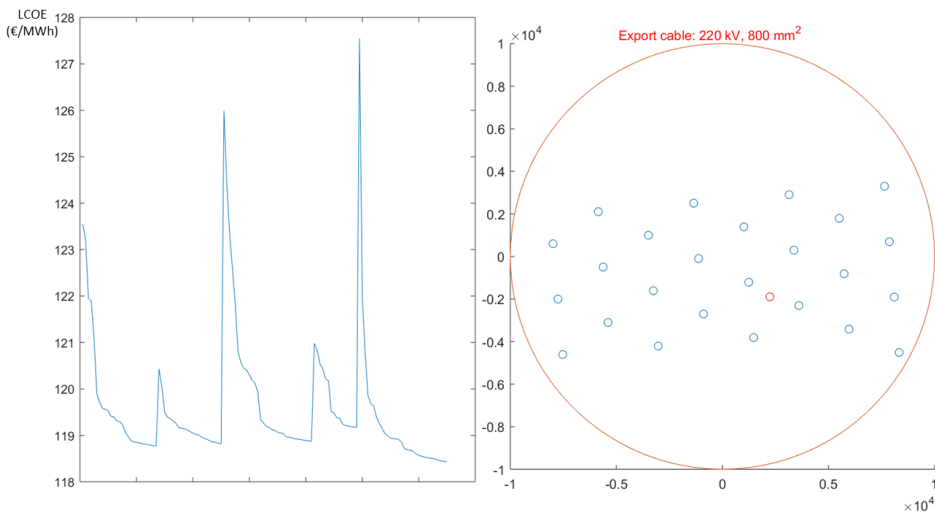


Figure 4.10: Example of simulation for 8 rows.

Therefore, given the consistent and better results obtained in Site 4 for the numbers of rows equal to 5,6,7 and 8 (although this last option provided quite unorganized layouts), the same simulations were then run for the rest of the sites. The average results of the five optimizations made in each case are shown in Table 4.6:

N. rows	2	3	4	5	6	7	8	Avg.
Site 4	119.26	119.04	119.07	118.67	118.79	118.72	118.81	118.91
Site 7	-	-	-	116.96	117.07	117.02	117.09	117.04
Site 8	-	-	-	120.85	120.98	120.912	121	120.94

Table 4.6: Average values of $LCOE$ in €/MWh obtained in each case.

Clearly, it is **Site number 7** the one that presents the best results with 5 and 7 rows. In all the cases, this first optimization process reduced in more than 2 €/MWh the value of the LCOE obtained in the previous step. As it can be deduced from the table, even though the energetic resource is better in Site 4, the optimization of the layout did not mean a significant improvement in the LCOE value with respect to the other two sites, and Site 7 still resulted to be the one with the lowest energetic cost. Once the best site has been chosen, the final layout is obtained in the last step.

4.2.5.3 Step 3: final optimization

In the last step of the process, the optimizations for Site 7 in the cases of 5 and 7 rows were carried out. In each case this was done in two ways to make sure that all the results span was covered. Each one of these types of optimization was run 10 times:

In the first type of optimization, the default PSO parameters of inertia, self and social adjustment weights were used (dynamic $\omega = 0.1 - 1.1$, $c_1 = 1.49$ and $c_2 = 1.49$). Furthermore, the five results obtained in the previous step were given to the algorithm as an initial solution (*InitialSwarmMatrix*). This could have two effects: either it makes the optimization start from a good solution (if it is considered to be close to the global optimal) and therefore it allows it to further improve it; or it prevents the algorithm to find other existent minimums that may be better.

Due to this second possibility, an alternative way to carry out the optimization was attempted: one of the optimal sets of PSO parameters proposed in literature (shown in Table 3.2) were used instead: $S = 63$, $\omega = 0.6571$, $c_1 = 1.6319$ and $c_2 = 0.6239$. In this case, no initial sets of decision variables were given to the algorithm, leaving this option to be randomly decided by the PSO as it has been done in Step 2.

After a long process that involved running the optimization ten times for each one of the four cases (each optimization taking an average of 30 to 60 minutes in the case

of the ones with the default variables and an hour to an hour and a half for those using the recommended parameters), the five best values obtained in each case are the following:

N. of rows	Parameters	1st	2nd	3rd	4th	5th
5	Default	116.7	116.71	116.71	116.71	116.71
	Recommended	116.56	116.59	116.71	116.73	116.75
7	Default	116.81	116.83	116.83	116.84	116.84
	Recommended	116.48	116.48	116.49	116.53	116.7

Table 4.7: Five best results of each optimization type in Step 3.

It is quite clear how the optimizations run with the default parameters that make use of the initial swarm from Step 2 provided results that slightly improved those from the previous step. However, when they are compared to the optimizations that make use of the recommended parameters, it is evident how the former are stuck in a localized minimum that may be improved.

In the next chapter, an argued choice of the possible final layout (or layouts) is presented, not only taking into account the LCOE results but also other qualitative aspects relevant in the study. The values obtained are analyzed and compared and a discussion is made about the technology.

CHAPTER 5

Results and Discussion

In the view of the results obtained and presented in the previous chapter, several final layouts were considered candidates to be chosen as the most convenient. Even though reducing the value of the *LCOE* of the project is the ultimate goal, other considerations also need to be taken into account.

Among the layouts that provide the best *LCOE* output, two clear groups of very similar arrangements were found. Within each of these two groups, the different solutions differ in small variations in the orientation angle or separation between platforms which result in the very small difference of *LCOE* observed in Table 4.7. These two main groups of arrangements are the following:

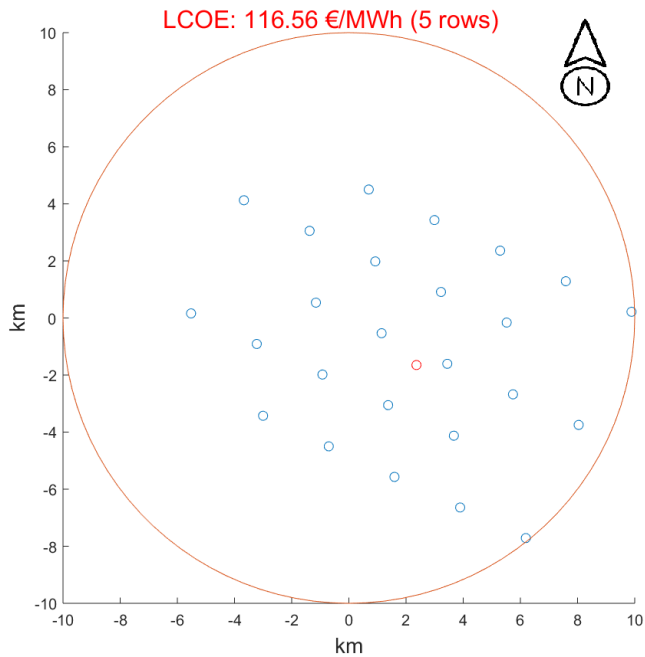


Figure 5.1: Layout of a possible final solution with 5 rows.

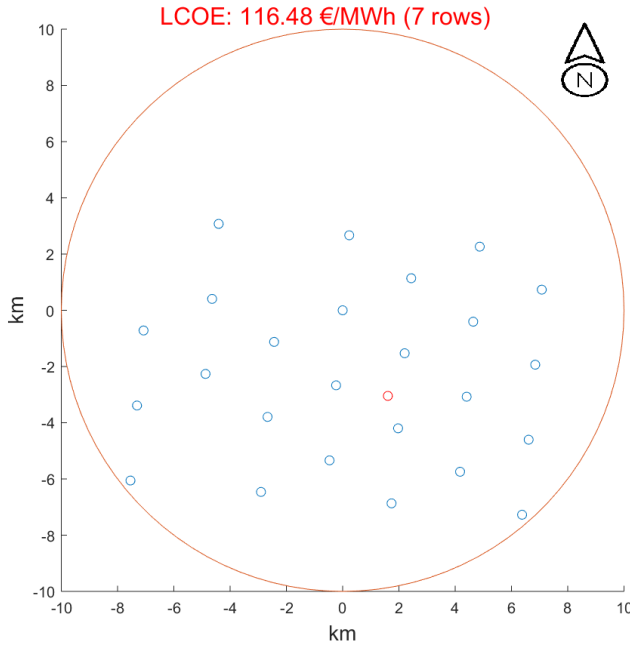


Figure 5.2: Layout of a possible final solution with 7 rows.

After considering the pros and cons of both layouts, it was decided that it is the first one, with five rows, the one that would be more convenient in a real case. On the one hand, the small difference of *LCOE* between both cases (0.08 €/MWh) is, most likely, below the error threshold of the model, and therefore it is not regarded as a determining factor. On the other hand, it has been considered that the second arrangement is quite unorganized, and therefore more messy for the visual impact (analyzed more in depth below). It also makes it more difficult to establish routes for vessels operating in the farm.

The input variables of the selected layout are shown in Table 5.1: respectively:

Separation between rows	2187.12 m
Separations between platforms in a rows	2535.44 m
Row offset	3798.86 m
Angle of orientation	-24.99°
x-coordinate of the substation	2364.55 m
y-coordinate of the substation	-1649.08 m

Table 5.1: Decision variables of the chosen layout.

In a first intuitive outlook of the the optimized input variables, it is easy to notice that these are quite logical. First of all, for every layout solution, the position of the offshore substation is always located in the fourth quadrant of the site (at its South-West), as it is the direction towards which the offshore substation is located in this case, as seen in Fig. 5.3.

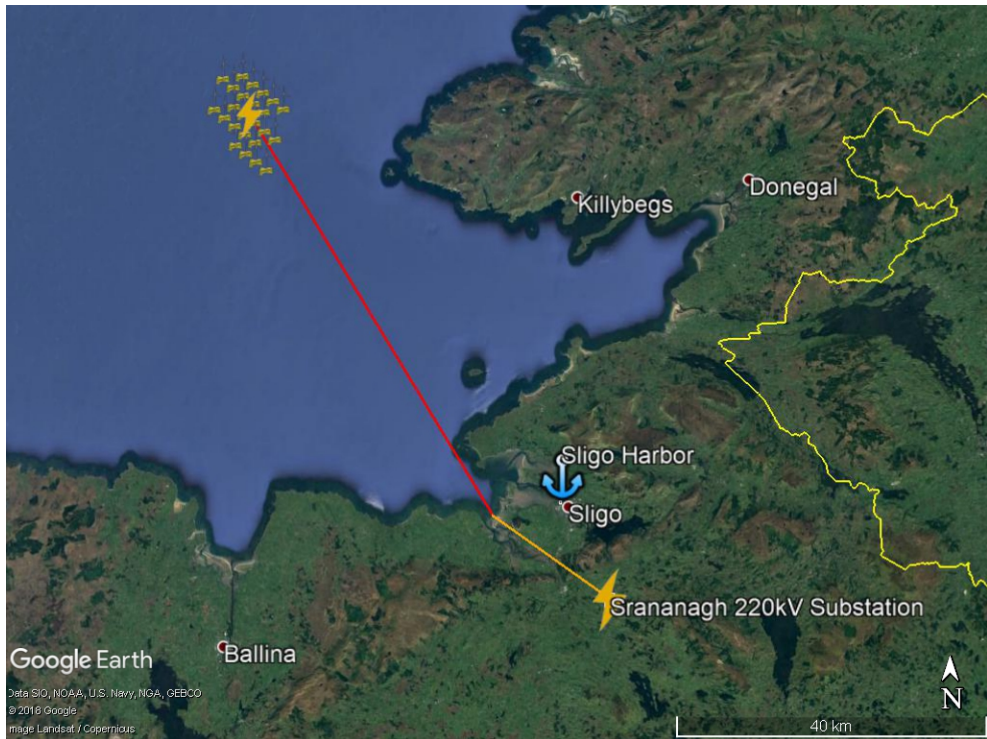


Figure 5.3: Location of the farm in the area. In red: the subsea stretch of the export cable. In orange: its inland stretch.

In the figure above, the distance from the farm to the onshore substation (about 80 km) and the harbor (in the order of 60 km) can be observed, being that to the closest land about 15 km. It should be remarked that the land closest to the farm is quite unpopulated, only finding very small villages in the surroundings, like Glencolmcille, with only a few hundreds of inhabitants.

A more close-up look to the site, depicted in Fig. 5.4, reveals more information about the farm. Given the influence of the inter-array cables cost, the offshore substation is quite centered in the site, as the algorithm finds a balance between the costs

and transmission losses of these two types of cables (the influence of the different depths in the mooring cost should not be forgotten either, although its cost contribution is quite low). Secondly, and with a higher influence in the *LCOE* output, it makes sense that the orientation of the rows and the position of the WTGs tend to minimize the wind wakes when the main directions of the wind are taken into consideration. For this reason, the rows directions have resulted to be perpendicular to the main wind direction observed in the wind rose.

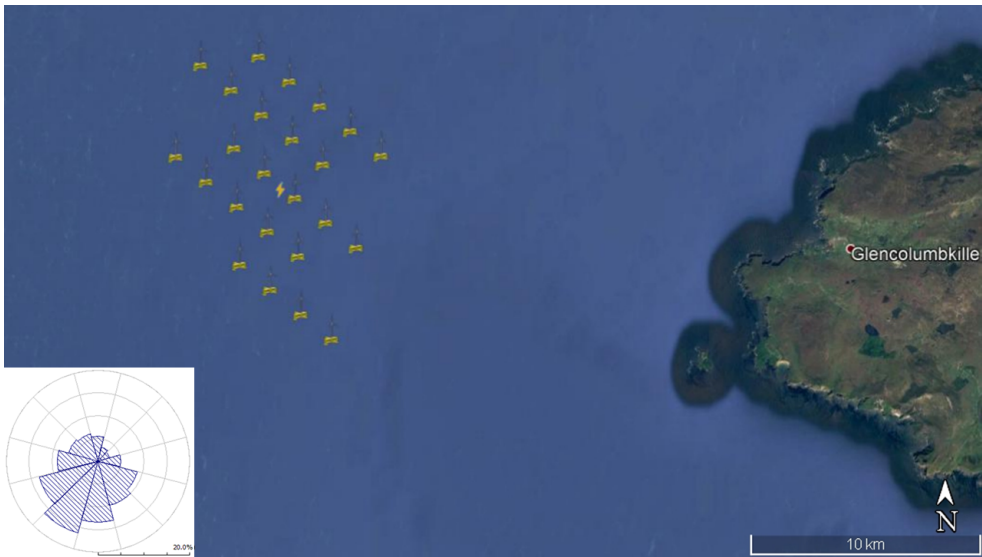


Figure 5.4: Farm arrangement, position of the offshore substation (bolt symbol) and wind rose of the site.

Given the presented arrangement of the wind farm, the energy values obtained in the model are those shown in Table 5.2. It is quite evident how the algorithm tends to minimize the wind wakes losses given its low values, one of the advantages of offshore areas with low spatial restrictions.

Furthermore, as advanced earlier on, the waves shadow range is quite smaller than that of the wind wakes and this is shown in the output values. In this case, the result is an energy loss due to the wave's shadows ten times smaller in proportional terms than that caused by the WTG's wakes. The rest of the parameters depicted are as dependent on the layout, but rather on the site's location and the technology.

AEP wind gross	1034.70 GWh
Wake losses	7.16 GWh (0.69%)
AEP wind net	1027.53 GWh
AEP waves gross	164.11 GWh
Shadow losses	0.08 GWh (0.05%)
Vanning losses	13.12 GWh (8%)
AEP waves net	150.90 GWh
Avg. downtime losses	123.2 GWh/year
Avg. transmission losses	1.73 GWh/year

Table 5.2: Output results of the chosen layout.

With regards to the economic figures of the calculation, the proportions depicted in Fig. 5.5 have been obtained in this case.

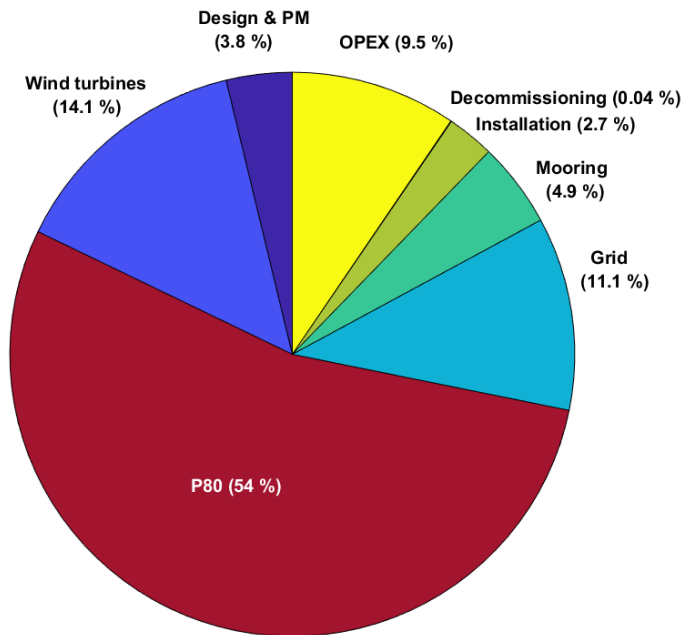


Figure 5.5: Piechart with the discounted costs proportions.

Several comments shall be made with regards to the costs. As it can be seen, most of the costs account for the CAPEX (around a 90%) and this is furthermore stimulated by the discount rate: the earlier the costs are executed, the bigger the proportional impact they will have in the final *LCOE* value. Even having considered the major planned maintenance operations, its total contribution to the discounted

costs does not reach the 10%. The opposite to the CAPEX occurs to the decommissioning costs, which apart from being low *per se*, the discount rate makes their influence insignificant.

As it was expected, among the CAPEX costs, the first contribution are those costs associated to the P80, and the devices that integrate it. Specially, the high amount of stainless steel that is needed for the platform structure increases the total cost significantly and its influence is, in fact, analyzed in the next section. The wind turbines represent the second highest cost of the projects and the grid costs the third. Their variation is also further analyzed.

Moving on from the strictly costs related aspects of the project, one of the issues that are originated by wind farms is their impact in the landscape, as it may be too invasive and, in some cases, they can even cause flickering due to the sun light going through the rotor blades. For these reasons, even though, as it has been said before, the area is quite unpopulated, the visual impact of the farm has been analyzed:

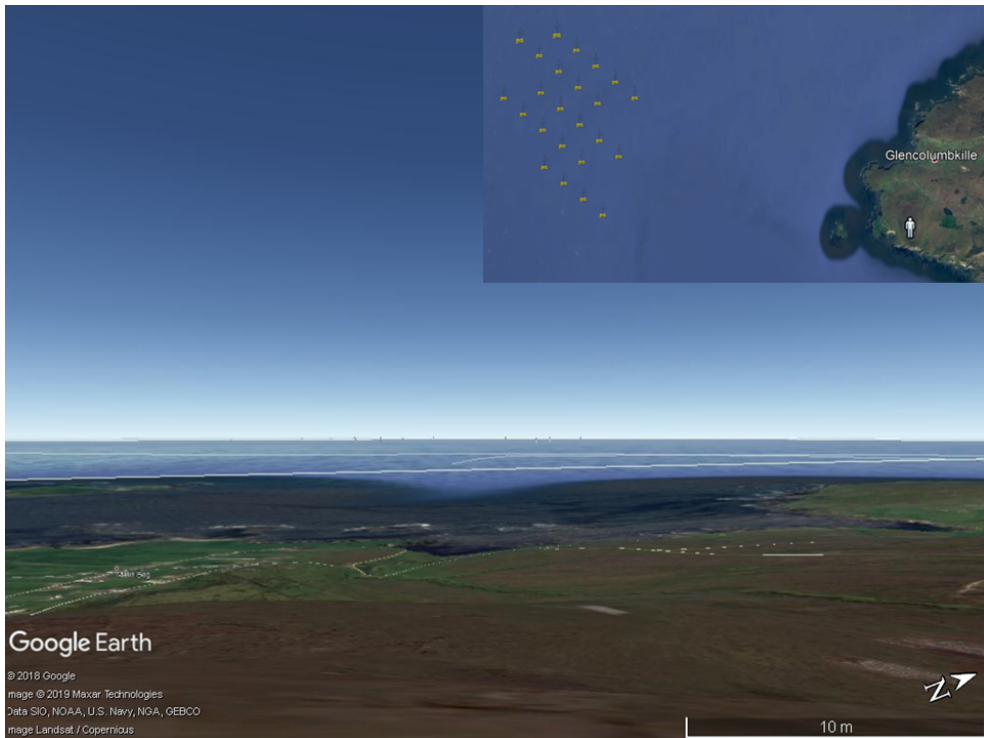


Figure 5.6: Visual impact from the highest point in the surrounding area.

The image (obtained through the combination of Google Earth and WASP) shows the farm, composed of 110 m tall wind turbines, from one of the very few points in land where it is visible, as the terrain is elevated. Even so, from this point only very small marks can be distinguished in the horizon, and the farm is completely invisible from any urban space in the area. Therefore, it can be concluded that the visual impact of the farm is irrelevant.

5.1 Sensitivity analysis

Once the main cost components of the project have been highlighted, the influence they have in the change of the *LCOE* needs to be studied. Naturally, even though all the costs related values have been researched and confirmed, as this is a hypothetical project that has not undergone thorough professional area specialized analysis, these values may be subject of variation for very diverse reasons: country specific conditions, change of market tendencies, resources availability, new technological considerations, legislation changes, etc.

The four parameters depicted in Fig. 5.7 are regarded as highly influential for the output *LCOE* value and they are also quite sensitive to change. The following sensitivity analysis has been applied to the optimal layout case presented above:

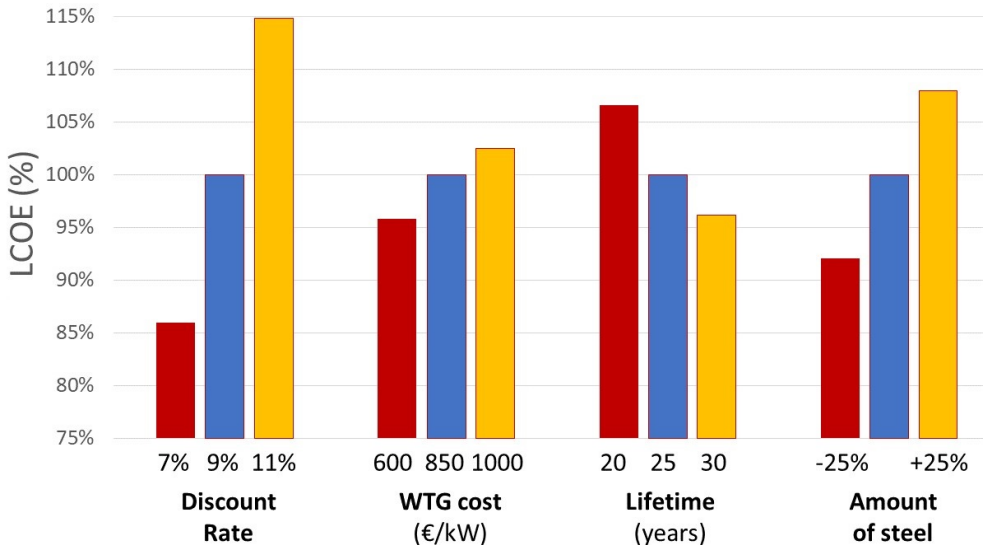


Figure 5.7: *LCOE* change with the variation of the main cost components.

From the four studied parameters, the **discount rate** is the most influential figure in the final cost as it can be seen in the graph. On the other hand, it is considered to also be the most uncertain of them all. As it completely depends on the investor's risk considerations, the value can only be estimated by carrying out surveys, consulting it with companies and comparing the concept with other similar and more mature technologies of which this parameter is known (the figures considered in this study and their sources are presented in Appendix A.5).

In fact, FPP considers a 7% discount rate that should even decrease after the technology has been tested and proved in small and eventually bigger projects like this one. The lower value implies a reduction in no less than almost a 15% of the *LCOE*. However, throughout this study the discount rate of 9% was used as it was compared to that of existent offshore wind farms, having the concept been regarded as a new technology that still needs to consolidate in the market. Anyhow, chances are that the value will decrease in the close future.

The second most influential parameter is the **amount of steel** needed to build the platform. As in most of the offshore floating concepts, this cost is definitely the first contributor to the final *LCOE* value of the project, and a reduction of 25% in the amount of steel would mean a decrease of as much as an 8% of the *LCOE*. Naturally, this involves a technological or geometrical change of the concept, as the buoyancy of the whole structure would change with the mass reduction, and therefore the amount of stored air would need to be different, but it is clear that there is a lot of room for improvement in this sense.

Regarding the **WTG costs**, this is a value that may be subject to change in both directions due to two main factors: on the one hand, the technology is constantly improving, and thus bigger and more efficient wind turbines keep being built at lower prices. However, as the wind energy market and more specifically the offshore wind one are in an up-wards tendency, the high demand of wind turbines may increase their cost (or at least stop its current down-slope price tendency). Paradoxically, also the presence of support schemes may encourage the manufacturers to increase the WTG price, given the consequent higher economical power of the developer. Anyhow, given the data found with regards to the costs (shown in Appendix A.2), the upper and lower values shown in the graph have been considered, meaning a change in the *LCOE* of 3-4%.

Lastly, the **lifetime** of the project has an important impact in the final cost too. As it has already been mentioned, it completely depends on the technology's design, and on climate related factors like the corrosion and the erosion of the materials, and the loads on the devices. As a P80 has never been tested offshore yet, these considerations are also somewhat uncertain. FPP works with a lifetime of 25 years, and it is the one that has also been assumed in this case, but in the sensitivity analysis it is shown the impact of a possible increase or decrease of 5 years. It should be mentioned

that an increase of the lifetime may also involve de rise of other costs like the O&M, and vice-versa. This must be taken into account when doing a more specific study on the matter.

Concurrently, it has also been studied the variation of the *LCOE* when applying specific changes that do not only have to do with the modification of certain costs, or of the values of certain parameters. Instead, these changes consist in the modification certain project or technology dependent procedures or characteristics. Figure 5.8 shows the *LCOE* reduction originated from three different variations: omitting the major planned O&M operations, excluding the electrical infrastructure costs (in case the state takes responsibility for it), and in a hypothetical case where the platform would be made of concrete instead of steel.

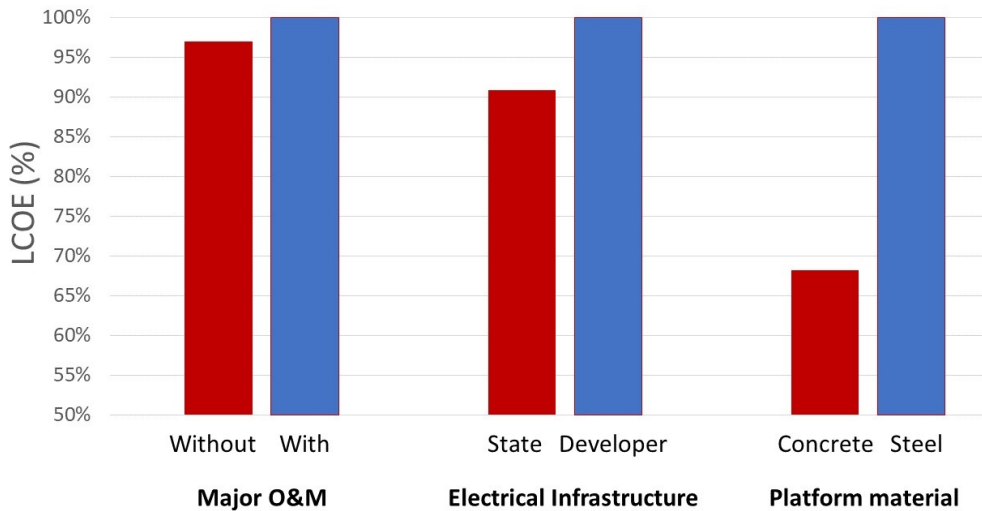


Figure 5.8: *LCOE* variation with concept and project related changes.

One of the main areas that is subject to change in FPP's current costs model is the O&M procedures, which are based on strategies normally carried out in offshore structures of the O&G sector, but they have not been able to be optimized or at least particularized for the P80 yet. In this sense, the main action considered to be avoidable is the **major planned O&M operation**, which, as explained in Section 3.3.3, consists in a periodical onshore inspection and maintenance service that involves towing the P80 to the harbor with the economical and downtime related expenses that this means. It has been found that avoiding this procedure reduces the *LCOE* in a 3% in the case studied. In general, this value depends on the distance to the operations harbor.

Without neglecting its cost impact, the action is actually not considered to be so significant, specially when taking into consideration that eliminating this big operation may involve having to increase the frequency of other types of planned operations, or it may force the concept to be out of service more often.

The second main project-related change that has been investigated is the case when **the state bears the costs related to the electrical infrastructure**. In this case, it has been considered that the developer would still be responsible for the costs associated to the acquisition and installation of the inter-array MV cables. Other than that, the costs of the offshore substation, onshore and offshore export HV cable and their respective installations are excluded from the costs model. In this case, a bigger impact has been found, having the *LCOE* been reduced by as much as a 9%.

As an extra remark on the matter, even though in this case the *LCOE* is considered to be reduced, in reality this cost still exists and, in general, and having a long-run perspective of a context where all renewable technologies' projects are feasible, the developer will probably have to take charge of these expenses. However, it is true that nowadays in some countries this cost is subject to be taken out from the equation, resulting in a significant improvement in terms of costs.

Finally, one last and arguably more hypothetical case where the **P80's platform would be made of reinforced concrete instead of steel** is studied. Some concrete floating offshore wind concepts already exist and the claim is that they are significantly cheaper due to the lower acquisition costs of the materials, the cheaper manufacturing process, the lower demand of O&M operations due to avoiding corrosion, and the possibility of increasing significantly the lifespan of the technology [62].

For this reason, given the amount of steel that conforms the platform, a few scenarios where it is used reinforced concrete instead of steel have been considered. They have been based on the following figures:

- Assumed current average cost of steel: 3.4 €/kg.
- Steel density: 8050 kg/m³.
- Assumed current average cost of concrete: 90 €/m³.
- Reinforced concrete estimated density: 2400 kg/m³.

It needs to be taken into account that changing the material of the structure has a lot of implications. In terms of buoyancy, the displaced volume of water depends on the materials' density difference if the structure's volume is kept constant, and therefore the air chambers that ensure this buoyancy need to be redesigned accordingly. Additionally, the materials' different resistances to distinct types of loads (compression, torsion, etc.) will condition the platform's walls' geometry and thicknesses.

Having these complex factors in mind (subject of a much more thorough study) and taking into account that concrete is in the order of ninety times cheaper than steel and three times lighter, the *LCOE* was then calculated in three cases: assuming the same volume of concrete as there is of steel currently, doing so with the mass, and an intermediate solution where a hypothetical optimized geometry is assumed.

In all three calculations it was found that concrete itself is so much cheaper than steel that the reduction of *LCOE* in all the cases was significant and very similar to each other, as the order of magnitude of the structure's materials cost completely changed: the *LCOE* has been reduced by about a 32%, the biggest impact among all the measures studied in the sensitivity analysis. In light of this notable cost reduction, it is considered that the cost can definitely be reduced this way in the future. If it is technically very difficult to design a structure completely made of concrete due to resistance or impermeability reasons, finding alternative solutions that combine the use of steel and reinforced concrete can still decrease this cost considerably, in the view of the results obtained.

As a general wrap up of the sensitivity analysis and moving back to more immediate costs variations, a case has been calculated (also using the optimal layout obtained earlier) with some of the parameters modifications presented above, which are considered as perfectly reasonable in the short-term. These are the following:

- Discount rate: 7%.
- The cost associated to the electrical infrastructure are assumed by the state instead of the developer.
- The major planned O&M operations are excluded.

The *LCOE* value obtained with these parameters is 87.71 €/MWh. The reduction from the original value is quite significant, and it is relevant specially when comparing it with the *LCOE* values of other technologies: commissioned onshore wind farms are currently in the range of 55 to 70 €/MWh, whereas some bottom-fixed offshore wind farms auctioned in 2019 and 2020 are expected to have an *LCOE* of 60 to 75 €/MWh [63].

The P80 costs in this case are still higher than those of its competing technologies. However, in the case of a farm with a higher number of platforms, where the wind and waves resources are stronger, the O&M is optimized, and where the WEC is purposely designed according to the specific site's conditions, the competitiveness of the technology is ensured. Not to mention the possible technological modifications discussed above that can eventually change the game in this sense.

5.2 Uncertainty analysis

As it has been remarked and reminded constantly throughout the report up to now, this model (as any other) is based on a series of assumptions and simplifications that make possible the calculation itself as, otherwise, the complexity of some of the phenomena involved would impede the feasibility of a study that involves such variety of factors. Furthermore, some of these simplifications make possible a fairly quick calculation that also allows an optimization process that would otherwise take much longer.

Having these premises in mind, the uncertainties of a prior analysis model of this kind need to be quantified when possible, and otherwise the user should be aware of the possible sources of inaccuracy. It must be mentioned that the uncertainty in specific values of parameters (like costs or rates as the ones seen in the sensitivity analysis) are not included in this study, as their accurate values can eventually be found with a more in-depth and resourceful research. The considered uncertainties are, in change, those due to the model construction itself, the assumptions made, and the source models of the resources inputs. In this case, the uncertainties have been classified into quantifiable and unquantifiable (or, at least, unquantified at this point):

Quantified uncertainties:

- The uncertainty of the wind speed profile provided by the WRF model (NEWA) was obtained by the developers after comparing results and observation. The error with the observations is $\Delta w.s. = 9 - 15\%$ [60].

- Similarly, when checking the reliability of the MIKE21 waves model, DHI found a maximum difference with measurements of $\Delta H_s = 0.25m$ [61].

- In the case of NO Jensen's wakes model, the uncertainty can have two sources: that due to the wave decay coefficient considered (showing a difference in the wake losses of $\Delta wakes = 30\%$ [64]), and that originated by the difference in the atmospheric stability (causing a change of $\Delta AEP_{wind} = 6\%$ [65]).

- Additionally, the observed difference between the used wakes model and the values obtained by WAsP is an average of $\Delta AEP_{wind} = 0.4\%$, and a maximum value of $\Delta AEP_{wind} = 0.9\%$.

- As commented in Section 3.1.1, another source of uncertainty is that due to the transformation of the scattered waves probabilistic matrices, obtaining a difference with time series values of $\Delta AEP_{waves} = 5\%$.

- The vanning efficiency uncertainty is not included in this study as the worst case scenario value of $\Delta AEP_{waves} = 15\%$ was adopted, a conservative enough value.

- Lastly, it is estimated that there can be an uncertainty due to the interpolation between the GWC standard heights. However, as a 110 m hub height has been used in this case, being very close to the reference height of 100 m, the uncertainty due to this interpolation is discarded.

Unquantifiable uncertainties:

- The waves shadow model is arguably the main unknown uncertainty as it could not be compared with an up-to-date non-linear model. However, it has been seen that the influence of the waves energy in the total $LCOE$ is much lower than that of the wind, and the waves shadow losses are really small due to the big distances between the platforms. Therefore, an error would not have a big impact in the calculation.

- An error associated to the power output matrix of the WEC, but its parameters were obtained from both numerical calculations and measurements, so the output values provided by FPP should be reliable.

- The land shadow influence on the wind speed at different parts of a site was assumed as negligible. This is one of the reasons why having real measurements of the site before carrying out a project is very important.

- The transmission losses model used is based on observed losses in real cables. However, the empirical values in which it is based could not be completely accurate for all cases. However, this uncertainty is unknown.

The graphs with the AEP_{wind} and AEP_{waves} variations due to the described quantifiable uncertainties are presented below:

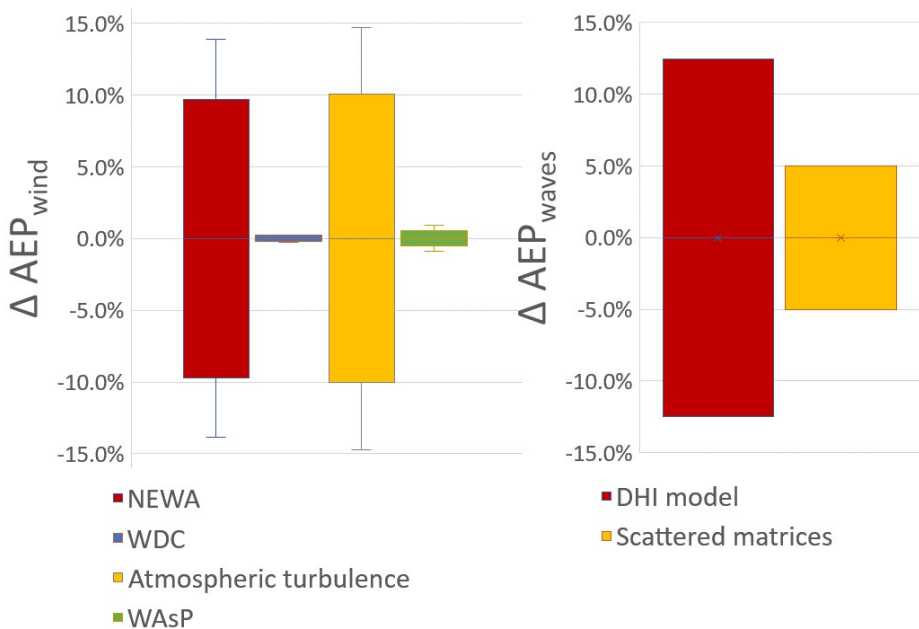


Figure 5.9: Uncertain factors effect on AEP_{wind} and AEP_{waves} .

In the first element of the left chart, it has been estimated that the difference in the wind speed means a variation in the power output of the WTG according to its power curve slope (assumed linear trend-line of 407 kW/m/s), and since the mean wind speed in this case is 10.65 m/s , the changes of 9% and 15% in the wind speed have an influence in the AEP_{wind} of 8.3% and 13.9% respectively. In order to get the variation of AEP_{waves} due to the waves height error of 0.25 m, the scattered probabilistic matrices were shifted 0.5 m (their minimum resolution), and the change in AEP_{waves} was then divided by two, obtaining the shown $\Delta AEP_{waves} = 12.5\%$.

Given that all the presented uncertainties are assumed to be stochastic independent processes, the combined average uncertainties can be calculated as follows:

$$\left(\frac{\Delta AEP_{wind}}{AEP_{wind}}\right)_{total}^2 = \left(\frac{\Delta AEP_{wind}}{AEP_{wind}}\right)_{NEWA}^2 + \left(\frac{\Delta AEP_{wind}}{AEP_{wind}}\right)_{WDC}^2 + \left(\frac{\Delta AEP_{wind}}{AEP_{wind}}\right)_{AT}^2 + \left(\frac{\Delta AEP_{wind}}{AEP_{wind}}\right)_{WAsP}^2 \quad (5.1)$$

$$\left(\frac{\Delta AEP_{waves}}{AEP_{waves}}\right)_{total}^2 = \left(\frac{\Delta AEP_{waves}}{AEP_{waves}}\right)_{DHI}^2 + \left(\frac{\Delta AEP_{waves}}{AEP_{waves}}\right)_{inputs}^2 \quad (5.2)$$

Obtaining a 11.9% uncertainty on the AEP_{wind} calculation and a 13.4% in the case of AEP_{waves} . And thus the uncertainty in terms of the $LCOE$ is defined as:

$$\left(\frac{\Delta LCOE}{LCOE}\right)_{total}^2 = \left(\frac{\Delta LCOE}{LCOE}\right)_{wind}^2 + \left(\frac{\Delta LCOE}{LCOE}\right)_{waves}^2 \quad (5.3)$$

Which provides a total uncertainty in the model's $LCOE$ calculation of 11.7%. Once this value has been obtained, it is convenient to mention that in order to minimize the effects of the uncertainties, the policy has been followed is to adopt fairly conservative values throughout the model and in this case analysis.

As a consequence of these results it shall be said that, even though these conservative assumptions have often been adopted, at the end this model can serve as a primary analysis of the costs and energy output that result of this type of project, which should be then followed by a thorough study of the site of interest in case of having the intention of actually carrying out a specific project. Both more in-depth research, and also site and technology specific physical measurements should be made in order to obtain accurate results that can be assured to match reality with all guarantees.

CHAPTER 6

Conclusion

The main objective of the present study was to develop a tool that allows the user to minimize the lifetime costs of an offshore farm composed of the Floating Power Plant's hybrid wind and wave concept. The different models or parts that conform the tool were built in MATLAB, followed by a demonstration of the tool through a case analysis. An easy-to-use philosophy, motivated by the objective of providing a useful tool, led to implementing all the inputs (divided into site, power converters and costs related inputs) through spreadsheets instead of directly in the code, so the parameters are easily modifiable. The tool consists of the waves, wind and costs models, and the layout optimization algorithm.

In the **wave energy model** (first undertaken part of the project), the most immediate challenge was the adaptation of the waves input in the form of three scattered matrices that depict the probability of occurrence of their energy defining characteristics: the significant height, the energy period and the direction. This data, freely accessible for FPP at any site, was transformed to a single three-dimensional probabilistic matrix with a wave energy output error of just a 5% in comparison to time-series data. Next, a wave shadows calculation model was adapted, introducing a relationship between the waves' zero-crossing and energy periods, correcting a mistaken length value, and decreasing its computing time to 4% of the original one. Finally, the WEC's power output matrix was integrated, an 85% vanning efficiency due to simultaneous waves directions was added, being then able to obtain the the wave's annual energy production.

The **wind energy model** was subsequently implemented. The input information, commonly in the form of Generalized Wind Climates, is transformed into a probability matrix that relates the wind speed and direction at a certain hub height. Two MATLAB wind wakes models based on N.O. Jensen's calculation method were acquired and compared with WAsP. The chosen model provides an average error of 0.35% in the wind energy output and a 3.5% error in the wake losses. It was observed that a resolution of 10° in the input data is needed to ensure a correct calculation. The wind annual energy production is then found by multiplying the WTG's power curves with the wind speeds after the wakes effect.

After obtaining the annual energy production, a **costs calculation** method was

defined to obtain the farm's Levelized Cost of Energy, a powerful indicator for investors. On the one hand, the energy generated undergoes further variations in this last module as downtime and transmission losses are discounted, finally obtaining the net energy sold to the grid each year. On the other, all the expenses were calculated using around 140 figures and parameters: the investment costs (CAPEX), applied before the start of the project except for the decommissioning; and the maintenance operational costs (OPEX) and downtime periods (applied throughout the lifetime). These costs depend on the site's distance to shore, to the harbor, and to the grid, as well as on the bathymetry. All in all, the *LCOE*, primary output value of the model is obtained, remaining the computing time of the entire tool below 5 seconds.

The last step to conform the tool was the **optimization** process that carries out the cost minimization by modifying certain decision variables. Given the problem's convex nature and the presence of discrete parameters, a metaheuristic algorithm is needed. After considering different options, the Particle Swarm Optimization (PSO), based on animal swarm behaviors, was chosen. The decision variables that were finally implemented are the platforms' positions (arranged in rows for visual and operational considerations), substation position, and the export cable choice. Furthermore, restraints and penalizations associated to the variables were implemented. The algorithm is able to find optimized solutions but a few issues were found regarding integer input variables, and when obtaining a consistent global minimum.

In the final phase of the project, a **case study** was carried out off the west coast of Ireland, an area with a convenient wind and waves climate. A farm size of 25 platforms and a grid connection through an onshore 220kV substation were chosen by means of a study of the area's grid strength. After a qualitative and quantitative process of elimination, Site 7 was chosen, with an *LCOE* of 116.56 €/MWh. The result was put in context, and relevant costs variations due to the most influential factors were investigated through a sensitivity analysis. The factor with the highest influence, also considering its degree of uncertainty, is the discount rate, with a variation effect on the *LCOE* of about a 14%, for a 2% change of the parameter (from its base 9% value to a 7%). Furthermore, situations with certain modifications were studied and a severe cost reduction was found if concrete was to be used instead of steel. A plausible short-term scenario with certain parameter variations was calculated, obtaining a result of 87 €/MWh, significantly closer to that of bottom-fixed wind farms currently being auctioned (60 to 75 €/MWh). It is considered that the technology presents good potential as there is room for costs reduction, specially in the structure's material (first cost component of floating concepts), where just a shift from steel to concrete could result in *LCOE* values in the range of 60 to 70 €/MWh.

Finally, an uncertainty analysis was carried out, resulting in an estimated variation of an 11.7% in the *LCOE* output, and highlighting relevant aspects regarding the input data, its processing, and the model construction, possible sources of inaccuracies. It is deduced that a study of this kind should only be serve as a preliminary tool

which must be followed by accurate site specific research. A special effort should be made in the wind and waves climate measurement, due to the important discrepancies between the existent data models.

6.1 Future work

A list of possible modifications, investigation fields and improvements to the model developed is presented below:

- The scaling effects of the WEC's shadows model should be investigated, as well as the linearities assumed by the numerical model in order to prove that it reproduces well the lab-scale measurements.

- A more specific O&M strategy should be modeled after offshore testing. A trustworthy aging rate could be defined and the O&M could be optimized for a certain lifetime of the project.

- A DC export transmission system (normally feasible for distances higher than 100km offshore) could also be modeled, allowing the optimization algorithm to choose between AC and DC.

- The power output matrices of different sized WEC should be developed so the algorithm would choose the most optimal one among the different possibilities. Similarly, it could be done so with the WTGs (two more decision variables).

- An optimization of the inter-array cables disposition can also be done (instead of exclusively connecting all of them to the substation individually), in order to study which is the most convenient arrangement in each case.

- A more advanced algorithm can be implemented for lay-out optimization: for example the Agent Swarm Optimization algorithm, that means a solution to other algorithms' issues.

- A translation to other programming languages of the model, like Python, would be interesting, as it could communicate, for example, with the upcoming PyWAsP or with TopFarm, and some routines could be run with these more specialized tools.

- Aside from the present model, a study should be made with regards to the technological feasibility of changing the platform's material from steel to concrete, given the high cost reduction potential.

Bibliography

- [1] NASA and S. Callery. (2019). Global climate change: Scientific consensus, [Online]. Available: <https://climate.nasa.gov/scientific-consensus>.
- [2] D. Wallace-Wells, *The uninhabitable earth*. Crown Publishing Group, 2017.
- [3] R. K. Pachauri, M. R. Allen, V. R. Barros, J. Broome, W. Cramer, R. Christ, J. A. Church, L. Clarke, Q. Dahe, P. Dasgupta, *et al.*, *Climate change 2014: synthesis report. Contribution of Working Groups I, II and III to the fifth assessment report of the Intergovernmental Panel on Climate Change*. Ipcc, 2014.
- [4] World Energy Council (WEC). (2015). Wind energy resource, [Online]. Available: <https://www.worldenergy.org/data/resources/resource/wind/> (visited on 2019).
- [5] W. Europe, *Wind energy in europe in 2018, trends and statistics*, 2018.
- [6] World Wind Energy Association (WWEA). (2019). Wind power capacity worldwide reaches 597 gw, 50.1 gw added in 2018, [Online]. Available: <https://wwindea.org/blog/2019/02/25/wind-power-capacity-worldwide-reaches-600-gw-539-gw-added-in-2018/> (visited on 2019).
- [7] Statista. (2019). Global offshore wind energy capacity from 2008 to 2018 (in megawatts), [Online]. Available: <https://www.statista.com/statistics/476327/global-capacity-of-offshore-wind-energy/>.
- [8] Global Wind Energy Council (GWEC). (2019). 51.3 gw of global wind capacity installed in 2018, [Online]. Available: <https://gwec.net/51-3-gw-of-global-wind-capacity-installed-in-2018/>.
- [9] G. R. Energy. (2019). Haliade-x offshore wind turbine platform, [Online]. Available: <https://www.ge.com/renewableenergy/wind-energy/offshore-wind/haliade-x-offshore-turbine> (visited on 2019).
- [10] “Floating offshore wind vision statement,” Wind Europe, Tech. Rep., 2017.
- [11] H. Stiedsal, “Tetraspar and tetrabase: Industrialized offshore wind turbine foundations,” Stiedsal Offshore Technologies, Tech. Rep., 2019.
- [12] C. Pérez-Collazo, D Greaves, and G Iglesias, “A review of combined wave and offshore wind energy,” *Renewable and Sustainable Energy Reviews*, volume 42, pages 141–153, 2015.

- [13] S. Astariz and G. Iglesias, “Enhancing wave energy competitiveness through co-located wind and wave energy farms. a review on the shadow effect,” *Energies*, volume 8, number 7, pages 7344–7366, 2015.
- [14] Floating Power Plant A/S. (2019). Invest in the future, [Online]. Available: <http://www.floatingpowerplant.com/>.
- [15] C. Pérez-Collazo, M. M. Jakobsen, H. Buckland, and J. Fernández-Chozas, “Synergies for a wave-wind energy concept,” 2013.
- [16] W. Power. (2019). Why wave power, [Online]. Available: <https://www.waves4power.com/why-wave-power/>.
- [17] H. de Sevin, “Development of an array design framework for a hybrid converter offshore farm,” Master’s thesis, Technical University of Denmark, 2014.
- [18] EMODnet. (2019). Bathymetry viewing and downloading service, [Online]. Available: <http://portal.emodnet-bathymetry.eu/?menu=19>.
- [19] A. Pecher and J. P. Kofoed, *Handbook of ocean wave energy*. Springer London, 2017.
- [20] K. Johannessen, T. S. Meling, S. Hayer, *et al.*, “Joint distribution for wind and waves in the northern north sea,” in *The Eleventh International Offshore and Polar Engineering Conference*, International Society of Offshore and Polar Engineers, 2001.
- [21] Danish Hydraulic Institute (DHI A/S). (2019). Waves data, [Online]. Available: <https://www.dhigroup.com/>.
- [22] J. Pastor and Y. Liu, “Wave climate resource analysis based on a revised gamma spectrum for wave energy conversion technology,” *Sustainability*, volume 8, number 12, page 1321, 2016.
- [23] S. Bellew, A. Köhler, A. Juliussen, P. Le Faucheux, A. Yde, and V. David, “Joint wind wave testing and validation of floating power plant’s renewable hybrid,” 2015.
- [24] A. Semedo, K. Sušelj, A. Rutgeresson, and A. Sterl, “A global view on the wind sea and swell climate and variability from era-40,” *Journal of Climate*, volume 24, number 5, pages 1461–1479, 2011.
- [25] R. Li, “Simulation of 8mw floating wind turbine,” Technical University of Denmark, Tech. Rep., 2018.
- [26] D. W. Energy. (2019). Wind atlas methodology, [Online]. Available: <https://www.wasp.dk/WASP/Details/Wind-Atlas-Generation/WindAtlasMethodology>.
- [27] —, (2019). Wasp, [Online]. Available: <https://www.wasp.dk/>.
- [28] A. Peña, P.-E. Réthoré, and O. Rathmann, “Modeling large offshore wind farms under different atmospheric stability regimes with the park wake model,” *Renewable energy*, volume 70, pages 164–171, 2014.

- [29] P. Sanderhoff, "Park-user's guide. a pc-program for calculation of wind turbine park performance," 1993.
- [30] L. Kitzling, D. Møller, and R. Bramstoft, "Feasibility studies of energy projects, lecture note 3: Levelized cost of energy," Technical University of Denmark, Tech. Rep., 2017.
- [31] M. Lerch, M. De-Prada-Gil, C. Molins, and G. Benveniste, "Sensitivity analysis on the levelized cost of energy for floating offshore wind farms," *Sustainable Energy Technologies and Assessments*, volume 30, pages 77–90, 2018.
- [32] G. L. Ohlsen, "Positioning of danish offshore wind farms until 2030 using levelized cost of energy (lcoe)," Master's thesis, Technical University of Denmark, 2019.
- [33] A. G. Gonzalez-Rodriguez, "Review of offshore wind farm cost components," *Energy for Sustainable Development*, volume 37, pages 10–19, 2017.
- [34] L. Castro-Santos, E. Martins, and C. G. Soares, "Cost assessment methodology for combined wind and wave floating offshore renewable energy systems," *Renewable energy*, volume 97, pages 866–880, 2016.
- [35] E. Camm and C. Edwards, "Reactive compensation systems for large wind farms," in *2008 IEEE/PES Transmission and Distribution Conference and Exposition*, IEEE, 2008, pages 1–5.
- [36] T. Cronin, "Grid connection. planning and development of wind farms," Technical University of Denmark, Tech. Rep., 2019.
- [37] J. F. Manwell, J. G. McGowan, and A. L. Rogers, *Wind energy explained: theory, design and application*. John Wiley & Sons, 2010.
- [38] S. Lundberg, "Performance comparison of wind park configurations," Chalmers University of Technology, Tech. Rep., 2003.
- [39] M. Alonso and H. Amarís, "Impact of wind farms in power systems," *Wind Farm*, 2011.
- [40] A. Kusiak and H. Zheng, "Optimization of wind turbine energy and power factor with an evolutionary computation algorithm," *Energy*, volume 35, number 3, pages 1324–1332, 2010.
- [41] G. Mosetti, C. Poloni, and B. Diviacco, "Optimization of wind turbine positioning in large windfarms by means of a genetic algorithm," *Journal of Wind Engineering and Industrial Aerodynamics*, volume 51, number 1, pages 105–116, 1994.
- [42] J. S. González, A. G. G. Rodriguez, J. C. Mora, J. R. Santos, and M. B. Payan, "Optimization of wind farm turbines layout using an evolutive algorithm," *Renewable energy*, volume 35, number 8, pages 1671–1681, 2010.
- [43] T. Back, *Evolutionary algorithms in theory and practice: evolution strategies, evolutionary programming, genetic algorithms*. Oxford university press, 1996.

- [44] S. Grady, M. Hussaini, and M. M. Abdullah, "Placement of wind turbines using genetic algorithms," *Renewable energy*, volume 30, number 2, pages 259–270, 2005.
- [45] A. Emami and P. Noghreh, "New approach on optimization in placement of wind turbines within wind farm by genetic algorithms," *Renewable Energy*, volume 35, number 7, pages 1559–1564, 2010.
- [46] R. Eberhart and J. Kennedy, "Particle swarm optimization," in *Proceedings of the IEEE international conference on neural networks*, Citeseer, volume 4, 1995, pages 1942–1948.
- [47] I. M. Arango, J. I. Sebastián, R. P. García, and J. B. M. Rodríguez, "Water distribution system design using agent swarm optimization," in *Water Distribution Systems Analysis 2010*, 2010, pages 747–763.
- [48] I. Montalvo, J. Izquierdo, R. Pérez-García, and M. Herrera, "Water distribution system computer-aided design by agent swarm optimization," *Computer-Aided Civil and Infrastructure Engineering*, volume 29, number 6, pages 433–448, 2014.
- [49] J. Stopa, D. Janiga, P. Wojnarowski, and R. Czarnota, "Optimization of well placement and control to maximize CO₂ trapping during geologic sequestration," *AGH Drilling, Oil, Gas*, volume 33, number 1, page 93, 2016, ISSN: 1507-0042. DOI: 10.7494/drill.2016.33.1.93.
- [50] Y. Shi and R. Eberhart, "A modified particle swarm optimizer," in *1998 IEEE international conference on evolutionary computation proceedings. IEEE world congress on computational intelligence (Cat. No. 98TH8360)*, IEEE, 1998, pages 69–73.
- [51] M. E. H. Pedersen, "Good parameters for particle swarm optimization," *Hvass Lab., Copenhagen, Denmark, Tech. Rep. HL1001*, pages 1551–3203, 2010.
- [52] Irish Examiner. (2019). Ireland second highest in europe for wind energy, [Online]. Available: <https://www.irishexaminer.com/breakingnews/ireland/ireland-second-highest-in-europe-for-wind-energy-910442.html>.
- [53] Wind Power Monthly. (2019). Ireland plans 12gw renewables boost, [Online]. Available: <https://www.windpowermonthly.com/article/1587884/ireland-plans-12gw-renewables-boost>.
- [54] Department of Communications, Climate Action & Environment of the Republic of Ireland. (2019). Renewable electricity support scheme, [Online]. Available: <https://www.dccae.gov.ie/en-ie/energy/topics/Renewable-Energy/electricity/renewable-electricity-supports/ress/Pages/default.aspx>.
- [55] Government of Ireland, "Renewable electricity support scheme. high level design," 2019.
- [56] EIRGRID and SONI, "All-island ten year transmission forecast statement," 2016.

- [57] Marine Traffic. (2019). Density maps, [Online]. Available: <https://www.marinetraffic.com>.
- [58] C. Desmond, J. Murphy, L. Blonk, and W. Haans, "Description of an 8 mw reference wind turbine," in *Journal of Physics: Conference Series*, IOP Publishing, volume 753, 2016, page 092013.
- [59] New European Wind Atlas (NEWA). (2019). Wind resource for wind farm siting, [Online]. Available: <http://www.neweuropeanwindatlas.eu/>.
- [60] B. Witha, A. N. Hahmann, T. Sile, M. Dörenkämper, Y. Ezber, E. G. Bustamante, J. F. Gonzalez-Rouco, G. Leroy, and J. Navarro, "Report on wrf model sensitivity studies and specifications for the mesoscale wind atlas production runs: Deliverable d4. 3," 2019.
- [61] Danish Hydraulics Institute, "Mike 21 wave modelling spectral waves fm short description," 2017.
- [62] R. Ebenhoch, D. Matha, S. Marathe, P. C. Muñoz, and C. Molins, "Comparative leveled cost of energy analysis," *Energy Procedia*, volume 80, pages 108–122, 2015.
- [63] International Renewable Energy Agency (IRENA), *Renewable power generation costs in 2017- key findings and executive summary*, 2017.
- [64] T. Sørensen, M. L. Thøgersen, P. Nielsen, and N. Jernesvej, "Adapting and calibration of existing wake models to meet the conditions inside offshore wind farms," *EMD International A/S. Aalborg*, 2008.
- [65] A. Peña and O. Rathmann, "Atmospheric stability-dependent infinite wind-farm models and the wake-decay coefficient," *Wind Energy*, volume 17, number 8, pages 1269–1285, 2014.
- [66] J. H. Larsen, H. C. Soerensen, E. Christiansen, S. Naef, and P. Vølund, "Experiences from middelgrunden 40 mw offshore wind farm," in *Copenhagen offshore wind conference*, 2005, pages 1–8.
- [67] I Slengesol, W. P. de Miranda, N Birch, J Liebst, and A van der Herm, "Offshore wind experiences: A bottom-up review of 16 projects," *Project ref. OW2010-002. Ocean Wind AS, Norway*, 2010.
- [68] ODE, "Study of the costs of offshore wind generation. technical report urn number 07/779," *Offshore Design Engineering (ODE) Limited, Renewables Advisory Board (RAB) & DTI*, 2007.
- [69] G. Gerdes, A Tiedemannm, and S. Zeelenberg, *Case study: European offshore wind farms-a survey for the analysis of the experiences and lessons learnt by developers of offshore wind farms*, 2006.
- [70] D. Westwood, "Offshore wind assessment for norway," *Oslo: The Research Council of Norway. North Sea Energy*, 2010.

-
- [71] International Renewable Energy Agency (IRENA). (2018). Wind costs 2010-2015, [Online]. Available: <http://resourceirena.irena.org/gateway/dashboard/?topic=3&subTopic=31>.
- [72] D. Energinet, *Technology data for energy plants for electricity and district heating generation*, 2016 (Updated in 2019).
- [73] BloombergNEF. (2018). 2h 2017 wind turbine price index, [Online]. Available: <https://about.bnef.com/blog/2h-2017-wind-turbine-price-index/> (visited on 2019).
- [74] X. ABB, *Submarine cable systems. attachment to xlpe land cable systems user's guide*, 2010.
- [75] G. Smith, C. Garret, and G. Gibberd, *Logistics and cost reduction of decommissioning offshore wind farms*. DNV GL, 2015.
- [76] Grant Thornton; Clean Energy Pipeline, *Renewable energy discount rate survey results - 2018*, 2018.
- [77] A. Myhr, C. Bjerkseter, A. Ågotnes, and T. A. Nygaard, "Levelised cost of energy for offshore floating wind turbines in a life cycle perspective," *Renewable Energy*, volume 66, pages 714-728, 2014.
- [78] Grant Thornton; Clean Energy Pipeline, *Renewable energy discount rate survey results - 2017*, 2017.
- [79] Offshore Engineer. (2019). Maintaining tension in subsea cable laying, [Online]. Available: <https://www.oedigital.com/news/461464-maintaining-tension-in-subsea-cable-laying>.

APPENDIX **A**

Costs Figures: Sources and Assumptions

The costs related figures used in the model and obtained from the literature through a research process are presented in the following Appendix. Their values, sources, and the decision-making process are depicted below. Nevertheless, FPP's specific Design and Project Management, Mooring, P80, Installation, O&M and decommissioning related costs, as well as the WEC power output matrix were left out, as they are specified in an alternative and confidential appendix in order to maintain the company's competitiveness in the market.

A.1 Design and project management

Country	Wind Farm	Cost	Cap [MW]	$k\text{€}_{2016}/MW$	
DK	Middelgrunden	2.98 M€	40	89	[66]
DK	Horns Rev & Nysted	0.1 M€/MW		109	[37]
NL	Prinses Amalia	10 M€	120	92	[67]
UK	ODE Costs Model	5.6 M£	108	88	[68]
UK	Scroby Sands	1.7 M£	60	52	[69]
UK	North Hoyle	0.8 M£/MW		144	[67]

Table A.1: Project management costs for commissioned offshore wind farms.

The design and project management strategy implemented was the one considered currently in FPP. However, a general alternative parameter was initially modeled, entailing an initial capital cost that has been observed to be dependent on the farm's total capacity and it has been implemented linearly in the model. As in many other cases, the difficulty of its estimation comes from the unavailability of real information and/or its low degree of specificity. In general, this cost involves several aspects such as bathymetric and meteorological investigation, resources monitoring, financing, li-

censing, legislation management, marketing, environmental impact assessment (EIA), stakeholders management and design engineering [33, 34].

For the model, a country based average was selected as the cost value of the design and project management. As an example, projects based in the UK have a cost of 94.67 k€/MW. In countries without relevant information, the world average of 97.57 k€/MW can be used instead.

A.2 Wind turbines

With regards to the cost of wind turbines, commercial secrecy and economies of scale make difficult to establish a clear relation between their price and capacity. The costs of wind turbines also depend greatly on the year of acquisition as the market is changing quickly, the capacity is constantly growing and the number of both manufacturers and promoters and their requests fluctuate quite a lot lately.

The turbines' costs can generally be split into three components: acquisition, shipping-assembling and electrical installation; the second one depending on the distance to shore and climate characteristics of the area [33]. Even though according to certain sources the cost of turbines may also include the acquisition and/or the installation of the foundation, the three main cost components are in average distributed as follows: 85% for the acquisition, about 5% for the installation (of the turbine only), and the last 10% accounts for the electrical part. [70].

Using data from several commissioned and yet-to-be commissioned wind farms (all prior to 2015), the following correlation between capacity and price was then found to fit quite acceptably the wind turbine total costs [33]:

$$Cost_{wt} [\text{k€}] = 1374 \cdot Capacity_{wt}^{0.87} \quad (\text{A.1})$$

Presenting those of the studied farms with turbines bigger than 5 MW a cost in the range of 1400-1600 k€/MW, and those smaller between 500 and 800 k€/MW.

On the other hand, focusing on somewhat more recent data, for turbines with diameters greater than 95 m, an average value of 1143 USD/kW is the turbine price index provided by Bloomberg NEF for 2015 [71], and a total cost of acquisition of 1107 k€/MW was determined by DEA and Energinet in 2015 [72].

All in all, in order to meet the available data, disregarding the 5% that supposedly corresponds to the installation, and taking into account the historical rate of costs decrease obtained from IRENA (91.8 USD/kW/year), the more conservative one predicted from DEA (48.6 €/kW/year) [71, 72], and Bloomberg's WTG costs

projection shown in Figure A.1, it has been determined a cost of wind turbine of 850 *k*€/MW by 2019.

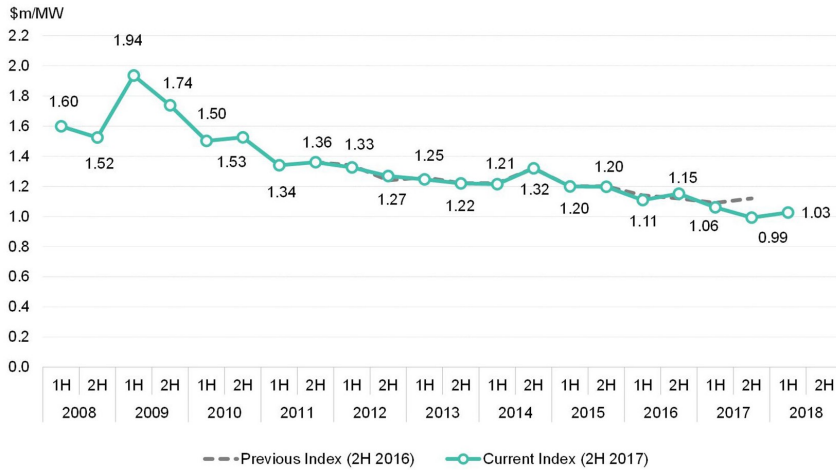


Figure A.1: Turbine price by delivery date as of 2017 [73].

A.3 Electrical infrastructure

Sixteen types of export cables were included in the model for this study, as presented in Table 4.4 (Section 4.2.4). Their associated costs are given in Table A.2 and they have been obtained from the progressions depicted in Fig. A.2

Cost (k€2016/km)	Section (mm ²)				
	500	630	800	1000	
Rated Voltage (kV)	110	436.75	529.2	597.25	702.75
	132	518	592	690	805
	220	843	946	1,061	1,214
	275	1,046.1	1,271.1	1,292.9	1,469.6

Table A.2: Costs of the cables used in the model.

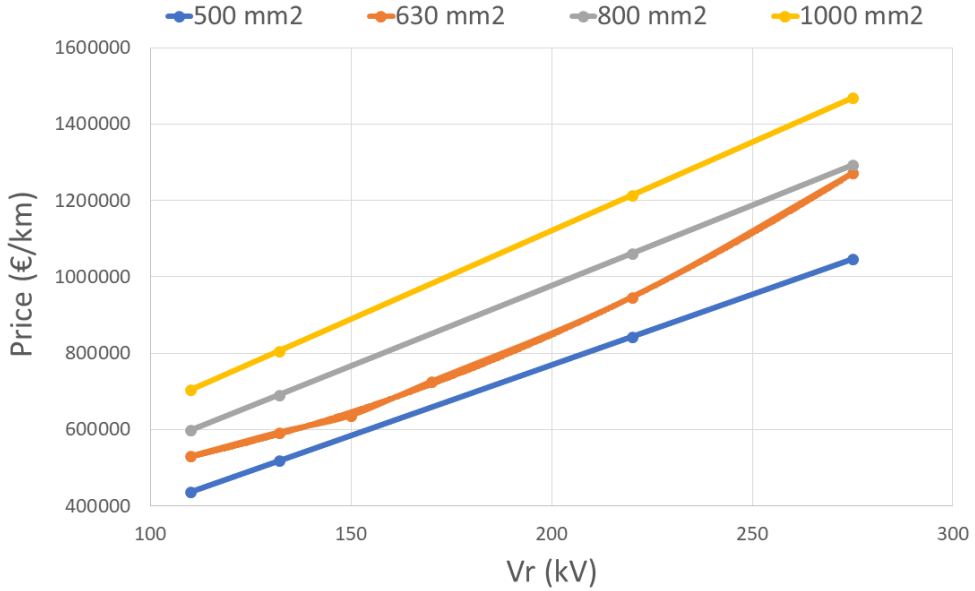


Figure A.2: Cables cost [33] (the values for the 110 kV and 275 kV cables were inter and extrapolated respectively).

In order to define their rated apparent power and transmission losses through the model presented in Section 3.3.4, the cable's sections, rated current and loss coefficients used in the model are presented below:

MV (V=10-90 kV)		HV (V= 100-300 kV)	
S (mm2)	I _{rated} (A)	S (mm2)	I _{rated} (A)
95	300	300	530
120	340	400	590
150	375	500	655
185	420	630	715
240	480	800	775
300	530	1000	825
400	590		
500	655		
630	715		
800	775		
1000	825		

Table A.3: Cables sections and rated current [74].

Voltage (kV)	P0	C0	Pk
11	5.01	0.0212	57656
22	13.08	0.0354	57656
33	21.48	0.0421	57656
45	38.40	0.0694	57656
66	70.71	0.1069	57656
110	149.70	0.149295	55566
132	200.87	0.1726	49470
220	530.30	0.2982	51211
275	878.4891	0.3606	55565.85

Table A.4: Transmission loss coefficients [38].

Having, again, been interpolated the coefficients of the 110 kV cable and extrapolated those of the 275kV cable as it is shown in Fig A.3.

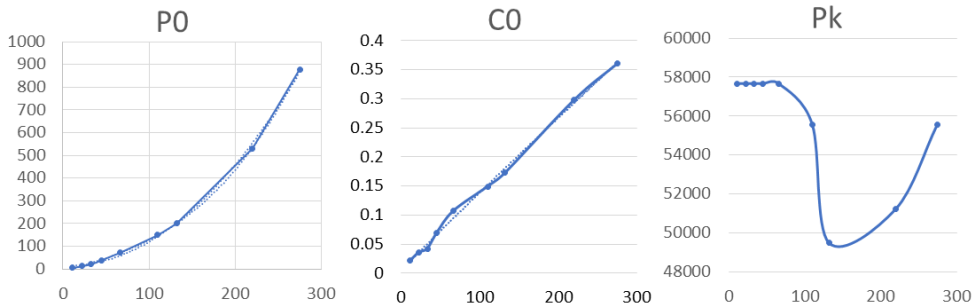


Figure A.3: Cables loss coefficient with respect to its voltage (in kV).

Regarding the inter-array cables and the rest of the electrical costs, this information was provided by FPP and therefore it is kept confidential.

A.4 Decommissioning

As it was done with the Design & Project Management costs, it has been used FPP's specific decommissioning costs. However, alternative figures based in existent wind farms and estimations can be used in general terms.

However, due to the fact that most of the offshore wind farms still have not arrived to the end of their lifetime, decommissioning still remains as a quite unknown process when it comes to its costs. This uncertainty is increased by the facts that

wind farms are currently being installed further offshore and wind turbines are considerably bigger, so the conditions are changing. Also, the moderate but incessant increase in the frequency of these decommissioning processes as offshore wind farms start reaching their lifetime in the upcoming years, might also have an effect in its costs. And evidently, more uncertain is the case when it comes to floating wind, not to talk about hybrid technologies. Arguably, offshore technology might imply somewhat lower costs, which may, on the other hand, compensate for the increasing distance offshore. [75].

A well fitted linear progression that uses values from future offshore projects estimates a fixed cost of 1606 k€_{2016} , with a capacity dependent slope of $114 \text{ k€}_{2016}/\text{MW}$, which provides a value of 13 M€ for a 100 MW farm [33]. As a contrast, available data from few past decommissions of wind farms with 3-4 MW wind turbines indicates quite higher costs, in the range of 300 to 500 $\text{k€}/\text{MW}$, and thus 30-50 M€ for a 100 MW wind farm [75].

As a solution of compromise and having the purpose of trying to match the rather contradictory data, the linear expression ?? was used.

A.5 Discount rate

The discount rate, also defined as the opportunity cost of capital, represents the risk cost of investing money in a specific project as opposed to doing so anywhere else, and it is a key parameter for investors to determine the actual market value of these projects [37, 76]. Of course, this risk depends highly on the type of technology used in the project and its maturity.

Its impact in projects is quite big but, as it is not an entirely objective value, it is a value difficult to estimate. It depends on investors and the studies they carry out when analyzing the convenience of investing in specific projects. Also, once again, secrecy makes the research of this value even more difficult.

As a first approach, when calculating costs of renewable energies, IRENA estimates a discount rate of 7.5% for OECD countries [63], which is not precise enough as there are quite different technologies with various risks and maturity in the wide range of renewables. Focusing on offshore installations it was observed a decrease with time of their discount rate. According to some studies, its value for offshore projects was estimated to be from 8% to 12% in 2013 [31, 77]. However, more recent data obtained from surveys made in 2017 and 2018 present somewhat lower average values:

Country		2017	2018
Ireland	Levered	9.50%	8.50%
	Unlevered	8.25%	6.50%
United Kingdom	Levered	9%	8.75%
	Unlevered	7.75%	7.25%
Nordic Countries	Levered	8.25%	8%
	Unlevered	7%	6.75%
Germany	Levered	8%	8.25%
	Unlevered	6.25%	6%
France	Levered	9.75%	9.50%
	Unlevered	8.25%	8%

Table A.5: Surveyed discount rate by country for offshore wind energy projects [76, 78].

Given the discount rate's uncertainty, taking into account the previous information and knowing, as it has been remarked, that the rate's trend is negative, but keeping in mind on the other hand that hybrid wind-wave technology is a yet-to-scale and therefore more risky technology, a rather conservative discount rate of 9% has been used in the model.

A.6 Vessel speeds

The following speeds of the boats involved in the installation, maintenance and de-commissioning of the farm are considered in the model:

- **Towing vessel:** cruise speed (return) of 14 knots (25.9 km/h) and towing speed of 5 knots (9.26 km/h).
- **Cable laying vessel:** cruise speed of 14 knots, and cable laying speed of 0.65 knots (1.2 km/h) [79].
- **General passenger O&M vessel:** average cruise speed of 20 knots (37 km/h).
- **Cable removal vessel:** cable removal speed of 0.5 knots (0.9 km/h).

APPENDIX **B**

Confidential data
from Floating Power
Plant A/S
